THE DEVELOPMENT AND EVALUATION OF ^{252}Cf NEUTRON IRRADIATION FACILITIES FOR TWO BIOMEDICAL APPLICATIONS USING DISCRETE ORDINATES, MONTE CARLO, AND EXPERIMENTAL METHODS

by

RODERIC IVAN PETTIGREW

B.S., Morehouse College
(1972)

M.S., Renssalaer Polytechnic Institute
(1973)

SUBMITTED IN PARTIAL FULFILLMENT
OF THE REQUIREMENTS FOR THE
DEGREE OF

DOCTOR OF PHILOSOPHY

at the

MASSACHUSETTS INSTITUTE OF TECHNOLOGY

13 JUNE 1977

Signature redacted

Signature of Author . . . . . .
Department of Nuclear Engineering, 13 June 1977

Signature redacted

Certified by. . . . . .
Thesis Supervisor

Signature redacted

Accepted by . . . . . .
Chairman, Department Committee

THE DEVELOPMENT AND EVALUATION OF ^{252}Cf NEUTRON IRRADIATION FACILITIES FOR TWO BIOMEDICAL APPLICATIONS USING DISCRETE ORDINATES MONTE CARLO, AND EXPERIMENTAL METHODS

by

Roderic Ivan Pettigrew

Submitted to the Department of Nuclear Engineering on June 13, 1977, in partial fulfillment of the requirements for the Degree of Doctor of Philosophy.

ABSTRACT

Two original ^{252}Cf neutron irradiation facilities have been designed using advanced transport calculations for two different biomedical applications.

The first facility is designed to irradiate 10 gram samples of blood or tissue loaded with 100 μg of ^{10}B so that the 0.48 MeV prompt gamma ray can be measured with 5% statistical precision in less than an hour, using a Ge(Li) detector. In addition, the designed facility is sufficiently compact (~1 m^3) and radiologically safe (~50 mrem/hr on surface) to allow an in-hospital siting. The constructed facility consists of four Bi-shielded 80 μg ^{252}Cf sealed sources moderated with 115 liters of D_2O in a cylindrical tank (50 cm diameter by 60 cm). Biological shielding consists of 20 cm of Li loaded polyethylene on all sides of the tank. Measurements of the thermal neutron flux distributions along three orthogonal directions within the D_2O, the fast neutron flux at the detector position, external surface does rates, and of ^{10}B loaded test samples were in excellent agreement with design calculations ($\leq$ 2 standard deviations).

The second facility is designed to measure small calcium changes within the human hand and wrist by activating ^{48}Ca with thermal neutrons and subsequently monitoring the 3.1 MeV decay gamma ray with large NaI detectors. This facility was designed so that a 1% statistical precision could be obtained with a fast neutron dose to the hand of less than 1 rad. Further, a sufficiently uniform thermal flux has been engineered so that the change in Ca activations for a 1 cm lateral hand displacement is in the range of 0.5%. This irradiator consists of eight 100 microgram sources where four sources are positioned symmetrically in each of two parallel annular Bi rings separated by 12 cm in a H_2O tank (50 cm diameter by 55 cm) which is shielded on all sides by 20 cm of polyethylene-Li. A Ca counts to hand dose ratio of

35,000 counts per rad (fast neutron) is estimated for this system.

Thesis Supervisors: Gordon L. Brownell
Professor of Nuclear Engineering, M.I.T.

Brian W. Murray
Research Associate,
Department of Nuclear Engineering, M.I.T.

ACKNOWLEDGMENTS

This thesis is dedicated to my grandparents, who would have cherished its completion, and to my parents whose encouragement and support added stability and peacefullness to the years spent in realizing this work.

I am also most appreciative of the support and assistance of my advisor, Professor G.L. Brownell. Extra special and most sincere expressions of gratitude are to be extended to Dr. Brian W. Murray and Professor Owen L. Deutsch whose personal and professional insights, resources of expertise, and guidance, were indispensable in the execution and completion of this research. Further, I have benifitted from and enjoyed the discourse with and the encouragement of Dr. R.G. Zamenhof and Ms. Myu Campbell, with whom I shared an office for the duration of my studies at M.I.T.

The careful and professional work of Mr. F. Woodworth, Mr. Ronald St. Jean, and the M.I.T. Nuclear Engineering Department machine shop staff is greatfully acknowledged.

I would also like to acknowledge full financial support from the USAEC (Traineeship) 1974 to 1976, and from the M.I.T. Health Sciences Fund, 1976-1977.

Finally, I would like to thank Mrs. Terry Crossley and Ms. Betty Wytias for their consideration and indulgence in typing a difficult manuscript.

TABLE OF CONTENTS

TABLE OF CONTENTS (continued)

TABLE OF CONTENTS (continued)

TABLE OF CONTENTS (concluded)

LIST OF FIGURES

LIST OF FIGURES (continued)

LIST OF FIGURES (continued)

LIST OF TABLES

I. INTRODUCTION

1.1 INITIAL CONSIDERATIONS

There are two specific areas in the application of neutron activation techniques in the life sciences where improved nuclear measurement techniques would constitute a significant advance. One area concerns the treatment of malignant brain tumors by boron neutron capture therapy, while the other involves the *in vivo* measurement of skeletal calcium, an important diagnostic parameter in the study and treatment of metabolic bone diseases.

This thesis reports the research leading to and culiminating in the design of two self-contained neutron irradiation facilities utilizing sealed ^{252}Cf sources. The first facility, designed to activate, *in vitro*, boron in human tissue samples, has been constructed, experimentally characterized, and evaluated. The second facility has been designed to measure, *in vivo* , the calcium content in the human hand and wrist with high precision and at a safe dose level.

Before undertaking the design of these facilities, a number of considerations need to be borne in mind. First, the radiation components encountered in such a facility will include, fast, epithermal and thermal neutrons, and photons over a wide range of energies produced by the neutron source, and by neutron scattering and capture events in the facility. Second, the wide

range of spatial transport characteristics of these radiation components results from a variety of possible radiation interactions. Since the dimensions of the contemplated facilities may be small with respect to the characteristic relaxation lengths, the radiation fields can be substantially affected by the proximity of boundary surfaces and radiation sources. The accurate description in these regions cannot be accomplished by the use of analytical methods nor by the results of calculations for large, single material source-moderator configurations. Third, because the different radiation components exhibit different Quality Factors (QF) in the assessment of radiation dose, the contribution of each needs to be known so that the estimate of dose equivalent can be made.

To arrive at an optimum design of a neutron irradiation facility and, bearing in mind the above considerations, two distinct paths can be followed. The first is to experiment with a single source, in a variety of geometries within different moderator materials, in order to measure all the important flux and dose distributions needed for the design contemplated. If the design criteria include a multi-source configuration, facility compactness, and an optimum design to satisfy human use requirements, a complete experimental approach may prove to be prohibitively

expensive. The second approach is to carry out the design using advanced neutral particle transport calculations. The neutron facilities described in this thesis were designed in this manner using a one dimensional discrete ordinates computer code called ANISN [Engle (1967)] and a general geometry Monte Carlo transport code called ANDY [Harris (1970)]. Both codes make use of an up to date 29 element, neutron-gamma ray coupled cross section data file compiled at the Los Alamos Scientific Laboratory [Sandmeier (1974)]. With these calculational tools, complex source-moderator-shielding configurations can be set up mathematically, tested, and modified with relative ease and a reasonable cost.

This thesis attempts to demonstrate that compact, self-contained, optimal neutron irradiation facilities using isotopic neutron sources can be accurately designed by the use of advanced transport calculations and engineering concepts. Since funds were available only for the construction of the boron assay facility, only this facility has been built, characterized and evaluated. The remarkable agreement between calculational estimates and experimental results for this facility adds confidence to the predicted results for the hand irradiation facility. The biomedical needs and rational for these facilities are discussed next.

1.2 Biomedical Rationale For the Development of Neutron Irradiation Facilities

1.2.1 Boron Neutron Capture Therapy

An interesting radiation therapy technique for the treatment of brain-tumor patients is boron neutron capture therapy. This radiation modality is based upon the selective loading of tumor cells with a ^{10}B enriched boron compound and then irradiating the tumor site with a thermal or epithermal neutron beam. This approach can be especially advantageous in sterilizing tumor cells interspersed within healthy tissue such as the margins of a glioma within the brain. The radiation dose is produced by the α and ^{7}Li particles released after neutron capture in ^{10}B, viz; $^{10}B(n,\alpha)\ ^{7}Li$. Figure 1.1 illustrates the α particle decay scheme from the excited state of ^{11}B. The total Q of the reaction is 2.79 MeV but in 94% of the decays, the recoiling ^{7}Li nucleus is in the 0.477 MeV excited state. As a result, the two heavy charged particles share an average kinetic energy of 2.33 MeV. The ranges in tissue for these particles is 10 μM or less, or about the diameter of a typical cell. This implies that the dose delivered in this therapy procedure will follow the ^{10}B distribution, even to the cellular level. In addition, the particles each have a high linear energy transfer (LET) in H_2O which enhances their local biologic radiation effect [Deutsch (1975)].

1.2.2 The Loading of ^{10}B in Brain Tumor

In order to load tumor cells in the brain with

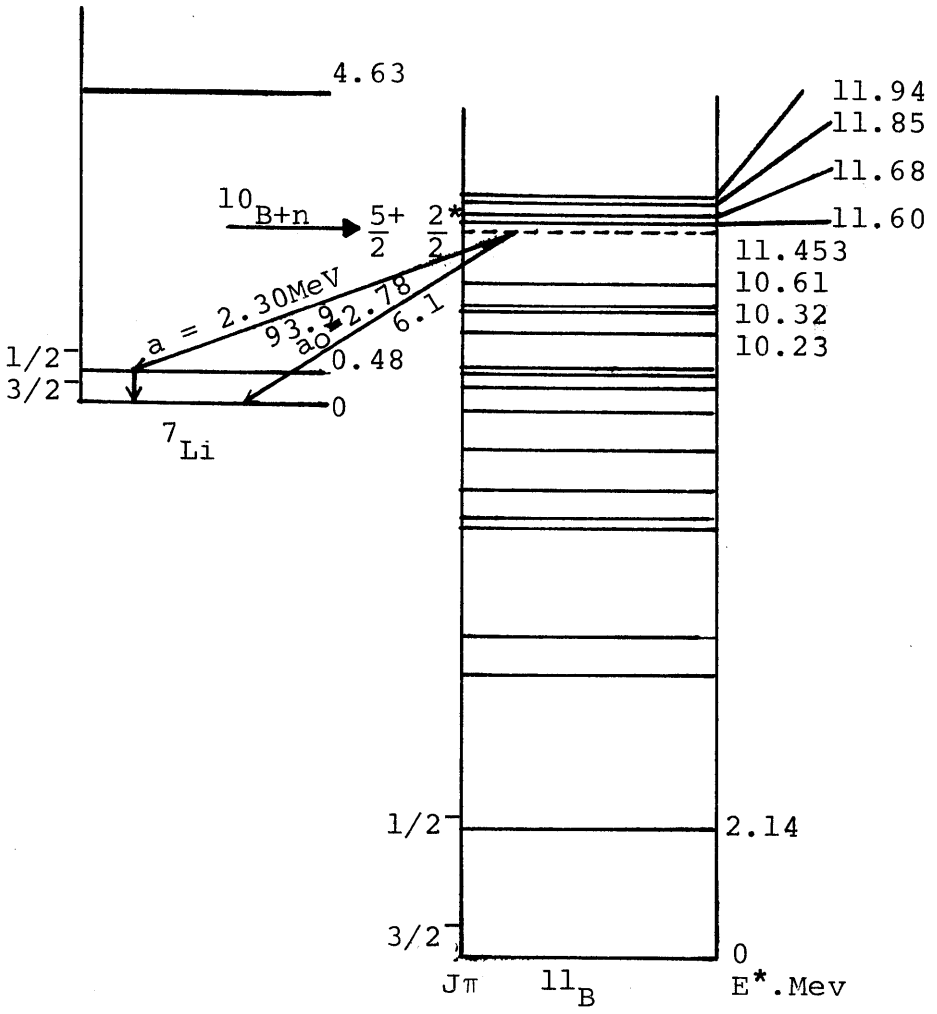

FIGURE 1.1 -- ENERGY LEVELS OF ^{10}B AND ^{7}LI SHOWING THE TWO ALPHA-PARTICLE DECAY CHANNELS FOR THE SLOW NEUTRON INDUCED REACTION $^{10}B(N, \alpha)^{7}LI$. FROM FODERERO (1972)

with ^{10}B preferentially to normal brain cells, the blood brain barrier is utilized. This barrier normally prevents most chemical compounds from entering brain cells from the bloodstream. For neoplastic cells, however, this barrier is compromised so that a ^{10}B compound within the bloodstream can enter such cells. At the present time this is the only practical approach for ^{10}B loading of brain tumors [Tolpin (1976)]. Although a high ratio of ^{10}B concentration in tumor cells to that in normal cells is realized (>10), the bloodstream can have a higher concentration of ^{10}B than the tumor cells. This situation can place the blood vessel walls at risk from the same charged particle dose as some tumor cells receive. This is the primary reason for the failure of the first trial of boron neutron capture therapy which took place at the M.I.T. facility during 1960-1961 [Brownell (1973)].

1.2.3 The Need For A Rapid Boron Assay Method

The standard method to assay small concentrations of boron in tissue samples generally involves the measurement of 1-5 micrograms of boron in 20-50 milligrams of tissue [Soloway (1964)]. The method generally requires 5-6 days to complete an assay with an accuracy of ±15%, particularly in blood samples. A rapid protocol of this method can measure boron samples in about three hours, but is seriously inaccurate for tissue samples larger than 500 milligrams or if the samples contain less than 1 microgram or more than

5 micrograms [Kaczmarczyk (1971)].

It is clear that a rapid means of boron analysis in the bloodstream is warranted before another trial can safely commence. If a rapid boron assay technique were available, a quantitative knowledge of the ^{10}B clearance from the patient's bloodstream could be obtained before irradiation so that an effective therapy protocol could be established [Brownell (1977)]. Essentially, what is required is a method to measure small blood and/or tissue samples, in vitro, with the following criteria:

(1) Sensitivity: Detection of ^{10}B at levels of concentration of the order of 10 μg ^{10}B/g sample in 10g samples.

(2) Precision: Statistical standard deviation of $\pm$5% or less.

(3) Time required to complete a measurement: less than one hour.

Another application of a rapid boron assay method lies in the development of new boron compounds that are being tested in animal models. For this development, small animals are normally used so that whole organs weights are often smaller than 10 grams. With such a method, the development and testing period could be substantially reduced from the present time consuming wet chemistry methods.

1.2.4 Prompt Gamma Ray Neutron Activation for the Rapid Assay of ^{10}B

A particularly attractive approach to the rapid assay of ^{10}B is prompt gamma ray neutron activation analysis. The sample containing the boron is placed in a low energy neutron flux to activate ^{10}B via $^{10}B(n,\alpha)\ ^{7}Li$. Since about 94% of the recoiling ^{7}Li nucleii are emitted in the first excited state, a prompt gamma ray with an energy of 0.477 MeV is emitted as the ^{7}Li de-excites to its ground state. If a high energy resolution Ge(Li) detector is present to monitor this gamma ray, then the area under the ^{10}B peak will vary directly with the amount of ^{10}B present in the sample provided the ^{10}B concentration is not too high. This peak is Doppler broadened to first order ($\pm v/c$) since the ^{7}Li nucleus has an initial velocity of 0.015c. [Murray (1975)].

Since a large number of boron loaded samples were contemplated, a dedicated neutron irradiation facility to carry out this rapid boron assay was needed. Hence, a compact, non-reactor neutron activation facility was envisaged. The design criteria stated above and the necessity of having a Ge detector near the sample in significant photon and fast neutron fluxes combine, to yield a very challenging nuclear engineering problem. How this was met, will be fully described in the calculations and experimental studies in the following chapters.

1.3 Rationale for the Measurement of Skeletal Calcium, In Vivo

The human skeleton contains about 99% of the total body calcium and about 80% of the total body phosphorous. These two minerals are indispensable for the growth and homeostasis of a healthy skeleton throughout life. Consequently, the strength and weight bearing capability of the skeleton is highly dependent upon its mineral content. The skeleton is made up of two fairly distinct types of bone; cortical and trebecular. Cortical bone has a very small normal turnover of calcium and phosphorous and is generally found in the shafts of long bones such as the humerus, radius and ulna in the arm. Trebecular bone has a metabolic turnover rate eight times that of cortical bone [ICRP (1975)]. This type of bone is found in the spine, at the epiphyses of long bones, and within the small bones of the hands and feet.

Normal bone metabolism during adulthood may be simply described as a continuous remodelling of bone, particularly in trebecular areas of the skeleton, with a concomitant turnover of bone mineral. Disorders in bone metabolism generally result in significant reductions of bone mineral mass which, in turn, can lead to disabling bone fractures and bone pain. These disorders stem from a variety of causes such as hyperparathyroidism, gut malabsorption of calcium, kidney or liver failure, loss of gravity or prolonged bed rest, or the absence of minerals in the diet [Neer (1977)]. Since a variety

of complex mechanism are involved, assessment of skeletal status, *in vivo*, should be a necessary part of good clinical management of patients with disorders in their bone metabolism. This assessment can be made in terms of several parameters but the primary parameter is the mineral content of bone. Since the normal variance (with a healthy population) of bone mineral content is significant (± 15%) [Cohn (1971] , the usual approach is to measure relative changes in mineral content for each individual over a period of time or after therapy has been initiated. What is urgently needed at the present time is a method to measure ± 5% changes in the Ca content of bone. This method should be safe, rapid, inexpensive, and preferably carried out within a hospital setting for a most efficient clinical management of patients. [Neer (1977)].

1.3.1 Available Methods of Skeletal Assessment In Vivo

The methods available to the clinician include calcium balance studies, photon absorptionmetry, bone biopsies, radiologic examinations and *in vivo* neutron activation analysis [Harris (1970)] . Calcium balance studies involve the complete elemental measurement of all food eaten by the patient and all the patient's exreta. These studies are sensitive to small changes in total body calcium but are expensive to carry out. Each patient must first equilibrate on the standardized diet for about fourteen days, followed by the measurement period of six days [Neer (1977)].

There have been questions raised about the overall accuracy of these studies since small errors in the elemental assays of food and excreta are additive [Hegsted (1976)]. Standard radiologic exams may not detect bone loss until as much as 40% of the skeletal calcium is lost [Colbert (1976)]. Bone biopsies, usually taken from the pelvis, are only single point measurements, and the histologic data is not readily interpretable [Catto (1973)].

Photon absorptionmetry is a technique to measure the mass absorption coefficient of bone using a low energy photon source, such as ^{125}I. [Cameron (1963)]. This technique has definite clinical advantages such as, high precision ($\pm$ 2-4%), rapidity (1-2 hours), low dose, and commercially available facilities for in-hospital siting. The most generally scanned region of the skeleton are the shafts of the radius and ulna in the forearm. This skeletal site has the advantage of accessibility and providing reproducible data, but has the distinct disadvantage of being a cortical bone region. Furthermore, the technique does not measure Ca or P mass directly, so that the mineral content changes that may occur from one measurement to the next must be inferred from the measurement data. As a result, this technique suffers from a lack of sensitivity of measuring small (<5%) changes in mineral content of the skeleton.

1.3.2 Neutron Activation Analysis to Measure Calcium In Vivo

The standard method to measure calcium and phosphorous, in vivo is by neutron activation analysis. A comprehensive review of this technique was recently completed at M.I.T. [Zamenhof (1977)]. To measure the total body content of Ca and P, the whole body is irradiated with fast neutrons in a bilateral fashion to create a uniform thermal neutron flux distribution in the body. After neutron activation, whole body counting is performed to measure all the radioactivities produced. The two reactions and characteristic γ-rays of interest for bone mineral measurements are:

$$^{48}Ca + n(\text{thermal}) \rightarrow {}^{49}Ca^{*} \xrightarrow[(T_{1/2}=8.8m)]{\beta \text{ decay}} {}^{49}Sc^{*} + 3.10 \text{ Mev } \gamma \text{ ray}(89\%)$$

$$^{31}P + n(E_n > 3.5\text{MeV}) \rightarrow \alpha + {}^{28}A\ell^{*} \xrightarrow[(T1/2=2.31m)]{\beta \text{ decay}} {}^{28}Si + 1.78 \text{ Mev } \gamma \text{ ray}(100\%)$$

Whereas a fairly uniform spatial distribution of thermal neutron flux is achievable by bilateral irradiation or by continuous rotation of the subject about a single axis [Cohn (1970), Vartsky (1976)], there is no easy way to obtain spatial uniformity of the fast activating flux for $^{31}p(n, \alpha)^{28}A\ell^{*}$ using neutron sources with energies of 14 MeV or less. This fact, together with the knowledge that all

of the body's phosphorous does not reside in the skeleton, means that Ca is the element that is relied upon for skeletal assessment *in vivo*.

Partial body neutron activation analysis is an alternate method to total body studies as a means to reduce the whole body dose of fast neutrons. However, a greater degree of engineering skill is required to achieve reproducible results. In addition, the choice of the measurement site within the skeleton needs to be chosen carefully to allow reproducible results, low whole body dose, and measurement data that may reflect significant bone mineral changes.

1.3.3 The Choice of the Hand for In Vivo Partial Body Calcium Measurements

If the main purpose of most *in vivo* calcium assays is to monitor change, clearly the trebecular regions of the skeleton are the sites of choice. The clinician's first choice is the spine since fractures often occur there first in patients with calcium metabolism disorders. The extremities are the next areas of choice, primarily because of accessibility and reduction of whole body dose. To make a knowledgeable choice, consider the following. The percentage mass of the skeleton in these sites are: spine and sacrum equal 8.33%, hand and wrist equal 1.52% and foot equal 5.82% [Spiers (1957)]. The whole spine and sacrum contain 95.8 gms of Ca in "standard man", the foot, 67.0 gms and the hand and wrist, 17.5 gms. [Guyton (1971)]. The ratio of trebecular

bone to cortical bone mass in "reference man" [ICRP (1975)], are 20/80 for the whole body and 40/60 for the spine. No figures are currently available for the extremeties but surely this ratio should fall between 20/80 and 40/60. Figure 1.2 illiustrates the bones of the hand and wrist, as well as the epiphyses of the radius and ulna. Altogether 29 separate bones are illustrated in which some portion of each contains trebecular regions.

There is one serious drawback to using the spine (or a portion of it) for a neutron activation site. A significant portion of the body's red marrow is contained in the spine. If a fast neutron dose of 3-10 rems is necessary for analysis, then the red marrow will be absorbing a substantial dose, particularly during sequential repeated measurements. The foot clearly has more calcium than the hand and wrist but a real problem exists in easily repositioning the foot in the neutron flux and in the detection system repeatedly.

Clearly the hand presents the largest number of positive features for partial body calcium assay; viz, accessibility, low dose to whole body and red marrow, ease of repositioning and a significant portion of trebecular bone. Other workers have also used the hand as the site for calcium measurements [Mazziere (1976), Catto (1973), Spinks (1976)]. A cursory glance at Figure 1.2 will indicate that the target geometry (number and configuration of bones) is indeed complex. Careful engineering will be needed to precisely measure this site

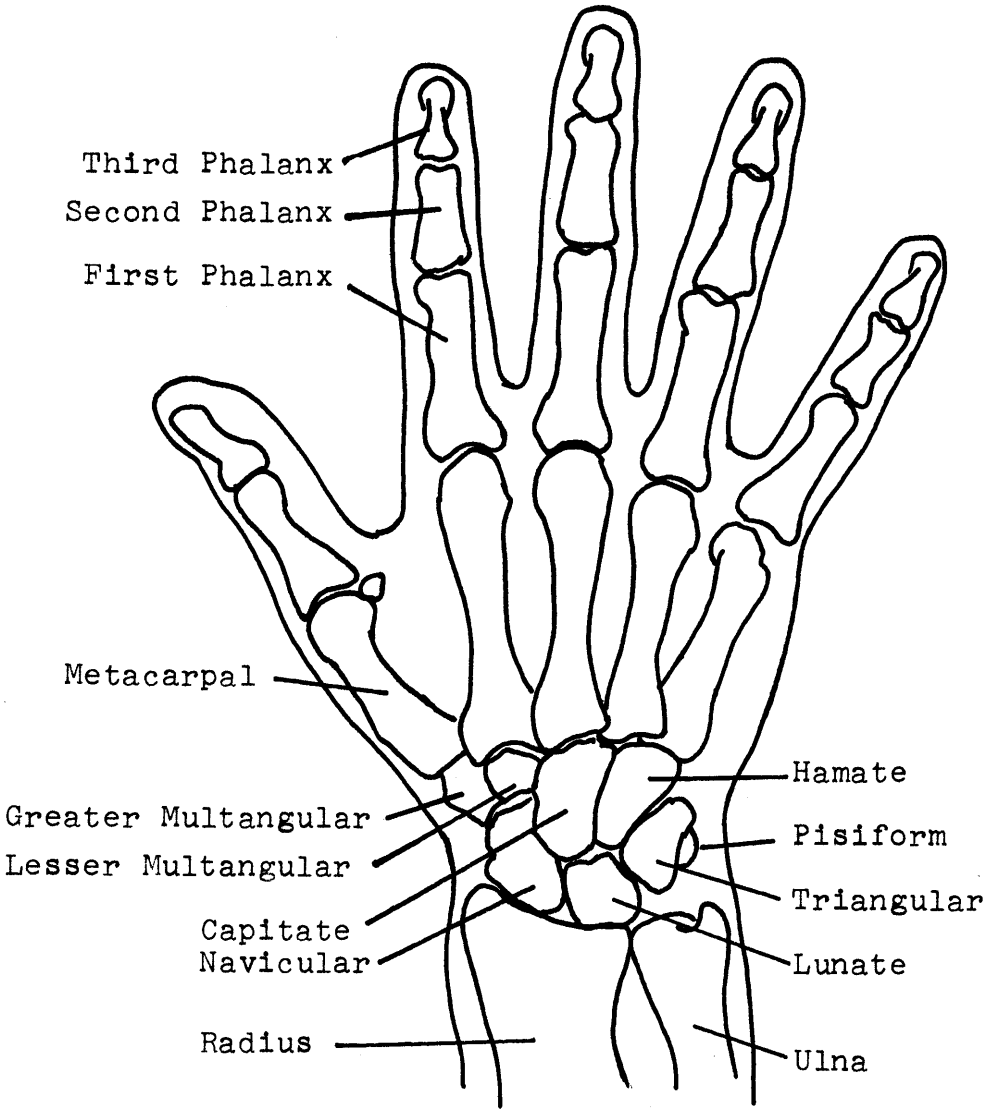

FIG. 1.2 - BONES OF THE RIGHT HAND AND WRIST

repeatedly over several years period. It is clear that to reduce repositioning problems, a large volume of uniform neutron activating flux is required and large NaI detectors are needed.

An advanced engineering design is needed to precisely measure the calcium content in the human hand and wrist while maintaining a safe dose level. A facility that can accomplish this and also be safely sited within a hospital environment can be a significant step forward in providing the means of studying metabolic bone disorders. Confidence in the described design for the hand irradiator is augmented by the good argument between theory and experiment for the boron assay facility. To begin, the transport calculations for this facility are described next.

II. CALCULATIONAL DESIGN STUDIES

2. DEVELOPMENT OF A RAPID BORON ASSAY FACILITY

2.1 Design Criteria and Objectives

In order for a boron assay facility to be useful during actual clinical trials of BNCT, as well as have applicability in the animal studies with ^{10}B compounds being developed and tested, it should meet the following specifications:

(1) SENSITIVITY sufficient to measure ^{10}B in amounts of the order of 0.1mg (corresponding to a concentration of 10μg ^{10}B/g in a 10g sample). This level of sensitivity is necessary since the levels of concentration of ^{10}B in blood samples during therapy trials are likely to range from 5-20 μg^{10}B/g sample in 10 g samples.

(2) PRECISION sufficient to make the above measurement with a statistical standard deviation of ± 5%. This should enable determinations of the ^{10}B concentrations in blood and tissue to within ± 1μg ^{10}B/g sample.

(3) RAPIDITY sufficient to make a measurement, satisfying (1) and (2), within an hour. Since the levels of ^{10}B in both blood and tissue vary as a function of time, it is highly desirable to understand the dynamic characteristics of each, leading up to and immediately prior to irradiation. This would allow optimization of the irradiation protocol as well as to ensure patient safety.

Accordingly, the boron assay facility was designed to meet the above requirements. Additional objectives include (a) a total facility sufficiently small and biologically safe to be sited within a hospital and (b) low cost and constructional simplicity.

2.2 Initial Considerations

2.2.1 Portable Neutron Source

While realizing the objective of in-hospital siting does not necessitate a radioisotopic neutron source, this type of portable source is most convenient for this application. In addition to portability, a radioisotopic neutron source has, when compared to other neutron sources, some other advantages that are important in this application. These advantages are reliability, flux levels which vary negligibly over measurement times, and very possibly lower long term cost [Crandall (1970)].

There are a number of available isotopic neutron sources [Reinig (1968), Crandall (1970)]. These include the (α, n), (γ, n), and spontaneous fission types. Of the presently available portable neutrons sources, the spontaneous fission neutron source, ^{252}Cf, surpasses all others in terms of neutron yield per unit activity, low heat generation, and cost per neutron [Renig (1968), Crandall (1970)].

The typical (α,n) sources (e.g., ^{238}Pu-Be, ^{241}Am-Be) emit from 2×10^6 to 4×10^6 n/sec-Ci, while the most widely used photoneutron source, ^{124}Sb-Be, has a neutron yield of

~1.6 x 10^6 n/sec-Ci. ^{252}Cf, however, emits 4.4 x 10^9 n/sec-Ci (Ibidem). This three orders of magnitude differential in neutron yield is one of two reasons for having selected ^{252}Cf as the neutron source for both biomedical applications discussed in this thesis.

The second reason involves the difference in the average energy of the source neutrons ($\bar{E}_N$). Because both applications addressed in this thesis involve activation of 1/v absorbers, it is desirable to use the neutron source with the "softer" neutron energy spectrum which would require less moderation and shielding. Californium-252, with an $\bar{E}_N$ = 2.3 MeV is preferable to the (α, n) sources which typically have an $\bar{E}_N$ ~ 4 MeV. Although ^{124}Sb-Be produces a monoenergetic neutron with an $\bar{E}_N$ = .025 MeV, the short lived 60-day ^{124}Sb, combined with the low neutron yield, and high gamma ray background make it undesirable. The pertinent characteristics of ^{252}Cf are the following:

> One gram of ^{252}Cf emits 2.3 x 10^{12} n/sec from a volume of less than 1 cm^3 with a heat production of <40 watts and a half life of 2.65 years. This quantity of ^{252}Cf emits 6.6 x 10^{12} prompt gamma rays per second, and 6.6 x 10^{12} equilibrium fission product gamma rays per second [Stoddard (1971)].

The neutron spectrum can be represented by the formula

$$N(E)=E^{1/2}\ EXP(-E/1.39\ MeV)$$ [Ortiz (1972)]

A tabulation of the photon spectrum can be found in [Stoddard (1971)].

2.2.2 Moderators and Dependent Parameters

Since ^{10}B is a 1/v absorber, a more efficient and effective use of the ^{252}Cf neutrons can be made if they are moderated to thermal energies. Thus the second step on developing a boron assay facility is to examine and evaluate several likely moderators for this application in terms of a number of important parameters which are moderator dependent. These parameters include:

(1) Thermal Neutron Flux Distribution Within A Finite Moderator

In moderated systems of the approximate dimensions under consideration here, approximately 90-98% (depending on spectrum changes) of the ^{10}B activations are due to thermal neutrons. Hence the thermal flux distribution gives a good indication of the ^{10}B activations produced in a sample as a function of the sample position.

(2) Fast Neutron Flux Distribution

The possibility of fast neutron detector damage is a serious problem which must be considered in designing a prompt gamma ray analysis system. Fast neutron fluences of the order of 10^9 n/cm^2 have been reported [Senftle (1970), Riggey (1975)] to be the maximum level a solid state detector can endure before a measurable degradation of the energy resolution is observed. Stelson et. al. (1971) measured a 50% decrease

in the resolution of a 50 cm^3 coaxial Ge(li) detector after an exposure of 6 x 10^8 n/cm^2 from a Pu-Be source. Similar results were obtained with ^{252}Cf neutrons. (This assumes that the damage is due to Ge recoil where the minimum neutron energy required to dislodge a Ge atom is approximately 500eV.)

Thus the detector longevity is directly related to the non-thermal (E_N>500eV) neutron flux level at the detector position.

(3) Photon Fluence Distribution

This distribution is important for two reasons. First, it is proportional to the counting rates in the detector as a function of detector position. Second, it gives a measure of the gamma ray background within the energy window about the boron peak as a function of detector location in the moderator.

(4) Neutron and Gamma Dose

The levels of the thermal neutron, fast neutron, and gamma doses at the surfaces of the moderators will determine the types and quantities of the materials which will be used as biological shielding around the moderator.

A relative evaluation of several moderators and various multiregion configurations was made using these parameters where appropriate.

2.2.3 Optimization of Source-Sample-Detector Positions

The third basic step in developing a boron assay facility is to optimize the basic configuration with special emphasis on source-sample, sample-detector, and source-detector distances. The objectives of achieving a high thermal activating flux at the sample, a low fast neutron flux at the detector, attenuation of the gamma ray background, and maximizing the gamma ray signal are not necessarily compatible. It is therefore convenient to construct a figure of merit which includes each of these concerns and which gives some measure of achieving the stated goals as a function of geometrical variations. Accordingly, in view of the design criteria outlined in Section 2.1 and the problems elucidated in Section 2.2.2, an appropriate figure of merit is: THE NUMBER OF 5% PRECISE MEASUREMENTS OF 0.1mg AMOUNTS OF ^{10}B PER DETECTOR LIFE. Here, detector life is defined to be the time required for a fast neutron exposure of 6×10^8 n/cm^2 [Stelson (1971)]. We construct this figure of merit in several steps:

1. First we require a number of counts sufficiently large for its standard deviation, σ, to be $\pm$ 5%. Thus, for a signal S and background B,

$$\frac{\sigma}{S} = \frac{[S+2B]^{1/2}}{S} = .05$$

and the number of counts we seek, denoted by S_5 is:

$$S_5 = \frac{1+2C}{(.05)^2} \quad \text{where } C = B/S \tag{2.1}$$

2. Next we determine the number of counts obtainable per detector lifetime, i.e. per 6 x 10^8 n/cm^2. This is

$$\frac{^{10}B \text{ Counts}}{\text{Detector Life}} = \frac{^{10}B \text{ Counts}}{\text{Unit } \phi_F} \times \frac{6\times10^8 \text{ n/cm}^2\text{-sec}}{\text{Detector Life}} \qquad (2.2)$$

$$= \frac{\phi_T \sigma_a \, N \, \Delta \, \varepsilon_i(.477) \times 6\times10^8 \text{n/cm}^2\text{-sec}}{\phi_F}$$

where

ϕ_T = thermal flux in n/cm^2-sec.

ϕ_F = fast (E_N>500eV) flux in n/cm^2-sec.

σ_a = absorption cross section of ^{10}B = 3837 barns.

N = number of ^{10}B atoms per sample (.1mg of ^{10}B)

Δ = solid angle subtended by detector.

$\varepsilon_i(.477)$ = intrinsic detector efficiency at .477 Mev

3. Equation (2.2) must be corrected for dead time counting losses, where the fractional counting dead time T is,

$$T = \sum_{g=31}^{42} \tau_g \phi_g \varepsilon_i(g) \times 13.85, \text{ where} \qquad (2.3)$$

g refers to the photon energy group, explained in Section 2.3.1.

τ_g = multichannel analyzer counting dead time in seconds for energy group g.

($\tau \approx$ [.01 (channel number of count) +7] x 10^{-6} seconds)

13.85 = surface area of detector face in cm^2.

4. Thus equation (2.2) corrected for dead time counting losses is simply

$$\frac{^{10}B \text{ Counts, D.T. corrected}}{\text{Detector Life}} = \text{Eq. (2.2)} \times (1-T) \qquad (2.4)$$

5. Finally, dividing equation (2.4) by (2.1) gives the desired figure of merit,

$$\frac{^{10}B \text{ Counts, D.T. corrected}}{\text{Detector Life}} \times \frac{\text{5\% Precise Measurement}}{S_5}$$

$$= \frac{\phi_T \, \Delta \varepsilon_i \times 3.93 \times 10^4 \times (1-T)}{\phi_F \, (1 + 2C)} \qquad (2.5)$$

= THE NUMBER OF 5% PRECISE MEASUREMENTS OF .1mg ^{10}B PER USEFUL DETECTOR LIFE

where, if we assume a 16 KeV window about the ^{10}B peak and a flat distribution of photons in photon group 41 (see Section 2.3.1) we can approximate C by

$$C = B/S = \frac{\phi_\gamma(g=41)}{\phi_T} \times \frac{16\text{KeV} \times 13.85\text{cm}^2}{\sigma_a N \times 400\text{KeV} \times \Delta} \tilde{=} 24\phi_\gamma(41)/\Delta\phi_T \qquad (2.6)$$

2.3 One Dimensional Moderators Studies

2.3.1 Description of Transport Code, ANISN

From sections 2.2.2 and 2.2.3 it is apparent that a number of important moderator dependent parameters must be computed and analyzed in developing and optimizing a neutron irradiation facility for the assay of boron. To effect these engineering calculations and comparative parametric evaluations of probable moderator configurations,

the one dimensional discrete ordinates code, ANISN, was used.

The ANISN code, developed at Oak Ridge National Laboratory, numerically integrates the time-independent, multigroup Boltzman transport equation in one spatial dimension by the discrete ordinates method [Engle (1967)]. Bell and Glasstone (1966) give a derivation of the transport equation. This equation is a statement of particle conservation balancing the removal rate and production rate in an infinitesimal volume of phase space, defined by three space variables (x, y, z), two angular variables (co-latitude and azimuthal angles), and one energy variable (E). The resulting equation is:

$$\underline{\Omega}\cdot\nabla\psi(\underline{r},\underline{\Omega},E) + \Sigma_T(\underline{r},E)\psi(\underline{r},\underline{\Omega},E)$$

$$= \int dE' \int d\underline{\Omega}' \; \Sigma_s(\underline{r},E'\rightarrow E,\underline{\Omega}'\rightarrow\underline{\Omega})\psi(\underline{r},\underline{\Omega}',E) + Q(\underline{r},\underline{\Omega},E) \qquad (2.7)$$

where

Σ_T = macroscopic total cross section

Σ_s = macroscopic scattering cross section

$Q(\underline{r},\underline{\Omega},E)$ = inhomogeneous source

The radiation field is described by the angular fluence, $\psi(\underline{r},\underline{\Omega},E)$. This is the average number of particles in a volume element dr^3 at $\underline{r}$ travelling within direction $d\underline{\Omega}$ around $\underline{\Omega}$, at energy E in dE.

The numerical solution of this equation yields the scalar fluence $\phi(r,E)$ as a function of position and energy. This is the quantity of interest from which all of the

parameters outlined in Sections 2.2.2 and 2.2.3 can be determined. The solution is effected by reducing the transport equation to a system of finite difference equations [Engle (1967)] for each neutron and each photon energy group. In this method, all the independent variables are introduced in a discrete form. A discrete energy variable is introduced through the multigroup approximation, and a discrete space mesh is used for the spatial coordinates. The angular distribution of the neutron flux is evaluated in nine discrete directions. The flux in other directions is computed by linear interpolation between the computed directions.

ANISN allows for general anisotropic scattering by including a specifiable number of terms of the Legendre polymonial expansion of the cross sections. The cross section set used in this study was the 42-group LASL neutron and gamma-ray coupled cross-section data set which accounts for anisotropic scattering by a third order Legendre Polynomial expansion. [Sandmeir (1974)]. The energy group structure is tabulated in Table 2.1.

The neutron and gamma ray fluences are computed by the code for each energy group, at the specified intervals along the axis of the neutron beam. ANISN allows group selection of diffusion theory, which throughout this study was used in group 30, i.e. the "thermal" group.

For small slab volumes, the ANISN code allows for trans-

NEUTRON FLUENCE-to-KERMA AND PHOTON FLUENCE-to-KERMA FACTORS

ENERGY GROUP NUMBER	ENERGY AT LOWER BOUNDARY	NEUTRON FLUENCE-to-KERMA & PHOTON FLUENCE-to-KERMA FACTORS (erg/gm/particle/cm^2)
1	15.0 MeV	6.75 (-7)
2	13.5	6.65 (-7)
3	12.0	5.93 (-7)
4	10.0	5.75 (-7)
5	7.79	5.12 (-7)
6	6.07	4.69 (-7)
7	3.68	4.25 (-7)
8	2.87	3.89 (-7)
9	2.23	3.28 (-7)
10	1.74	2.97 (-7)
11	1.35	2.66 (-7)
12	.823	2.37 (-7)
13	.500	1.79 (-7)
14	.303	1.47 (-7)
15	.184	1.08 (-7)
16	67.6 KeV	7.20 (-8)
17	24.8	3.60 (-8)
18	9.12	1.60 (-8)
19	3.35	5.60 (-9)
20	1.24	2.20 (-9)
21	.454	7.55 (-10)
22	.167	3.02 (-10)
23	61.4 eV	1.45 (-10)
24	22.6	1.11 (-10)
25	8.32	1.35 (-10)
26	3.06	2.11 (-10)
27	1.13	3.35 (-10)
28	.414	5.61 (-10)
29	.152	8.85 (-10)
30	.000193	2.94 (-9)
31	9.0 MeV	2.45 (-7)
32	8.0	2.25 (-7)
33	7.0	2.05 (-7)
34	6.0	1.85 (-7)
35	5.0	1.64 (-7)
36	4.0	1.43 (-7)
37	3.0	1.21 (-7)
38	2.0	9.63 (-8)
39	1.0	6.71 (-8)
40	0.5	3.82 (-8)
41	0.1	1.51 (-8)
42	0.01	7.42 (-9)

TABLE 2.1 -- LASL 42 ENERGY GROUP STRUCTURE AND FLUENCE-TO-KERMA CONVERSION FACTORS

verse neutron and gamma-ray leakage with a buckling-type correction. To accomplish this, the macroscopic absorption cross section Σ_a is modified for each energy interval according to the following:

$$\Sigma_a' = \Sigma_a + \frac{\Sigma_T}{3}\left(\frac{\pi}{Z\Sigma_T+1.4209}\right)^2 + \frac{\Sigma_T}{3}\left(\frac{\pi}{Y\Sigma_T+1.4209}\right)^2 \qquad (2.8)$$

Σ_a' = modified cross section

Z,Y = transverse dimensions in cm of a rectangular slab normal to the beam direction

This was used in the calculation described in Section 3.5.

As an option, ANISN can also solve the equation which is adjoint to the transport equation. A complete description of this equation can be found in [Bell and Glasstone (1966)]. This physical significance of the adjoint solution can be understood from the following. Consider a steady state system which contains an arbitrary source $Q(\underline{P},\underline{\Omega},E)$, and at some point a neutron detector based on a neutron absorption reaction. This neutron detector could, as in Section 3.5, be the hand in which calcium absorbs neutrons with a response proportional to its macroscopic cross section Σ_a. In a more convenient notation than before, the transport equation can be written as,

$$\underline{L}\psi = -Q \qquad (2.9)$$

where $\underline{L}$ can be identified by comparison with the first form of the transport equation, equation (2.7).

A corresponding adjoint operator, $\underline{L}^+$, is defined by the

requirement that

$$\int\int\int \psi^{+} \underline{L} \psi \; dr^{3} d\underline{\Omega} dE = \int\int\int \psi \underline{L}^{+} \psi^{+} \; dr^{3} d\underline{\Omega} dE \qquad (2.10)$$

The adjoint equation with the source term Σ_a is

$$\underline{L}^{+} \psi^{+} = \Sigma_a \qquad (2.11)$$

By employing the relationship which defines the adjoint operator, the transport equation, when multiplied by ψ^{+}, and the adjoint equation when multiplied by ψ, can be subtracted (one from the other) to yield a physically interpretable relation:

$$(\psi \Sigma_a) = (\psi^{+} Q) \qquad (2.12)$$

(brackets indicate an integral over all variables)

The quantity $(\Psi \Sigma_a)$ is proportional to the response of the detector to the neutron source Q. For the application in Section 3.5, the adjoint function is proportional to the absorption of neutrons by calcium in the hand as a function of source location. The physical significance of the adjoint solution, may be interpreted as the fractional increase in the Ca activations due to a single neutron at a point. The beauty of this solution is that with one calculation, the hand's Ca activation rate can be determined for various source positions and for various source spectra Q(E).

2.3.2 Modeling

For the studies pertaining to the design of the boron assay facility, all of the ANISN calculations were done

in spherical geometries. A point ^{252}Cf source was located at the center of 30 cm spherical moderators in all cases except one. In this case, the moderator (D_2O) was a 50 cm sphere. For the ANISN calculations of various parameters which were only comparatively evaluated, an arbitrary source normalization of 10^{10} neutrons-second^{-1} was used, and is noted where appropriate. For the estimation of actual measurement characteristics, i.e., count rates, dead time, fast neutron detector damage etc., a source strength of ~7×10^8 neutrons/sec. is used. This is the neutron emission rate from the ~320 micrograms of ^{252}Cf presently in use.

In the various graphs, as well as throughout this thesis, the thermal flux is the group 30 flux. The fast flux is defined as the summation of the fluxes in groups 1 through 21. This includes the lowest energy neutron which can dislodge a Ge atom from the crystal, and is used to estimate the potential fast neutron damage to the detector. The ϕ_γ is the group 41 photon flux which is proportional to the background at the energies of interest (.468 - .486 MeV).

2.3.3 Fluence-to-Dose Conversion

The calculation of the dose rates at the surface of the moderators and shielding materials is accomplished by using the KERMA factors, for Rossi tissue, tabulated in Table 2.1 [Zamenhof (1975)]. KERMA (kinetic energy released in matter is defined [ICRU (1962)] as the ratio $\Delta E/\Delta M$, where

ΔE, is the sum of the initial kinetic energies of all charged particles produced by incident neutrons or gamma rays in a mass, ΔM, of matter. The gamma ray conversion factors were computed using the GAMLEG-69 code [Renkin, (1969)] and are taken from Zamenhof (1975). This conversion includes the kinetic energy imparted to photoelectrons, Compton-scattered electrons, and electron-positron pairs.

2.3.4 Calculations and Results

2.3.4.1 H_2O, Be, D_2O, and D_2O + 0.5% H_2O

The three basic materials which were considered as moderators are light water (H_2O), heavy water (D_2O) and beryllium. D_2O with 0.5% H_2O was also considered as an approximation to reactor grade heavy water. Figure 2.1 gives the thermal neutron flux distributions generated in these moderators by a point ^{252}Cf source of 10^{10} n/sec. Simply stated, these calculations were carried out to determine which of these basic moderators is best suited for this application. Graphite was not included in this study since calculations in the literature [LASL (1971)] indicate that graphite in this geometry, would produce a lower thermal neutron flux and higher fast neutron flux than either D_2O, Be, or H_2O. The thermal neutron flux in pure D_2O is approximately 7% lower than in reactor grade D_2O over the entire thermal neutron flux distribution. The increase in the gamma flux at the surface of the reactor grade D_2O, due

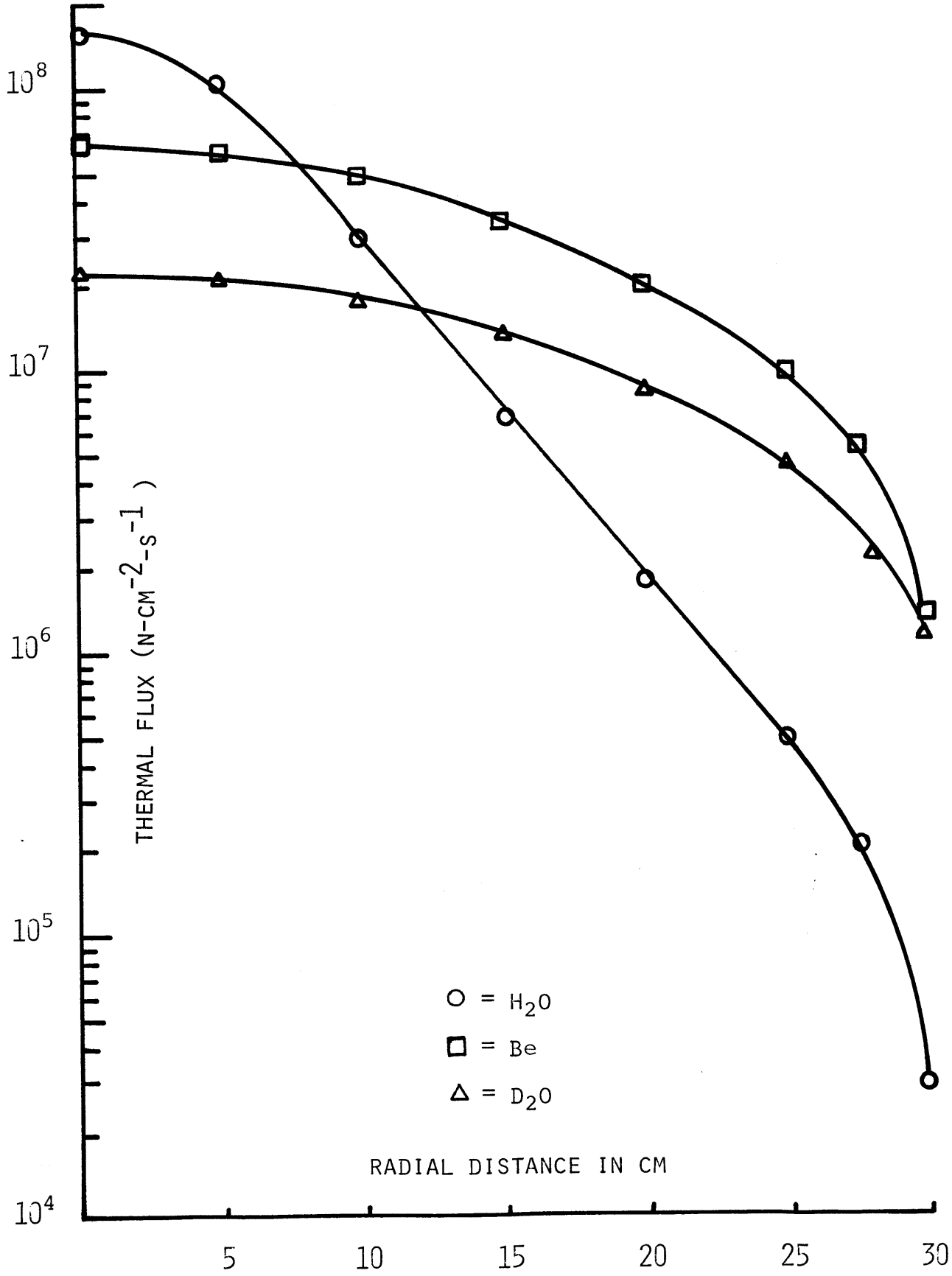

FIGURE 2.1 -- THERMAL NEUTRON FLUX DISTRIBUTION IN 30 CM SPERES OF H_2O, Be, AND D_2O.

MODERATOR	DOSE AT SURFACE OF 30 CM SPHERE IN REM/HR. FOR 10^{10} SOURCE NEUTRON/SEC			
	THERMAL N	FAST N	GAMMA	TOTAL
H_2O	0.11	2.33	5.67	8.11
Be	5.15	7.00	4.86	17.01
D_2O	4.33	6.37	4.04	14.74

TABLE 2.2 -- Thermal Neutron Flux Distribution in Various Multiregion Moderator Configurations

to the 2.22 MeV radiative capture gamma rays from the hydrogen is ~9%. Since the simulated reactor grade D_2O was a closer approximation to the D_2O which would actually be used, all of the remaining calculations were done with D_2O + 0.5% H_2O.

As a result of the calculations presented in Figure 2.1 and Table 2.2, both H_2O and Be were discarded as inferior moderators, relative to D_2O, for this application. Although the peak thermal flux realized in H_2O is seven times higher than the peak thermal flux in D_2O, H_2O is inferior in this application for several reasons. First the gamma production solely from the $^1H(n,\gamma)^2H$ reaction in this volume of H_2O is large enough to cause counting dead times of 30% with the detector at the surface of the moderator. Second, because of the small quantities of ^{10}B to be detected and the levels of the thermal flux, the detector has to be near the sample in order to monitor an adequate number of activations. Thus, with the sample in the region of high thermal flux (r = 1-10cm), the detector would have to be in a region of fast neutron flux ($\phi_F \sim 10^7$ n/cm^2-sec-320μg ^{252}Cf) which is too high to make this geometry propitious. Conversely, in regions where ϕ_F is sufficiently low, ϕ_T is lower than for D_2O. Because H_2O has a higher fast neutron removal cross section and absorption cross section than either Be or D_2O, the dose at the surface of the H_2O is lower (52%) than at the surface of Be and lower (45%) than at the surface of D_2O (Table 2.2). This relative

deficit in the shielding ability of either Be or D_2O can however be easily compensated for with additional shielding.

The higher thermal flux in Be when compared to D_2O would not appear to be sufficient to offset the high cost, and the machining and handling problems incurred with brittle and toxic forms of Be. Further, compared to D_2O, Be has no shielding advantages.

Consequently, for the boron assay facility, D_2O is the moderator of choice. We now seek to improve the important moderating parameters outlined in Section 2.2.2 by combining D_2O with small premoderating regions of H_2O, Pb, and with a region of D_2O reflector.

2.3.4.2 Multiregion D_2O + 0.5% H_2O Spheres

Although 30 cm of D_2O is sufficient to moderate ^{252}Cf neutrons to thermal flux levels adequate for this application, the photon background from primary gammas is too high to make a measurement tractable. Efforts to improve the ratio of the thermal flux to the gamma flux (i.e. signal to background) as well as the ratio of the thermal flux to fast flux (i.e. activations per unit detector damage) resulted in the calculations presented in Figures 2.2, 2.3, and 2.4. Figure 2.2 gives the thermal neutron flux distributions in four multiregion reactor grade D_2O configurations:

(1) 2 cm sphere of H_2O surrounded by 28 cm of D_2O.

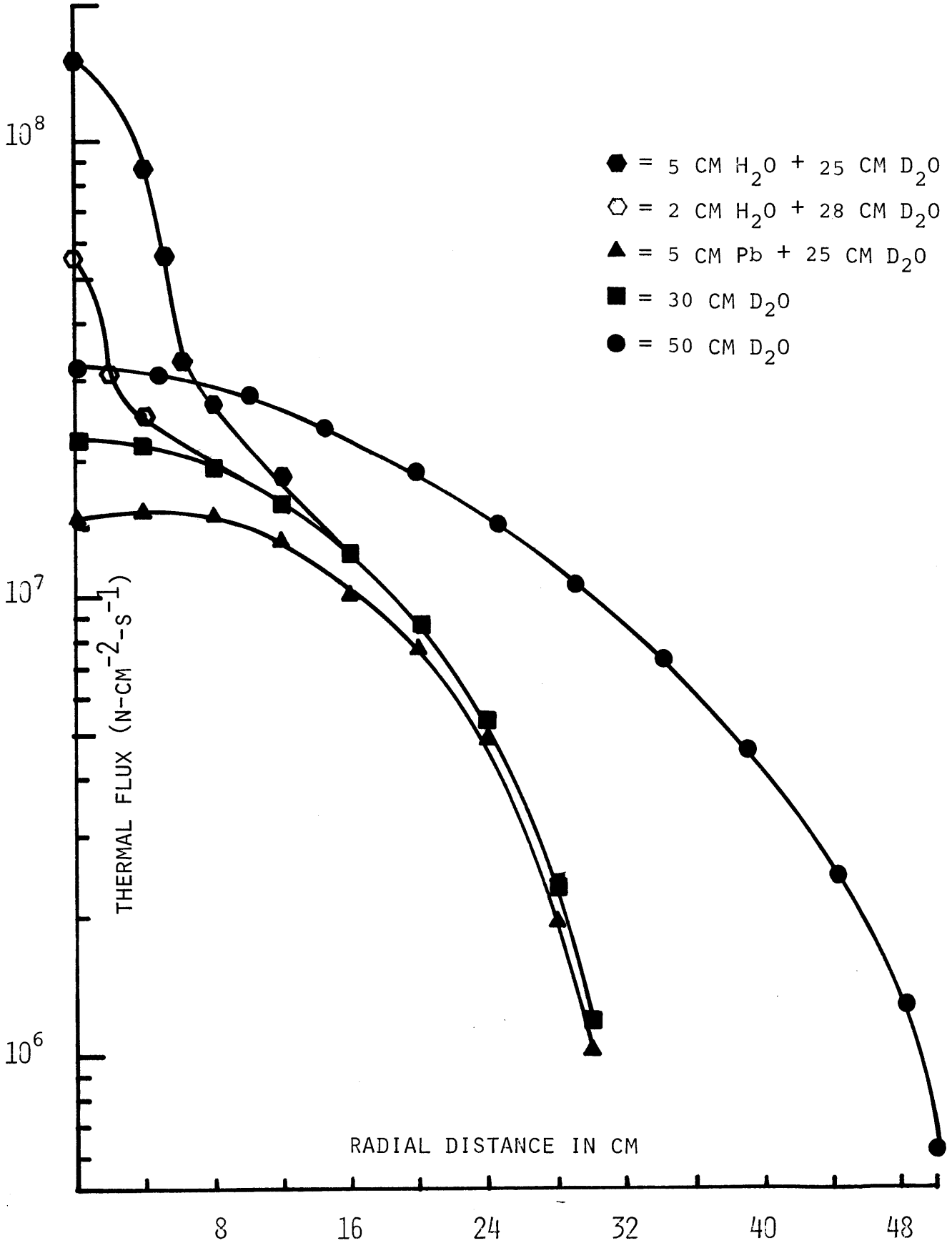

FIGURE 2.2 -- THERMAL NEUTRON FLUX DISTRIBUTIONS IN VARIOUS MULTI-REGION MODERATOR CONFIGURATIONS

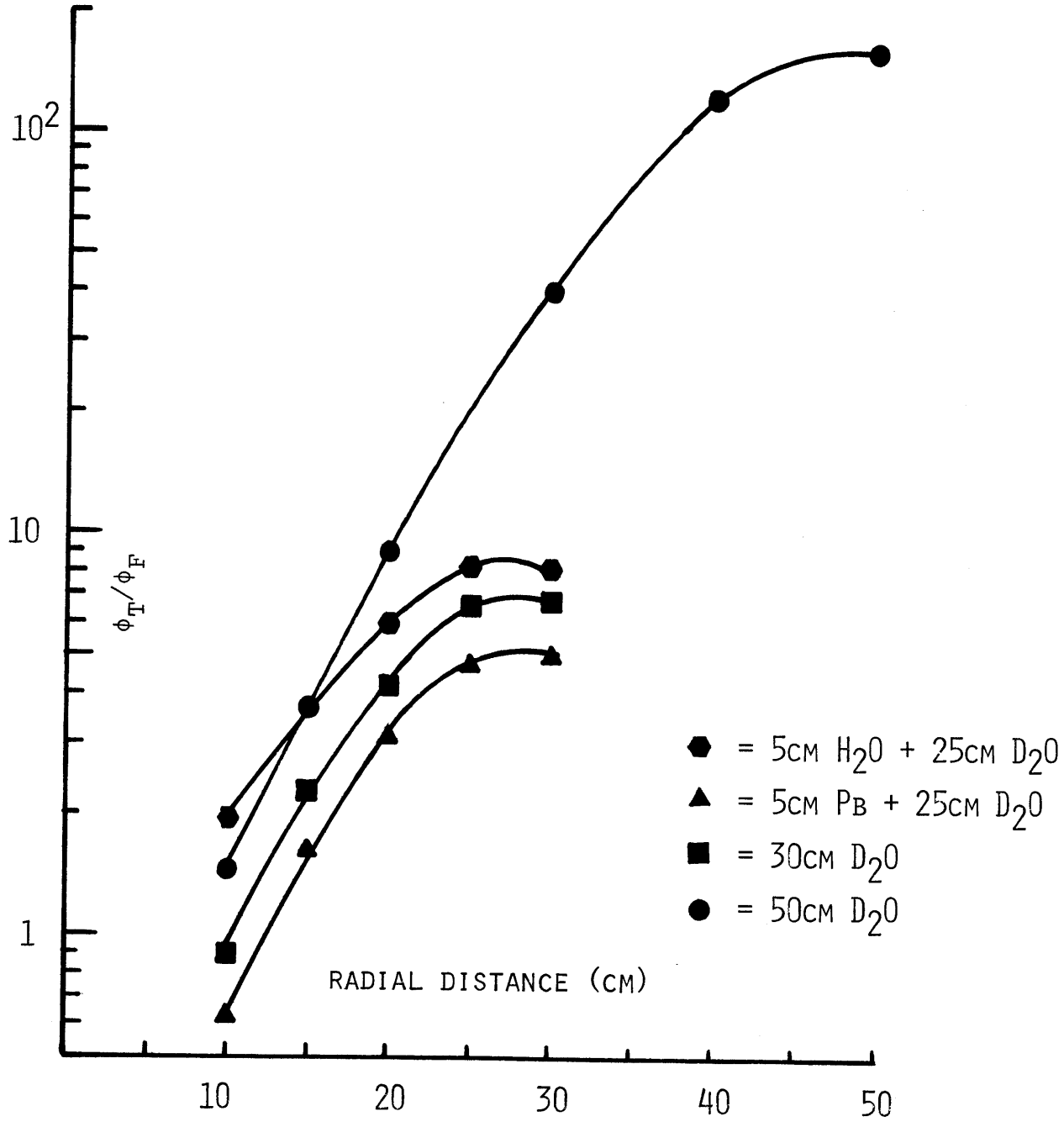

FIGURE 2.3 -- RATIO OF THE THERMAL NEUTRON FLUX TO THE FAST NEUTRON FLUX AS A FUNCTION OF DISTANCE IN VARIOUS MULTIREGION MODERATOR CONFIGURATIONS

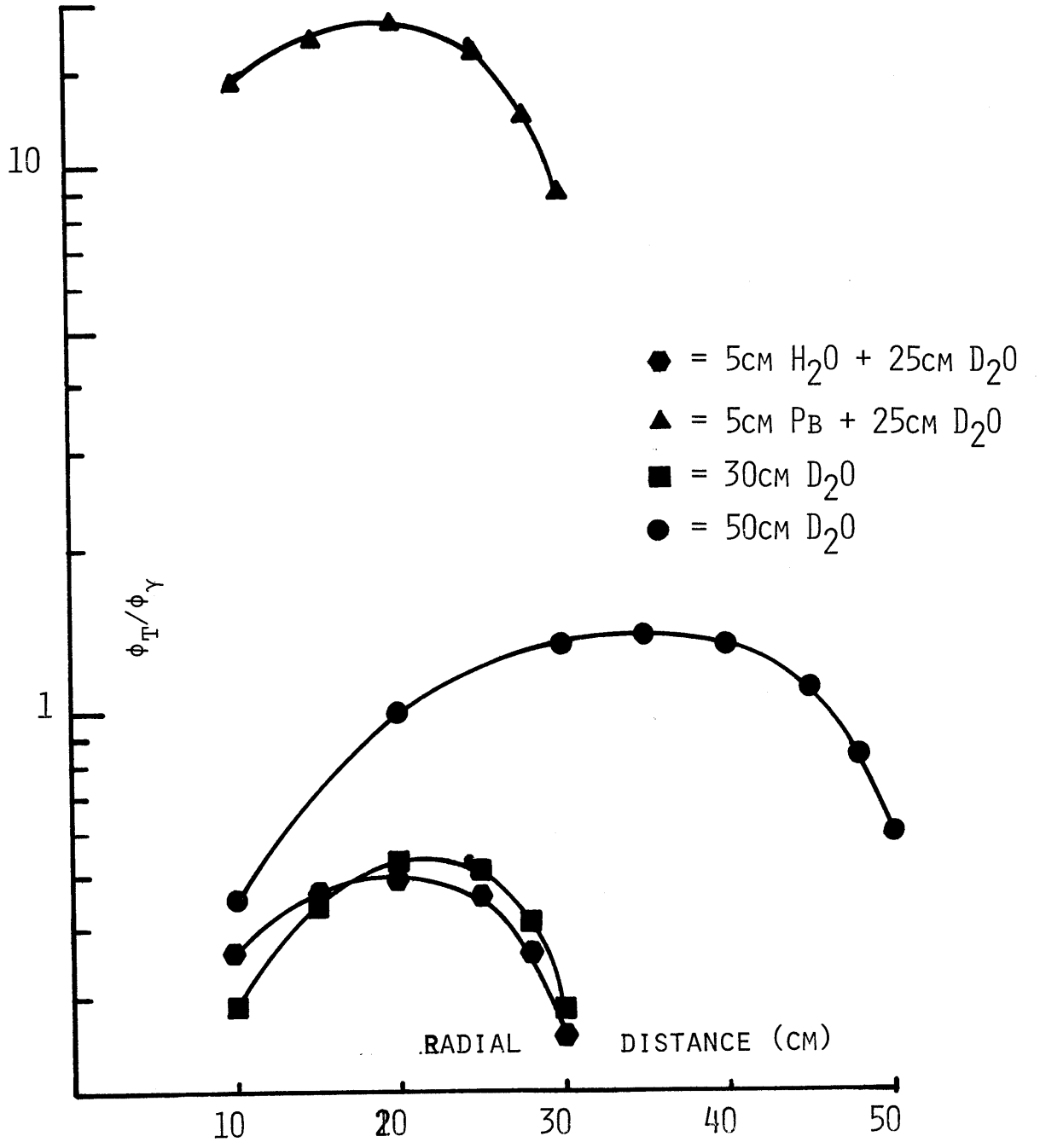

FIGURE 2.4 -- RATIO OF THE THERMAL NEUTRON FLUX TO THE FAST NEUTRON FLUX AS A FUNCTION OF DISTANCE IN VARIOUS MULTIREGION MODERATOR CONFIGURATIONS

Adding the 2 cm of premoderator around the source effected an increase in thermal neutron flux closely follows that observed in D_2O only. The fast neutron flux was decreased by ~6%.

(2) 5 cm sphere of H_2O surrounded by 25 cm of D_2O

The effect observed with 2 cm of H_2O premoderator was studied further by extending the H_2O region to 5 cm. The same general behavior was observed as before, but with the thermal flux now being increased by a factor of ~7 at the origin. Note that the thermal flux; (1) in the first 12 cm of this configuration follows that observed in 30 cm of H_2O, and (2) in the last 18 cm follows that observed in 30 cm of D_2O. Since after 12 cm (in Figure 2.1) ϕ_T in D_2O is larger than in H_2O, there appears to be little value in increasing the region of H_2O in the present configuration.

Figure 2.3 gives the radial distribution of the ratio of the thermal flux to the fast flux ($\phi_F = \sum_{g=1}^{21} \phi_g$) for the various moderator configurations. Note that by replacing the first 5 cm of D_2O with H_2O the ϕ_T/ϕ_F ratio increases by approximately 14%. (Replacing the 5 cm of Pb with H_2O in the next configuration increases this ratio by 60%.) The ϕ_T/ϕ_γ ratio [ϕ_γ(E=.1-.5MeV)], however, drops by approximately 10% because of the hydrogen capture gammas. In comparison

with D_2O only, this combination offers an overall improvement theoretically in the number of measurements possible per detector life if the background photons can be shielded to satisfactory levels. This shielding is necessary since the absolute ϕ_γ levels are high enough to cause the multichannel analyzer to be saturated with counts from primary gammas. If coupled with either source or detector shadow shielding, the advantages in fast flux reduction which this configuration offers could be exploited. An investigation of such an arrangement, which was omitted in this study, is therefore warranted for future study.

(3) 5 cm sphere of Pb surrounded by 25 cm of D_2O

In this configuration, the first 5 cm of D_2O is replaced by Pb which completely encapsulates the source. The object of this source shielding is a reduction of the gamma background count rates to a tolerable level. Since the dead time at the surface of the 30 cm of the D_2O sphere would be approximately 300%, the required thickness of Pb shielding is 7-8 half value thickness. Thus, for the model energy (~900 KeV) of the ^{252}Cf prompt gamma spectrum [Hyde (1964)], a two-orders of magnitude attenuation requires approximately 5 cm of Pb.

A reduction in the peak thermal flux of approximately 30% is observed by replacing the first five cm

of D_2O with Pb. Thereafter, the difference systematically decreases to approximately 10% at 24 cm and remains at this relative level throughout the remainder of the moderator. Despite this loss in the thermal flux and a corresponding decrease of 30% in the ϕ_T/ϕ_F ratio (Figure 2.3), this arrangement is superior because (1) of the ~96% net reduction in the total gammas, (2) a factor of 5 increase in ϕ_T/ϕ_γ (Figure 2.4), and (3) both the thermal flux level and the ϕ_T/ϕ_F (Figure 2.4) are still adequate for a satisfactory measurement.

(4) 50 cm of D_2O

Calculation of the parameters in Figures (2.2-2.4) for this configuration was at first primarily an academic exercise since the arrangement in part (3) seemed promising, and the additional volume of D_2O would increase projected cost by approximately 400-500% and the total facility size roughly by a factor of 4. In light of the experience gained with the constructed facility, however, this calculation has important application in the redesign discussed in Section 7.3.

2.3.4.3 Comparison with Other Data

Thermal neutron flux distributions in 30 cm of H_2O, Be, D_2O, and C were computed with discrete ordinates code DTF-IV and reported by LASL(1971). A comparison of these calculations with the corresponding ones in Figure 2.1 reveals

the following:

(1) H_2O

The ANISN and DTF-IV results agree to within 5% from 0 cm to ~23 cm. Near the boundary, 23-30 cm, the DTF-IV results are as much a factor of 2 higher.

(2) Be

The ANISN and DTF-IV results agree at the endpoints (i.e., 0 cm and 30 cm) but systematically differ in between. The maximum difference occurs at ~20% higher.

(3) D_2O

Again we observe a systematic difference. The DTF-IV results are ~30% higher at the origin but gradually taper to the same value as was computed by ANISN at 30 cm.

These DTF-IV calculations differ from the ANISN calculations primarily in that (1) the DTF-IV code solves the transport equation to determine the thermal flux, whereas ANISN employs diffusion theory and (2) the DTF-IV calculations were done with a 25 group cross section set.

An experimental measurement of the thermal neutron flux distribution, in a cylindrical tank of H_2O, has been made and reported by Magnuson (1968). The radius of the tank was 48 cm. These measurements agreed with the ANISN calculations to within ~5-15% throughout the distribution.

Finally, a student in the Nuclear Engineering Department of M.I.T. has reproduced the ANISN thermal flux distributions in Figure 2.1 to within 10%, by using a combination of Fermi Age and diffusion theory. He uses Fermi Age theory to compute the slowing down density, which then serves as the source term in the diffusion equation. The resulting equation is solved by the method of eigenfunctions to yield $\phi(r)$. A complete report on this work should be forthcoming soon. [M. Gottlieb (1977)].

2.3.5 Investigation of Biological Shielding Materials

Two basic materials were considered for "biological" shielding to be placed around the moderator. This shielding is required, to reduce the unshielded dose levels to tolerable levels of 10-30 mrem/hr. at the surface of the shielding. Since the dose rate at the surface of the 5cm Pb + 25 cm D_2O configuration is predominantly due to the fast neutrons (~60%) and thermal neutrons (~40%) polyethylene and glycerin were considered as shields because of their fast neutron removal cross sections. For the purpose of abatement of the thermal neutron dose rate, lithium ($^6Li, \sigma_a$ = 960b) loading in each of these materials was considered. The findings were the following:

(1) A thickness of 15-20 cm of hydrogenous shielding is required to reduce the surface dose rate to 10-30 mrem/hr. An equivalent amount of glycerin is about equally as effective. Stoddard (1971)

however, reports that for shielding thicknesses of 30 cm or more, glycerin becomes increasingly superior to H_2O. For thicknesses of 140cm, the neutron dose rate in glycerine is ~ two orders of magnitude lower than in water, and ~ one order of magnitude lower than in polyethylene. We were able to reproduce (with ANISN) Stoddard's results for glycerine but produced results for water that were equal at the origin but were one order of magnitude higher at 140 cm. Since Stoddard's calculations were also done with ANISN and for the same geometry, there is no apparent reason for this large discrepancy.

(2) Solubility experiments were conducted with lithium acetate in both water and glycerin. Despite its reported high degree of soluability [CRC Handbook of Chemistry and Physics (1971)], a maximum loading of ~4 wt.% Li and ~5 wt.% Li was obtained for water and glycerin respectively.

2.4 Preliminary Design of the Rapid Boron Assay Facility

2.4.1 Choice of Moderator

The information presented in Table 2.1 and Figures 2.1-2.4 was the basis for an initial design. The first step, was the selection of an appropriate moderator configuration. The characteristics of the considered

configurations have already been discussed in Section 2.3.4.2. It was shown that while all of these configurations generate sufficiently high thermal neutron fluxes, the unshielded background photon flux is too high to make measurements trackable. Since this background photon intensity was the overriding concern, the 5cm Pb + 25 cm D_2O was selected for this application. Further, the ϕ_T/ϕ_F ratio, while smallest for this configuration, was judged acceptable. It should be noted that this is not necessarily the optimal configuration. A better arrangement, for example, might be 5cm of H_2O surrounded by a few centimeters of Pb followed by D_2O. This however, was not investigated but is recommended for future study.

2.4.2 Geometry Optimization

By employing the figure of merit defined in Section 2.2.3, and the calculations in Figures 2.2-2.4, the optimal sample and detector positions within the reactor grade D_2O can be determined. This figure of merit is plotted in Figure 2.5 as a function of the appropriate sample or detector position for three limiting sample-detector geometries. These are:

(1) The sample is positioned at a point where ϕ_T is a maximum and farthest away from the source (r = 8cm). The detector position is varied radially within the moderator.

FIG. 2.5 -- NUMBER OF 5% PRECISE MEASUREMENTS PER GE(LI) DETECTOR LIFETIME FOR VARIOUS SAMPLE DETECTOR POSITIONS IN A 5CM PB + 25CM D_2O MODERATOR CONFIGURATION

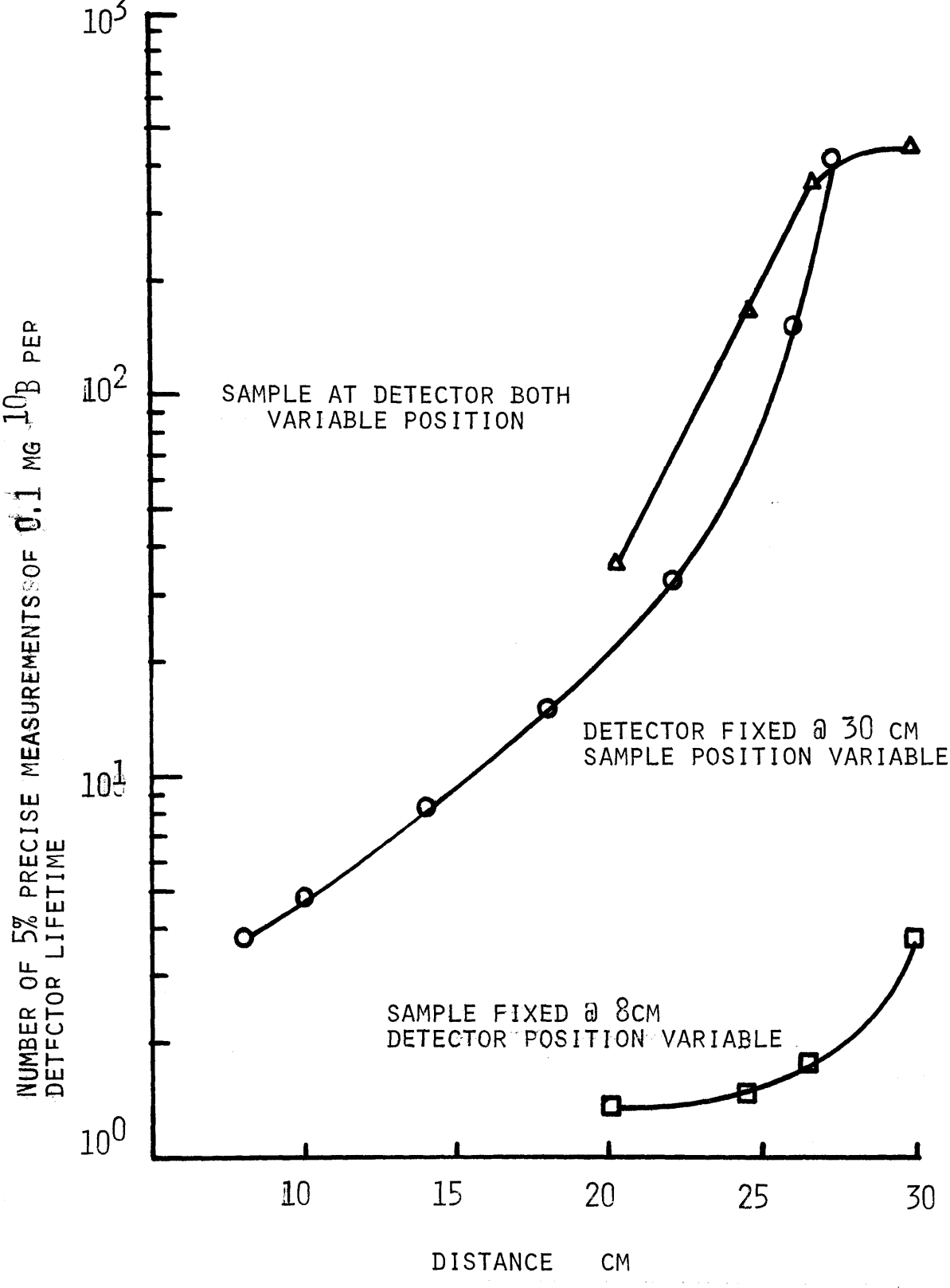

(2) The detector is positioned at a point where ϕ_F is a minimum (r = 30cm). The sample position is varied radially within the moderator.

(3) The sample is fixed at the detector face and the radial position of both, as a unit, is varied within the moderator. The center of the sample is assumed to be 2.5 cm from the detector. The sample container is assumed to be 7 ml cylindrical vial, 5cm in length and a 0.8 cm radius.

(4) The independent movement of both the detector and sample is not included since this geometry produces figure of merit values less than those obtained with geometry (3).

The curves of Figure 2.5 show that the best sample and detector locations are at the boundary for the detector with the sample approximately at the detector face. Note further that the worst arrangement by far is with the sample fixed where ϕ_T is a maximum.

2.4.3 Choice of Biological Shielding Material

At this point in the development of the boron assay facility, both of the shielding material discussed in Section 2.3.5 were judged as being satisfactory and roughly equally effective. Consequently both were considered further in the subsequent three-dimensional studies.

2.4.4 Conclusions

The findings of the ANISN one dimensional calculations may be summarized as follows:

(1) A suitable moderator configuration is 5cm of Pb photon shielding around the source with an addtional 25cm of D_2O around the Pb. As seen below, this provides thermal neutron flux levels and photon background flux levels which are adequate for assaying boron while meeting the design criteria.

(2) The optimal sample and detector locations are at the boundary for the detector with the sample approximately at the detector face. At these locations, the thermal flux at the sample is ~1.8 x 10^5 n/cm^2-sec-320 μg ^{252}Cf, and the fast neutron flux at the detector is ~1.5 x 10^4 n/cm^2 -sec-320 μg ^{252}Cf. These parameters should allow ~400 required boron measurements before redrifting is needed.

(3) 1 5 - 2 0 centimeters of either lithium-loaded polyethylene or lithium-loaded glycerine will adequately serve as biological shielding around the 30 cm (radius) of moderator.

We next consider a more realistic set of three-dimensional calculational experiments to further optimize the facility prior to construction.

2.5 Three Dimensional Monte Carlo Design Studies

Because precise calculations of the required performance parameters of a complicated three-dimensional design are beyond the scope of ANISN, a generalized geometry Monte Carlo neutral particle transport code was employed to design the three dimensional configuration to perform as required. In the absence of actual physical experimentation, this code enables the execution of a series of computational experiments with three-dimensional models in order to systematically develop, evaluate, and optimize a complete rapid boron assay facility. Note that the effect of the actual geometry on the radiation field in such a system is apt to be significant since the particle leakage from the basic design of the boron assay facility under consideration may be considerable (since the 30cm radius of moderator is ~1/4 of a diffusion length).

2.5.1 Description of Transport Code, ANDY

The Monte Carlo calculations included in this study were carried out using the ANDY code. Developed at the Los Alamos Scientific Laboratory, this code numerically integrates the transport equation by probabilistically simulating the nuclear interaction processes which govern the propagation of neutrons and photons in matter [Deutsch (1975)]. From the outcome of repeated, independent random trials for the simulation of many particles' trajectories (throughout their "life histories"), the fluxes and currents can be statistically inferred.

The particle interaction processes are simulated according to two basic physical principles. The first is that particles (neutrons, photons) interact with matter only by discrete collisional events. The second is that between collisions, particles undergo free streaming spatial translations. These translations are assumed to be linear, and the distance between collisions is assumed to be a random variable which is exponentially distributed. During the simulation process, each mathematical analogue is represented by a set of coordinates which generally include position, angle, energy and time. All of the possible collisional events, i.e., absorption, elastic scattering, inelastic scattering, (n, 2n) and (n, γ) interactions, Compton photon scattering and annihilation reradiation, are believed to be probabilistic in nature. Consequently, all of the pertinent information can be extracted from relevant probability distributions which are contained in the nuclear cross section data.

ANDY features a general geometry capability with a flexible three-element topology [Deutsch (1975)]. Multigroup energy dependence with generalized scattering treatment enables the calculation of neutron and photon transport simultaneously. The ANDY code uses the 42 group LASL neutron photon coupled cross-section data file. These neutron-photon coupled cross section sets allow calculation of neutron-induced gamma rays. The scalar fluence in a region of

interest may be estimated by either of two techniques. The first estimation procedure involves tallying the total number of collisions in a region and dividing by the product of the region's volume and macroscopic total cross-section (i.e., estimating the fluence from the collision density). The second procedure involves tallying the total track length of all trajectories through a region, and dividing by the region's volume (i.e., estimating the fluence from the alternate definition of neutron fluence as the total track length traveled by the number of neutrons in a volume).

In all of the ANDY calculations which follow, the track length flux estimator was used for particles in all energy groups except group 30. For particles in this group, the collision flux estimator was used except in evacuated regions, in which the track length estimator was used. A conversion of fluence to dose was achieved by employing the fluence-to-dose conversion factor that were used with the ANISN studies (Section 2.3.3).

For most of the geometrical configurations involved in this study, generally 2 - 8 x 10^4 neutron histories were required to obtain a suitably low variance of the means (10%-20%) of the various computed parameters. These calculations ranged from \$150-\$450 in cost when run at the lowest possible priority (at M.I.T.'s Information Processing Center).

2.5.2 Monte Carlo Model I&II

2.5.2.1 Specific Objectives

The first Monte Carlo calculations were carried out to investigate the following:

(1) The feasibility of a smaller moderator volume and complete assay system than was considered in the ANISN studies.

(2) The optimal sample-detector location in a realistic complete geometry which includes a detector portal within the moderator.

(3) The dose rates at the surfaces of the facility.

2.5.2.2 Geometry

Both the first and second models consisted basically of an aluminium cylinder of D_2O encased by a concentric cylindrical annulus of polyethylene loaded with 10% wt lithium. The volume of D_2O in the first model was approximately 31 liters contained in a cylinder of radius 15 cm, height 50 cm and with a wall thickness of .16 cm. The polyethylene-Li annulus was 15 cm thick. Thus the outer cylindrical dimensions were 60 cm outside diameter, and 80 cm in length.

The calculational model is shown in Figure 2.6, (and has 26 surfaces, 54 surface segments and 24 regions). Region 1 is lithium loaded polyethylene, region 2 is aluminum, all other regions are D_2O except regions 6-9 which were made voids

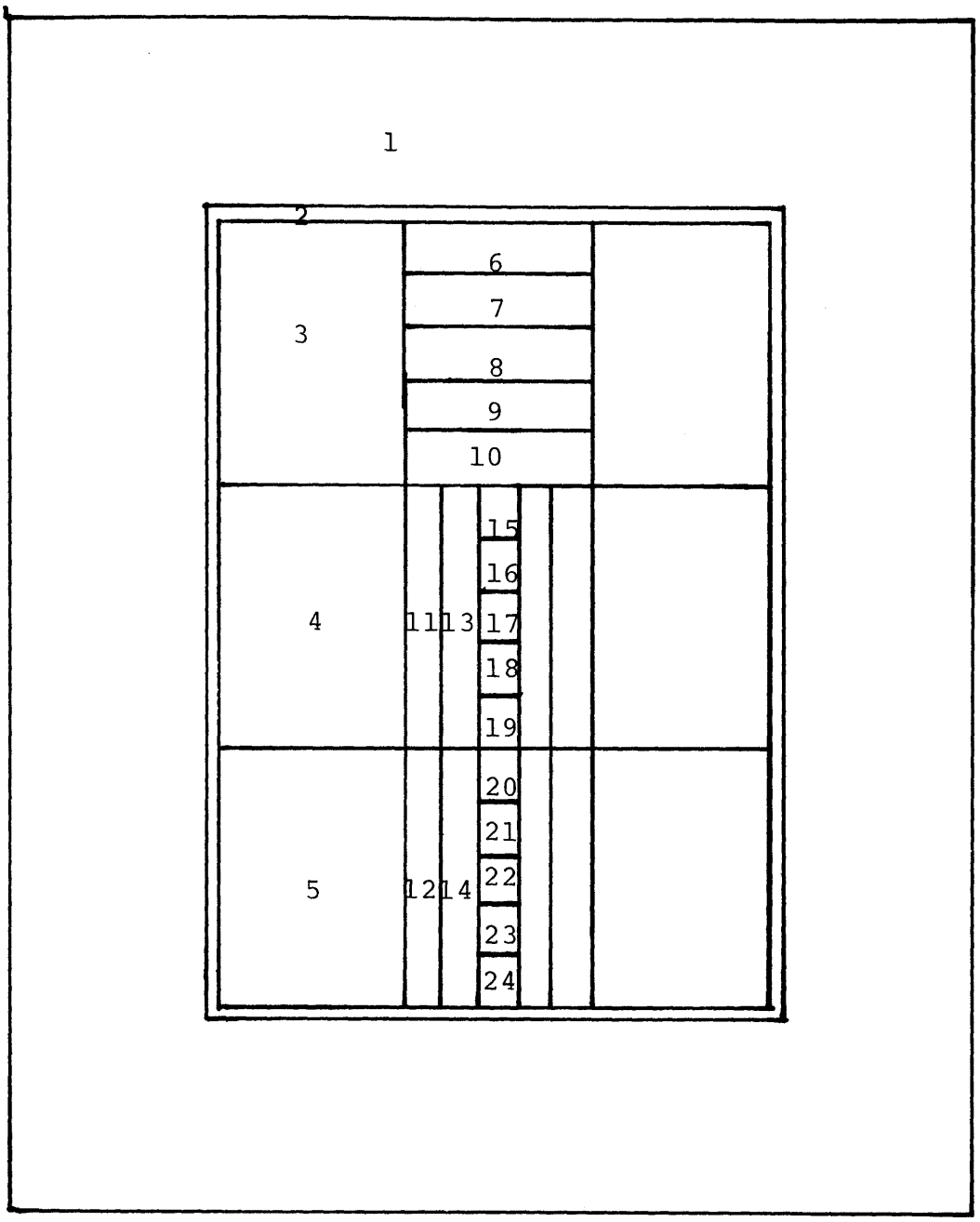

FIGURE 2.6 -- MONTE CARLO MODEL I & II OF THE BORON ASSAY FACILITY.

in order to investigate probable detector location. Regions 6-10 and 15-24 are "edit" regions in which volume averaged fluxes are computed. Regions 3-5 and 11-14 serve to divide the entire tank region into small regions. Each of these regions is bounded by a smaller number of surface segments than the total tank region would be bounded by if it were not so divided. Thus, these regions were not included for flux calculations but rather to prevent the number of surface segments bounding a region from being undesirably high (greater than ~12), so as to minimize the calculation time and cost.

The second model differs from the first in two respects only. First, it is larger with the moderator volume being increased to approximately 115 liters. The dimensions of the aluminum tank are 50 cm diameter and 60 cm in length. The outer polyethylene-Li annulus is 15 cm thick on the side and 15 cm thick, top and bottom. Secondly, regions 8-10 are now D_2O. Regions 6-7 remain voids.

2.5.2.3 Results of Calculations

The thermal fluxes in regions 10-24 for the Monte Carlo model I and in regions 8-24 for the Monte Carlo model II are given in Figure 2.7. These calculations have been normalized to 8.9×10^8 source neutrons/sec., the neutron emission rate from 400 μg of ^{252}Cf. The dose rates at the outer surfaces are given in Table 2.3. Calculations with primary gammas were not done since

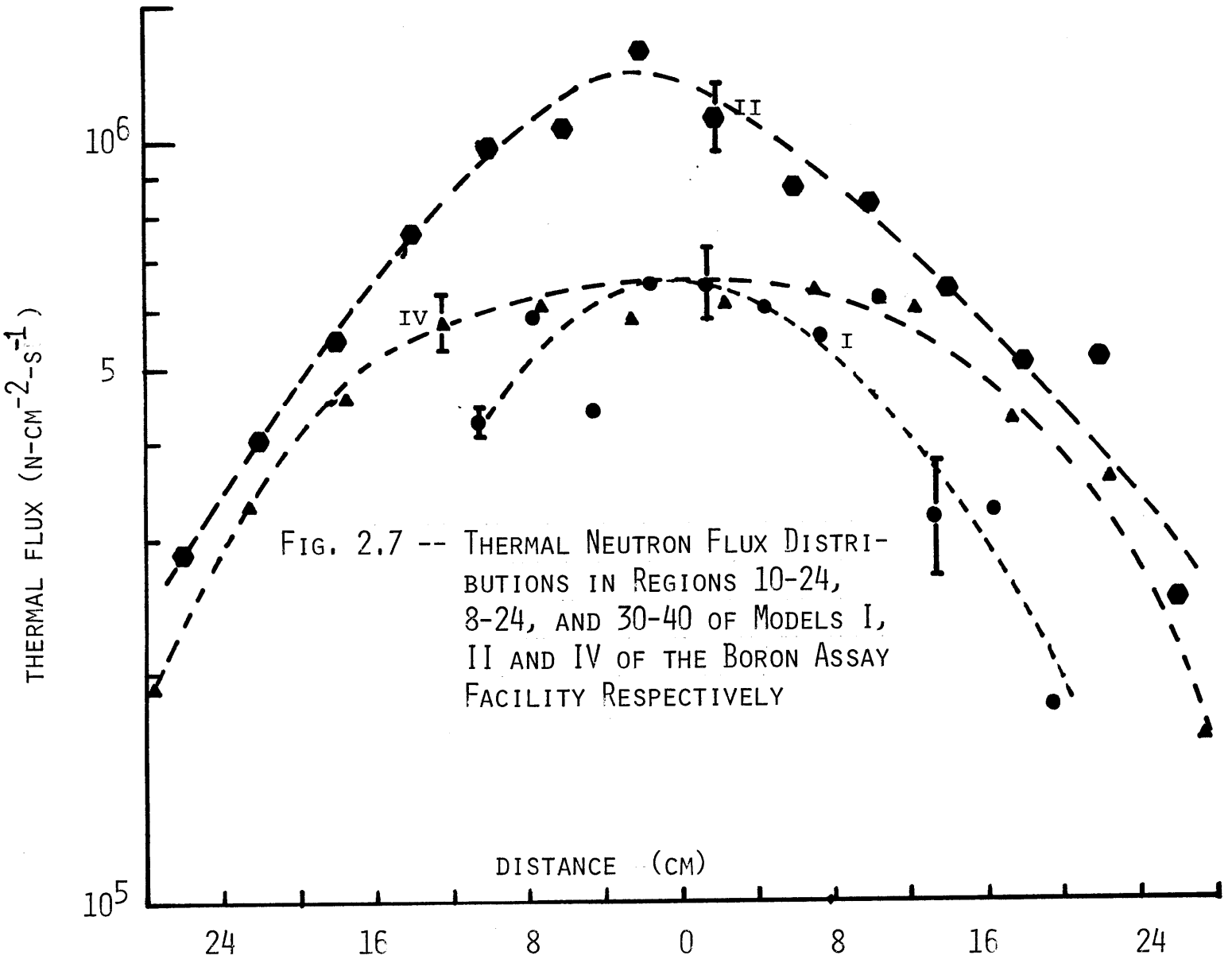

FIG. 2.7 -- THERMAL NEUTRON FLUX DISTRIBUTIONS IN REGIONS 10-24, 8-24, AND 30-40 OF MODELS I, II AND IV OF THE BORON ASSAY FACILITY RESPECTIVELY

FIGURE 2.7

the calculations with source neutrons and induced gammas alone indicated that these designs were unsatisfactory. Nonetheless, several useful observations were made with each calculation:

(1) The absolute thermal flux ($\phi_T \sim 10^4$ n-cm^{-2} s^{-1}) in the first model (31 liters of D_2O) are adequate for this application, but the fast flux levels make the design impractical. The calculated fast flux levels make the design impractical. The calculated fast flux ($\phi_F = \sum_{g=1}^{21} \phi_g$) ranges from 4.46×10^5 n/cm^{2}sec in region #10 to 1.19×10^5n/cm^2-sec in region #6. Again assuming 6×10^8 n/cm^2 as the maximum fast neutron fluence which the detector can tolerate, we compute ~1.4 hours as the total cumulative time the detector can spend in region #6. The induced gamma flux (ϕ_g=41) ranges from 3.77×10^3 γ/cm^2-sec in region #10 to 2.44×10^3 γ/cm^2-sec in region #6, corresponding to counting dead times due to induced gammas only) of approximately 9% to 5% respectively. This demonstrates the degree to which the lithium loaded polyethylene is effective in suppressing gamma production. The lack of a calculation of the primary background gammas prevents an exact calculation of our figure of merit at this point, however,

estimating from the ANISN calculations that $\phi_g = 41 \approx 8 \times 10^5$ n-cm^{-2}-sec with 5cm of bismuth around the sources, we get in region #6 an approximate figure of merit which is less than 1, but the highest for regions #10-#6. This proved to be the best sample detector location in this geometry. The fast neutron dose rates (Table 2.3) indicate this size system to be impractical. Attaining a ressonable level of safety require that the fast neutron dose levels at the side of the system be reduced by an order of magnitude. To achieve this and the reduction of the fast neutron dose rates at the detector site, the dimensions of the first assay facility model were increased to those of the second.

(2) Increasing the D_2O volume from ~31 liters to ~115 liters increased the thermal flux level by a factor of 2 (Figure 2.7). The fast flux level at comparative points was decreased roughly by a factor of ~2 however, the fast neutron flux in region #6 of the second model was one order of magnitude lower than in the smaller model. This means that the detector can spend a maximum of ~14 hours (before receiving a fast fluence of 6×10^8 n-cm^{-2}) in region #6, the least damaging region in the model. The induced gamma flux in region #6 is

$1.740^{3}\gamma$-cm^{-2}-s^{-1}. Again, estimating the $\phi_{\gamma}(E_{\gamma}=.1\text{-}.5)$ flux in region #6, the figure of merit is estimated to be approximately one. Of the several detector regions investigated, region #6 has the largest figure of merit in both models, which concurs with the ANISN results that indicated the optimal sample and detector locations to be the points farthest away from the source.

The dose rates at the surface of this second facility are adequately low (<30 mrem -hr^{-1}) as itemized in Table 2.3. These neutron does equivalent rates were computed using quality factors of 10 for the neutrons and one for the gamma rays.

2.5.2.4 Conclusions

Several conclusions can be drawn from the above considerations:

(1) The 31 liters of D_2O in the configuration consider in model I is inadequate for this application for two reasons. First, the fast neutron flux the detector would be exposed to is unsatisfactorily high (~1.2 x 10^5 n-cm^{-2}-sec). Second, the outer surface fast neutron dose rates are likewise undesirably high (~160 mrem -hr^{-1}).

(2) Increasing the D_2O volume from 31 liters to 115 liters increases the thermal flux level by a factor of two. The outer surface dose rates of the second

facility are ~1/5 the dose rates at the outer surface of the first. The fast flux level at the detector site is ~1.2 x 10^4 n-cm^{-2}-sec in the second facility. This is still undesirably high, since it will permit only 14 hours of counting time.

(3) The best location for the sample and detector, as indicated by the ANISN calculations, is the position in the moderator farthest away from the source.

(4) Neither of the two models is a satisfactory design for assaying boron since the maximum figure of merit in both is about one or less.

2.5.3 Monte Carlo Model III

2.5.3.1 Specific Objectives

The objective of this calculation was to determine the effectiveness of the following changes (in the previous model) in improving the figure of merit for the assay of boron as well as investigate glycerin as a biological shielding material. These changes and the points to be investigated are the following:

(1) The position of the detector portal has been moved to a far corner of the D_2O tank, rotated 90° and recessed 5 cm into the shielding (Figures 2.8 and 2.9). To minimize the roll-off of the thermal neutron flux at the new detector position, a cylindrical "cup" of D_2O was extended from the

tank wall to the detector face. In this position, the detector is obviously farthest away from the source in accordance with the conclusions in Section 2.5.2.4. Furthermore, the solid angle subtended by the detector at the source is reduced, and ~7 cm of glycerin now shields the detector from fast neutron. This new detector location should improve the figure of merit by increasing the ϕ_T/ϕ_γ and ϕ_T/ϕ_F ratios as well as reducing the counting dead time.

(2) To reduce the total gamma background and the corresponding counting dead time further, two lead shields were introduced in this third Monte Carlo model of the boron assay facility. First, the detector has been shielded by a 5 cm thick Pb annulus around the detector portal. Second, a 5 cm thick Pb "shelf" (region 24 in Figure 2.8) was included to provide further detector "shadow" shielding.

(3) The lithium loaded polyethylene has been replaced by glycerin ($C_2H_2O_2$). The glycerin has no lithium loading, since it has been assumed that enough lithium can be dissolved in the glycerine to suppress the radiative capture gammas production from hydrogen. This change was made to investigate the reported [Stoddard (1971)] superiority of glycerin in comparison to polyethylene as a shielding material.

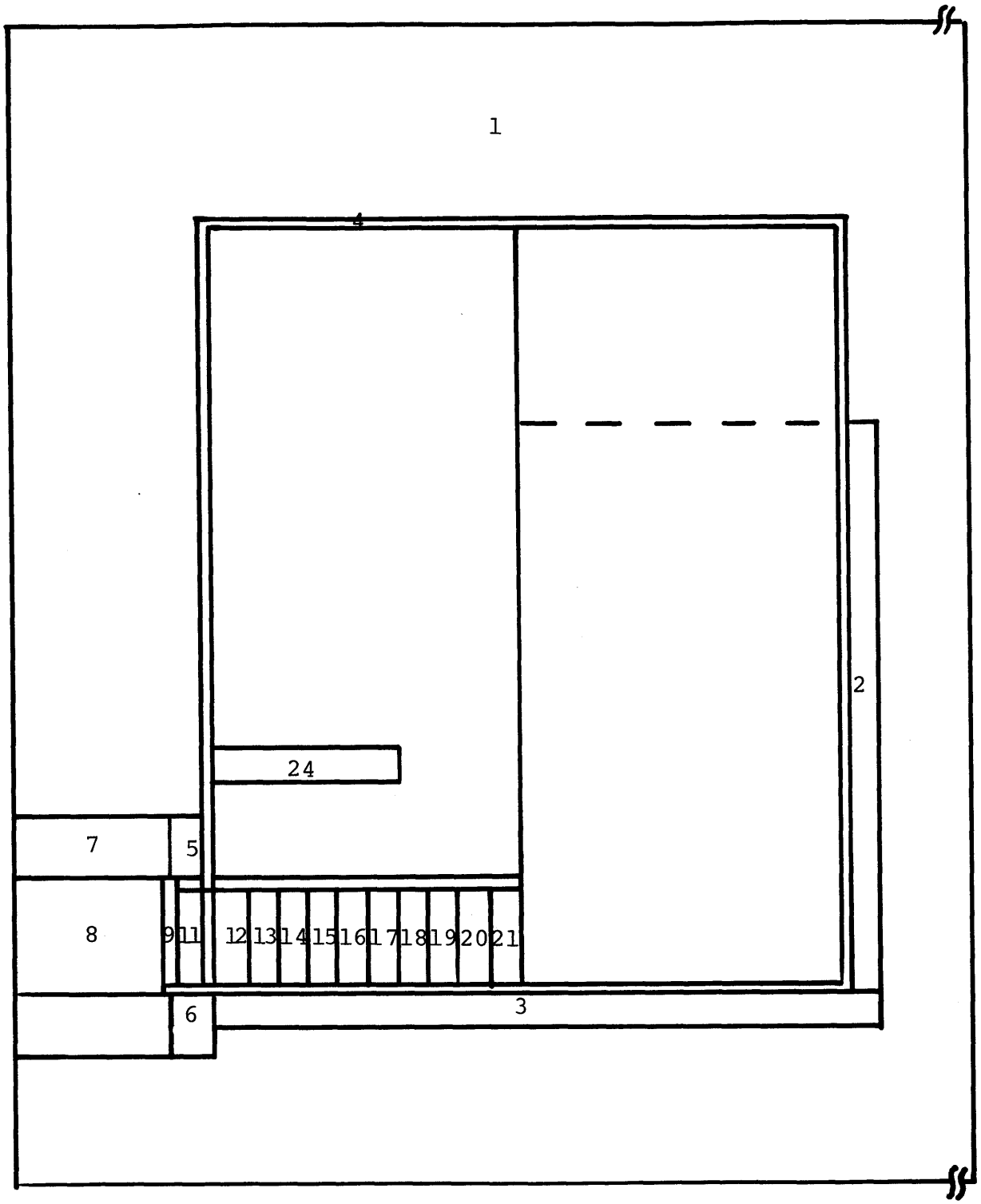

FIGURE 2.8 -- MONTE CARLO MODEL III OF THE BORON ASSAY FACILITY. SIDE VIEW.

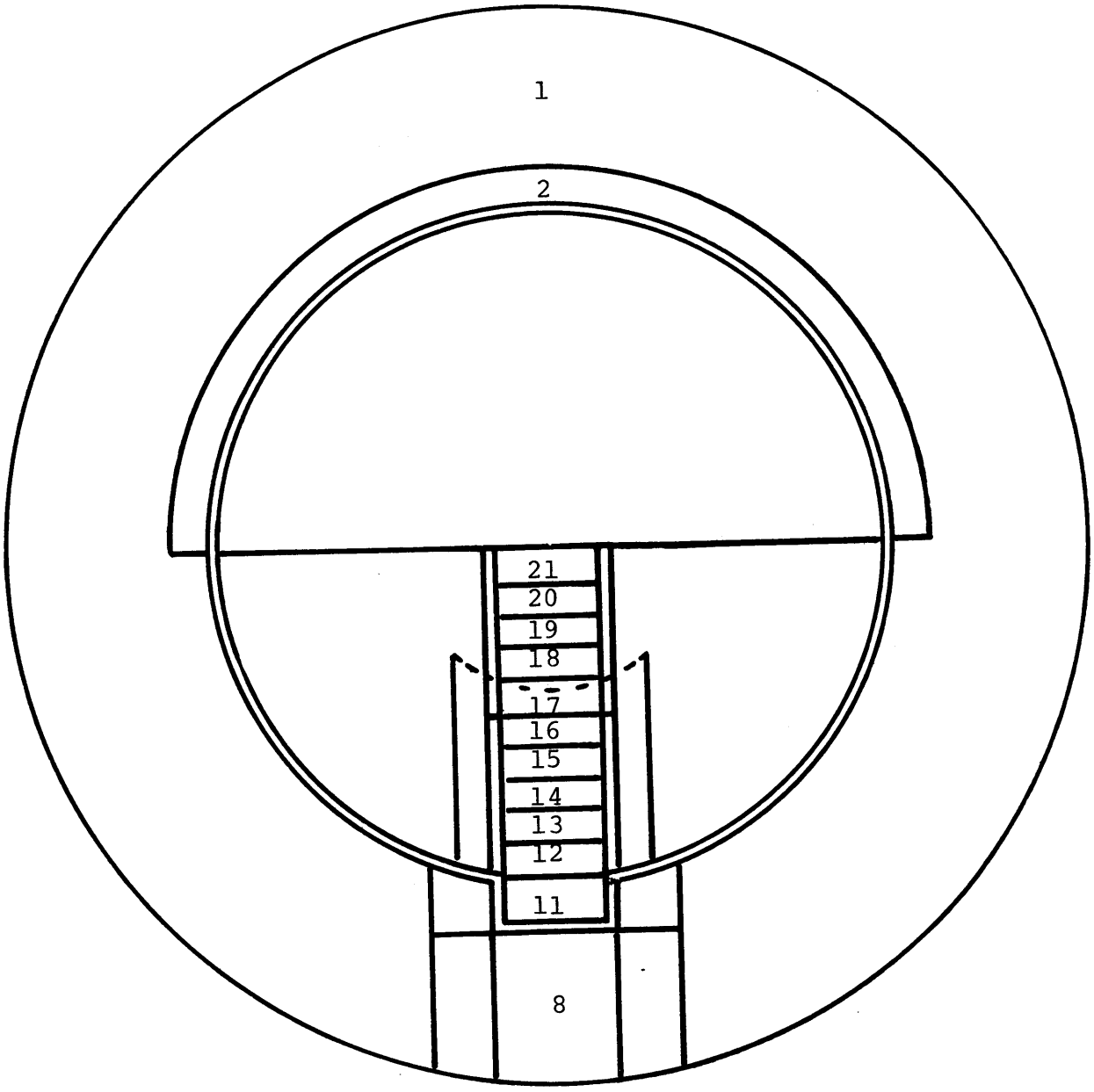

FIGURE 2.9 -- MONTE CARLO MODEL III OF THE BORON ASSAY FACILITY. TOP VIEW.

FIG. 2.10 -- THERMAL NEUTRON FLUX DISTRIBUTIONS IN REGIONS 11-21, AND 14-19, OF MODELS III AND IV OF THE BORON ASSAY FACILITY RESPECTIVELY

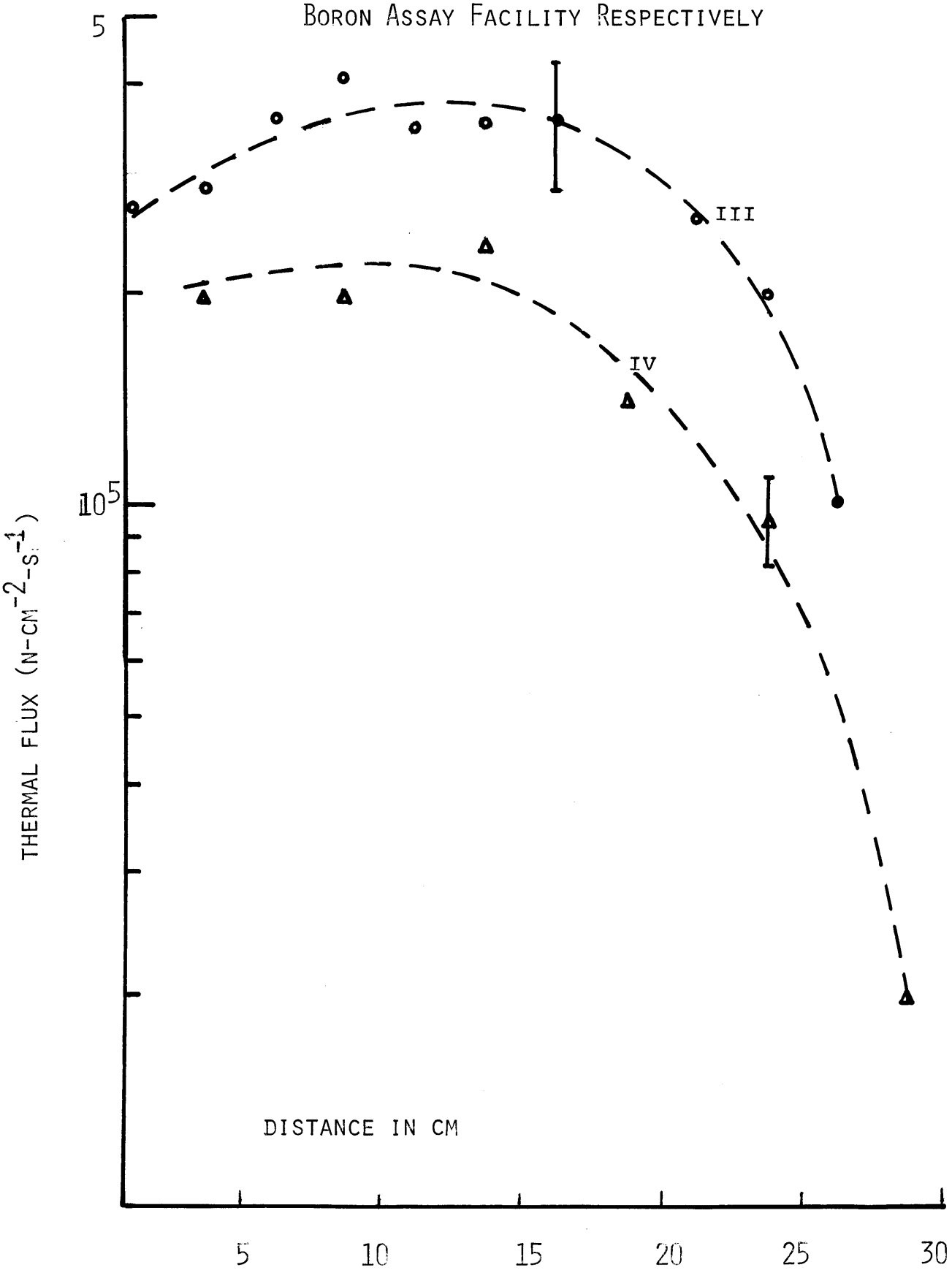

MONTE CARLO MODEL	DOSE (MREM/Hr.)			
	THM n	FAST n	IND γ	PRI γ
I				
SIDE	.02 ± 9%	158.0 ± 1%	3.1 ± 1%	-
TOP	.01 ± 27%	50.0 ± 11%	2.1 ± 7%	-
BOTTOM	.01 ± 27%	54.6 ± 10%	22.1 ± 7%	-
II				
SIDE	~.02	28.0 ± 9%	2.0 ± 15%	-
TOP	<.01	7.8 ± 51%	1.5 ± 19%	-
BOTTOM	<.01	12.0 ± 51%	1.2 ± 10%	-
III				
SIDE	.09 ± 23%	11.2 ± 13%	18.8 ± 1%	44.8 ± 1%
TOP	< 01	3.3 ± 71%	12.0 ± 7%	19.2 ± 2%
BOTTOM	<.01	2.9 ± 65%	12.8 ± 7%	25.3 ± 1%
IV				
SIDE (Avg.)	<.01	39.4 ± 15%	15.6 ± 5%	3.6 ± 1%
TOP	<.01	16.8 ± 22%	16.6 ± 30%	3.1 ± 1%

TABLE 2.3 -- CALCULATED DOSE RATES AT THE SURFACES OF MONTE CARLO MODELS I, II, III, & IV OF THE BORON ASSAY FACILITY

2.5.3.2 Geometry

The side and top views of the third model are given in Figures 2.8 and 2.9. Most of the changes that were made in the second model have already been described in the previous section. Additional changes include the addition of the horizontal regions along the D_2O tank's bottom (regions 11-21) in which the various particle fluxes are computed. The central vertical regions of the previous model have been eliminated, and the four point sources have been rearranged as in Figure 2.9. The objective of this new source configuration was an increased in the thermal flux levels at the probable sample position (i.e., at the detector face).

The following regions of the third Monte Carlo model contained the materials as indicated:

Region	Material
1- 6	Glycerin
7-24	Pb
8	Evacuated
11-23	D_2O
25-26	D_2O
Others	Fe

2.5.3.3 Calculation Results and Conclusions

The thermal neutron flux distribution in regions 11-21 is given in Figure 2.10 for a source normalization of 8.9×10^8 n-sec^{-1} (from 400μg ^{252}Cf). The

outer surface dose rates are given in Table 2.3, where the source normalization is 7×10^8 n-sec^{-1} (from 320μg ^{252}Cf, the present source size). In addition to these graphed and tabulated results, the following parameters were computed in region 8, which is the modeled detector portal:

$$\phi_T = 7.1 \times 10^4 \pm 35\% \quad \text{n-cm}^{-2}\text{-sec}$$

$$\phi_\gamma = 7.0 \times 10^3 \pm 71\% \quad \gamma\text{-cm}^{-2}\text{-sec where } \frac{\text{primary}\gamma}{\text{induced}\gamma} \approx 4$$

$$\phi_F \approx 2 \times 10^3 \text{ n-cm}^{-2}\text{-sec (note: too few fast neutron}$$

particles entered this region to estimate the error.)

All of these values were compted using a source normalization of 7×10^8 n-sec^{-1}. The above values of ϕ_T, ϕ_γ, and ϕ_F combine to yield a figure of merit of ~700, which is a rough estimate of the number of 5% precise measurements of 0.1 mg ^{10}B that can be made per exposure of 6×10^8 fast neutrons -cm^{-2} to the detector. Note that the possible detector residency time has increased from ~14 hours to ~80 hours. If we assume a detector repair cost of ~$1600, the effective cost per measurement would be ~$2.30. The final facility was therefore constructed on the basis of this model. Although the results in Table 2.3 indicate glycerin to be a good fast neutron shield, it was not used in the constructed facility because of its high radiative capture gamma production from hydrogen (Table 2.3) and the difficulties in loading glycerine with lithium (Section 2.3.5) to suppress gamma ray production. Polyethylene with a 10% wt lithium

loading was used instead. In this particular shielding material, only ~2% of the absorbed neutrons are captured by hydrogen (N_H and N_{Li} are on page 69). Had glycerin-Li been used, the gamma production would be ~2 times higher than with the polyethylene-Li (Section 2.3.5). Glycerin, however, does appear to be a better fast neutron shield than polyethylene in this configuration (see Table 2.3 but note that only the top and bottom of models II & III have the same thickness of polyethylene and glycerin respectively). Therefore, fear of substantial Compton background from the hydrogen radiative capture gamma ray was the impetus for electing to use lithium loaded polyethylene as biological shielding.

2.5.4 Monte Carlo Model IV and Final Design of Boron Assay Facility

2.5.4.1 Specific Objectives

The constructed boron assay facility differs from the third Monte Carlo model in several ways that are important in terms of neutron and photon transport (Section 2.5.4.2). Therefore, an experimental verification of the calculated parameters of the third Monte Carlo model is not possible. In addition, the calculations from this third model cannot be used to help estimate and interpret parameters and effects that are not easily determined experimentally (e.g., the relative contributions to

the dose from fast and thermal neutrons, induced and primary photons as well as the relative sources of the induced gamma ray dose, the neutron spectrum etc.). Consequently a (fourth) Monte Carlo model, which exactly corresponds to the constructed facility, was fashioned in order to facilitate experimental and calculational comparisons as well as aid in characterizing the radiation fields within the existing facility.

2.5.4.2 Geometry

The fourth Monte Carlo boron assay facility is presented in Figure 2.11 and Figure 2.12. A schematic drawing of the constructed facility is given in Figures 4.1 and 4.2. As indicated above, this Monte Carlo model has, as does the facility itself, a number of features not present in the third model.

First, each of the four 80 μg ^{252}Cf sources is encapsulated in a cylinder of bismuth as primary gamma ray shielding. These bismuth cylinders have a radius of 5.69 cm and are 12.58 cm in length. Second, the Pb annulus around the detector portal has been removed and replaced by polyethylene-Li to increase the amount of detector fast neutron shielding. Third, three sample tubes were introduced into the facility. These, as shown in Figures 2.11, 2.12, 4.1 and 4.2, include one vertical tube (a Z cylinder) near the tank center, a horizontal tube (y cylin-

der) which passes between the row of three Bi cylinders and the fourth Bi cylinder, and one horizontal tube (x cylinder) which extends across the tank's bottom into the D_2O "cup". The wall thickness of these iron tubes is 0.124 cm. The final difference is in the geometrical arrangement of the biological shielding as well as the shielding material. The best description of this shielding configuration is given by the illustrative drawing in Figures 4.1 and 4.2. This configuration consists of a series of concentric 5 cm thick boxes of polyethylene-Li shielding, so as to produce a rectangular box of shielding 20 cm thick on the sides and 15 cm thick on the top and bottom. This box is centered around the 115 liter tank of D_2O. The individual slabs of polyethylene are arranged in this step-like fashion in order to prevent fast neutron streaming along unobstructed air paths.

The materials which comprise each region of the model are as follows:

Region	Material
1	Polyethylene-Li $\{N_H=5.05\times10^{22}\,cm^{-3}$, $N_{Li}=1.07\times10^{22}\,cm^{-3}$
2, 41	Evacuated
48-53, 3	Fe
5-8	Bi (actually Pb where 1/5 σ_a^{Pb} was used)
All tube regions	Evacuated
Others	D_2O

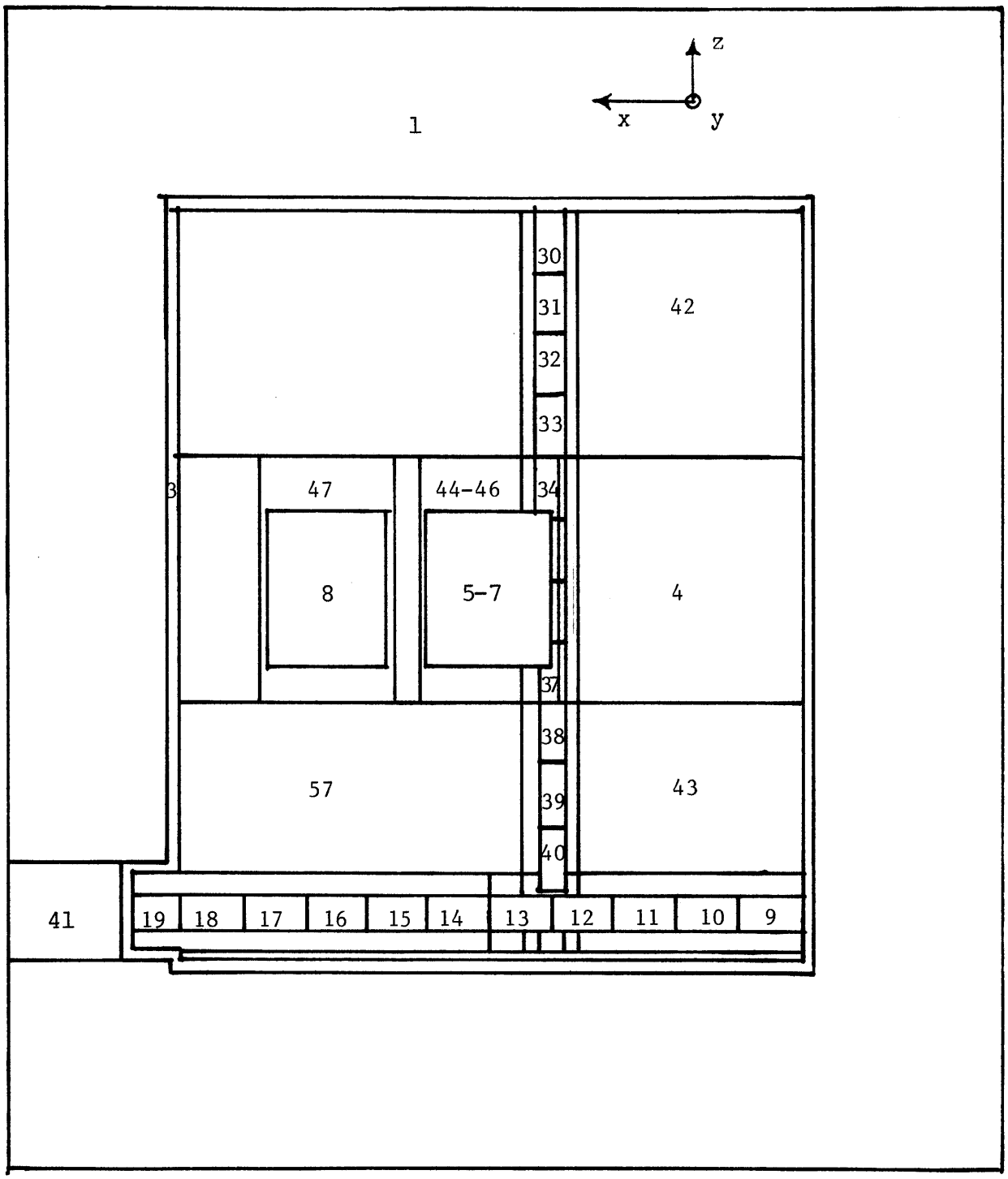

FIGURE 2.11 -- MONTE CARLO MODEL IV OF THE BORON ASSAY FACILITY. SIDE VIEW.

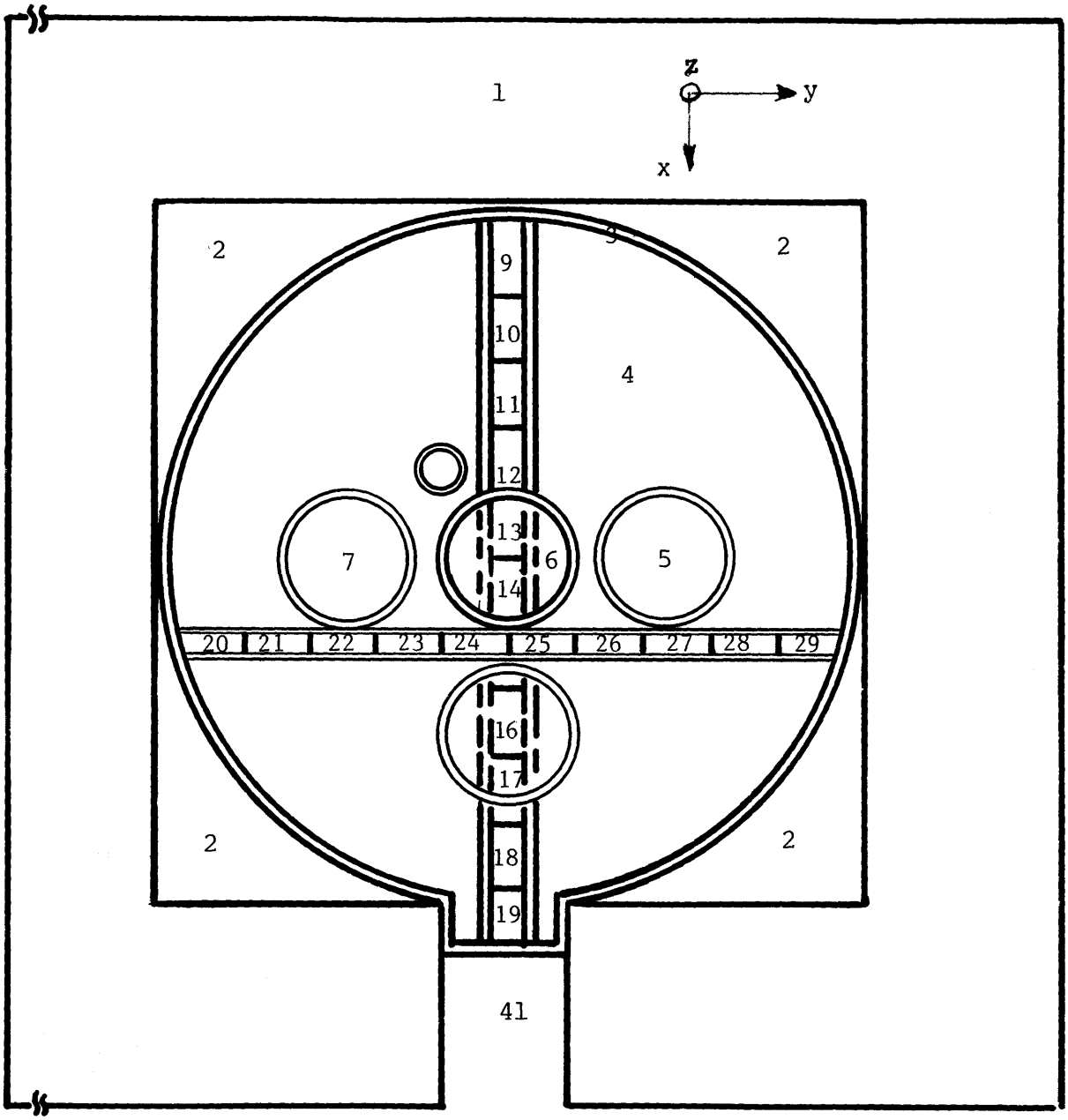

FIGURE 2.12 -- MONTE CARLO MODEL IV OF THE BORON ASSAY FACILITY. TOP VIEW.

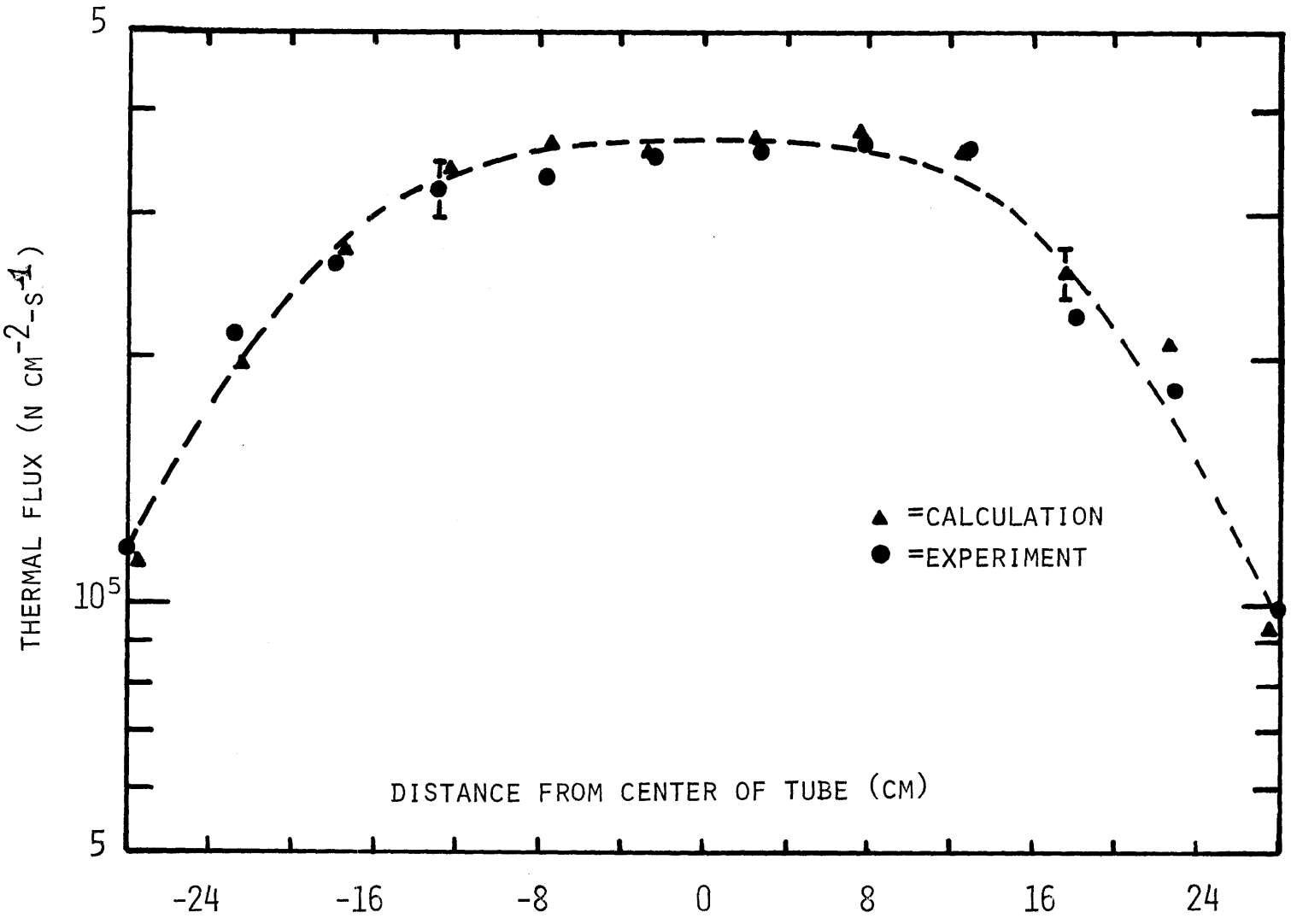

FIGURE 2.13 -- THERMAL FLUX DISTRIBUTIONS IN TUBE #1

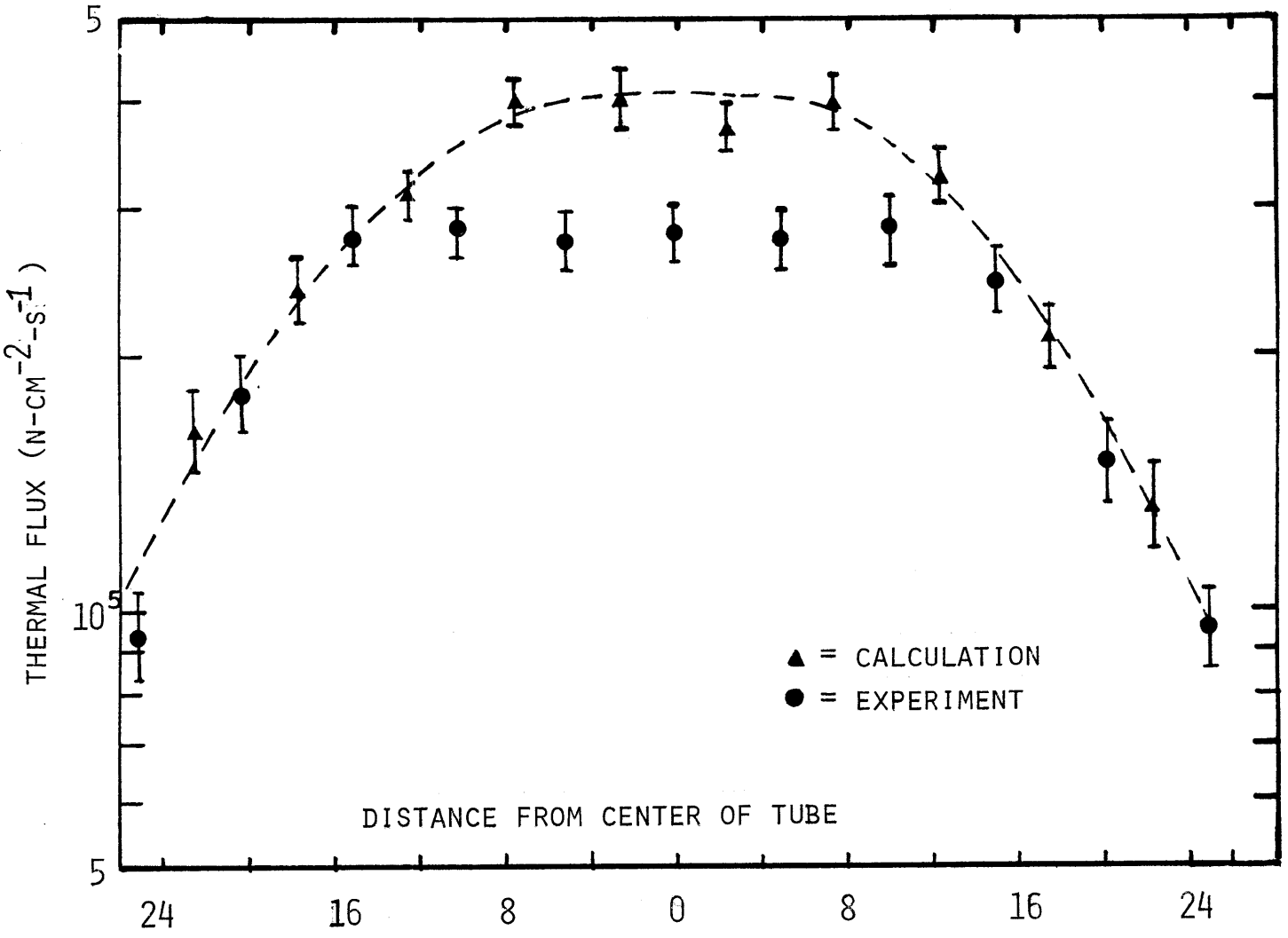

FIGURE 2.14 -- THERMAL FLUX DISTRIBUTIONS IN TUBE #2

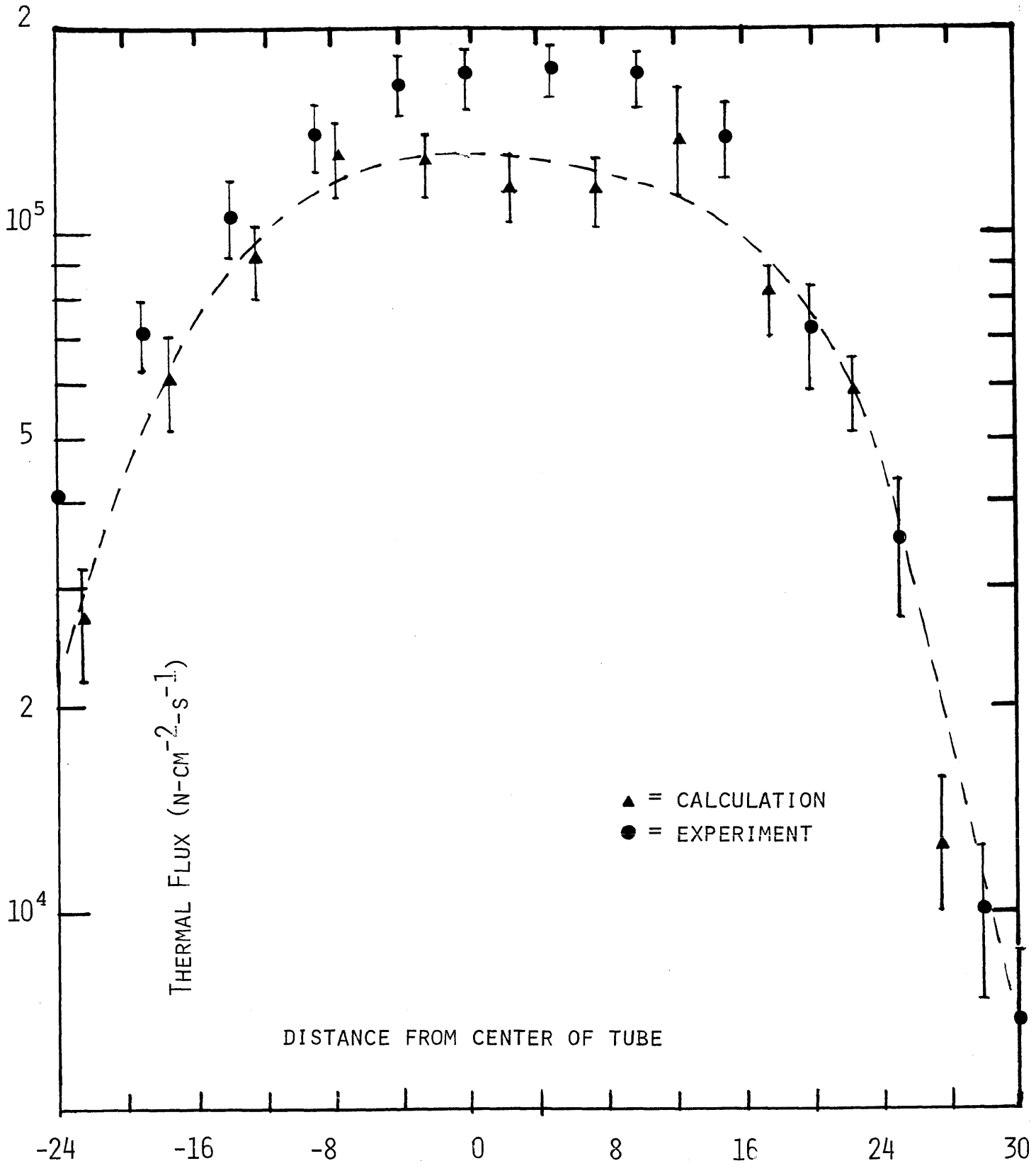

FIGURE 2.15 -- THERMAL FLUX DISTRIBUTIONS IN TUBE #3

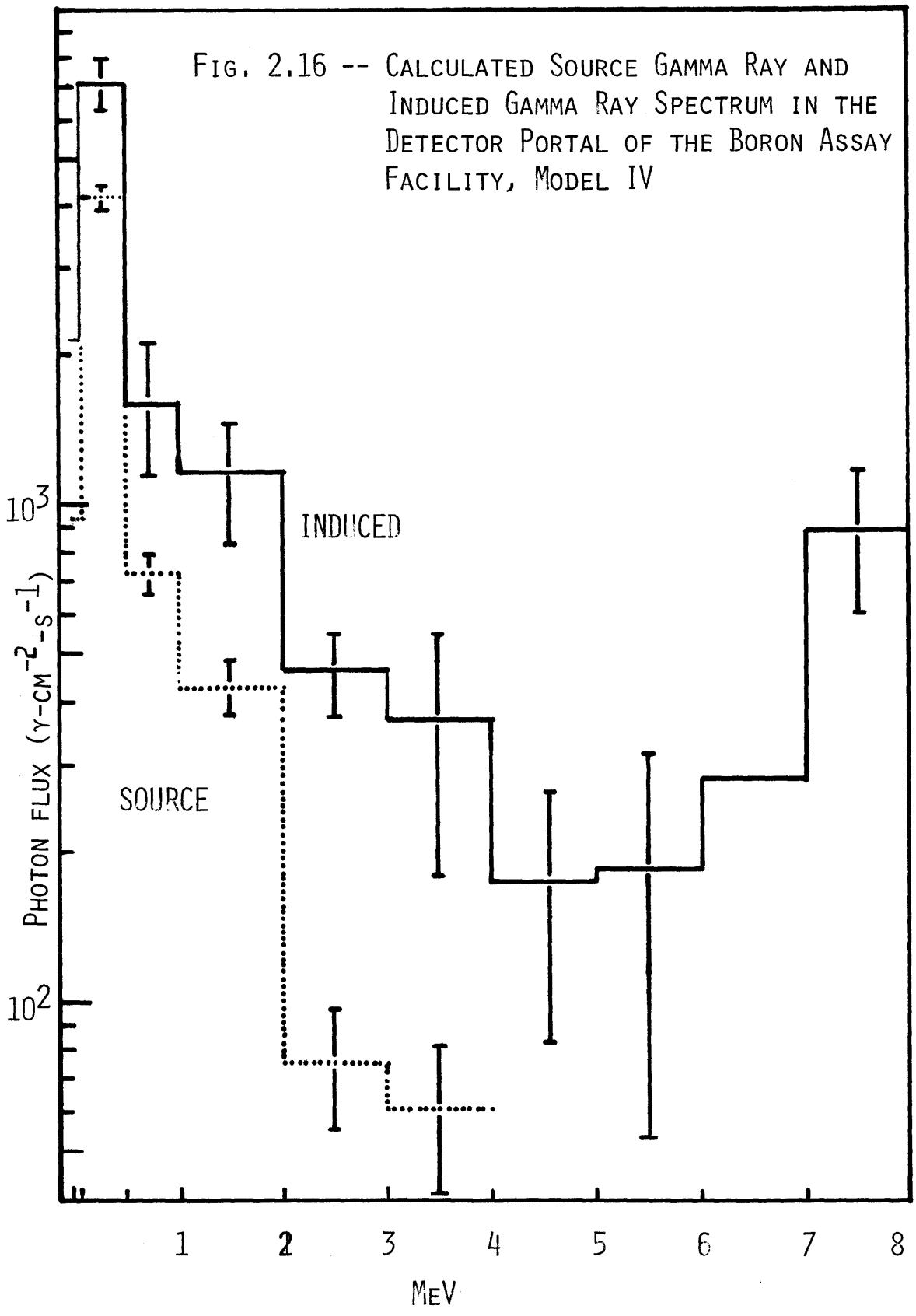

FIG. 2.16 -- CALCULATED SOURCE GAMMA RAY AND INDUCED GAMMA RAY SPECTRUM IN THE DETECTOR PORTAL OF THE BORON ASSAY FACILITY, MODEL IV

2.5.4.3 Calculational Results

A number of important parameters were calculated with this fourth model. The thermal flux distribution along each of the three sample tubes was computed and is presented in Figures 2.13, 2.14 and 2.15. The negative distances along the ordinates refer to the negative haves of the sample tubes as defined by the coordinate system indicated on the Model Carlo models in Figures 2.11 and 2.12.

The induced and primary gamma spectra in the detector portal are given in Figure 2.16. The error for each energy group gamma flux calculated was approximately by taking the inverse of the square root of the number of particles in that respective energy group which entered region #41 through the bounding side and end surfaces. The differential flux value for the energy group covering 6-7 MeV has no error estimate, since only one particle contributed to the flux in this group.

The doses at the top and bottom surfaces, and a dose value averaged over the four sides are given in Table 2.3. A more complete itemization of the surface doses is given in Table 4.1. A discussion of these results, and of the important previous results is given in the Section 2.5.5.

2.5.5 Conclusions

(1) Of the moderators considered for the boron assay facility, D_2O is the most applicable because of the adequate thermal neutron flux and small induced gamma ray flux generated in it, (by 320 μg of ^{252}Cf).

(2) The intensity of the source photons from 320 μg of ^{252}Cf requires that these sources be shielded to reduce the gamma ray dose rates, the background gamma ray flux, and counting dead times to acceptable levels. 5 cm of Bi around the sources reduces the photon flux and dose rates by approximately 95% at the surface of a 30 cm sphere of D_2O while reducing the thermal flux in the last 15 cm of D_2O by only 10%.

(3) Approximately 30 gallons of D_2O seems to be the minimum amount of moderator to be recommended for this application. This quantity of moderator and the source-sample-detector arrangement discussed in the last section should permit approximately 300 5% precise measurements of 0.1 mg of ^{10}B per detector lifetime. Considering only detector repair cost ($1600), the effective cost per measurement is estimated to be about $5.

(4) The calculations that were carried out with the third Monte Carlo model of the boron assay facility estimated that 700 5% precise measurements of 0.1 mg of ^{10}B per detector lifetime would be possible. Recall that the

source-sample-detector distances are the same in both the third and fourth Monte Carlo models. The factor of 2.3 difference in this figure of merit is due to the larger thermal flux level in the third model. Since this figure of merit is directly proportional to the square of the thermal flux, the factor of 1.5 difference between the thermal flux levels in the two models (figure 2.10) accounts for the observed difference in the estimated number of required measurements that can be made. The thermal flux level in the third model is higher because pure glycerin was used as the biological shielding material in this model whereas Lithium loaded polyethylene was the biological shielding in the fourth model. The glycerin, with the higher albedo, served as a better reflector. This arrangement, however, is not practical because of the H radiative capture gamma ray production in glycerin.

(5) Although glycerin does appear to have some fast neutron shielding advantages (compared to polyethylene) for the dimensions of the models that were considered (Table 2.3), the ability to load more lithium in polyethylene makes it (polyethylene) more desirable for biological shielding in this application. At least 20 cm of shielding, in addition to the 25 cm of D_2O is recommended for ~320 μg of ^{252}Cf.

3. IN VIVO NEUTRON ACTIVATION FACILITY FOR PARTIAL BODY MEASUREMENT OF SKELETAL CALCIUM

3.1 Design Criteria

The utility of a neutron activation facility for the measurement of Ca *in vivo* is based on several factors. The most important of these, is the precision with which small calcium changes within an extremity can be measured. The precision of serial measurements depends upon the uniformity of the activating neutron flux, errors in repositioning, forearm activation as a source of noise, and the reproducibility of monitoring the $^{49}Ca^{*}$ activity with NaI detectors. Equally important considerations are the dose to the patient's whole body and to the extremity (hand) in which the Ca is being activated.

The object of this study, therefore, was to design a facility which would meet the following criteria during each of several serial measurements over a period of years:

(1) 1% statistical precision

(2) low repositioning error

(3) <10 rem dose to the hand (per measurement)

(4) <10 mrem dose to the whole body (per measurement)

3.2 One Dimensional Moderator Studies

Several important parameters are moderator dependent. These include the magnitude of the thermal flux, the uniformity of the thermal flux, and the Ca activation rate to hand dose

rate ratio. Because of the geometrical complexity which the hand presents as an activation target (see introduction), a uniform thermal neutron flux is required if precise measurements are to be made. A large thermal flux is desired in order to minimize the time required to complete an irradiation. A short irradiation time would minimize the activation of the hand's Na($T_{1/2}$ = 15 hr.) and therefore the interference under the $^{49}Ca^*$ peak from the ^{24}Na 2.75 MeV peak. A high thermal flux to dose ratio is obviously desirable if a low dose per measurement is to be realized. Therefore, the two most practical and promising moderators (from the previous boron assay studies) were investigated with respect to these parameters.

3.2.1 Bilateral Irradiation

Recall Figure 2.1, which gives the thermal neutron flux distributions generated by a ^{252}Cf point source in 30cm spheres of H_2O, D_2O and Be. From this figure, note the uniformity of the flux distribution in D_2O, and the magnitude of the thermal flux in H_2O. Although heavy water (D_2O) has the more uniform thermal flux from a single source, the magnitude of the peak thermal neutron flux is one order of magnitude larger in H_2O. In this moderator the thermal flux distribution, which is less uniform than for one point source in D_2O, can be made more uniform by superposition of the distributions of two or more sources. From Figure 2.1 note that at 6cm the thermal

flux in H_2O is one-half its maximum value and that at 12cm it is ~1/10 its maximum value. Therefore, two sources 12cm apart should yield a uniform thermal neutron flux with a magnitude approximately equal to the peak thermal flux for one source.

3.2.2 Calcium Activations Per Unit Dose

As mentioned earlier, another important consideration which is also moderator dependent is dose. Figure 3.1 shows the activating fluence per unit dose (in rem) as a function of radial distance in the two moderators under consideration. This may also be viewed as the signal to dose ratio as a function of hand to source distance in the moderator. Note that for hand to source distance greater than 15cm, D_2O gives a better signal to dose (rem) ratio, whereas for hand to source distances of less than 15cm this ratio is higher in H_2O. The determination of which moderator to use was based on the following practical consideration. Approximately 45-50 cm of hydrogenous material is required to shield the dose rates from 400μg of ^{252}Cf to levels in the range of ~50 mrem/hr. Since each 400μg ^{252}Cf source will require ~45 cm of moderator plus shielding, the total diameter of a facility containing two such sources separated by xcm will simply be ≈2 x (45 cm + xcm). Thus, if a source to hand distance of 15cm is used in a bilateral configuration employing two 400μg ^{252}Cf sources the two sources would be spaced 30cm apart and the total diameter of the facility would

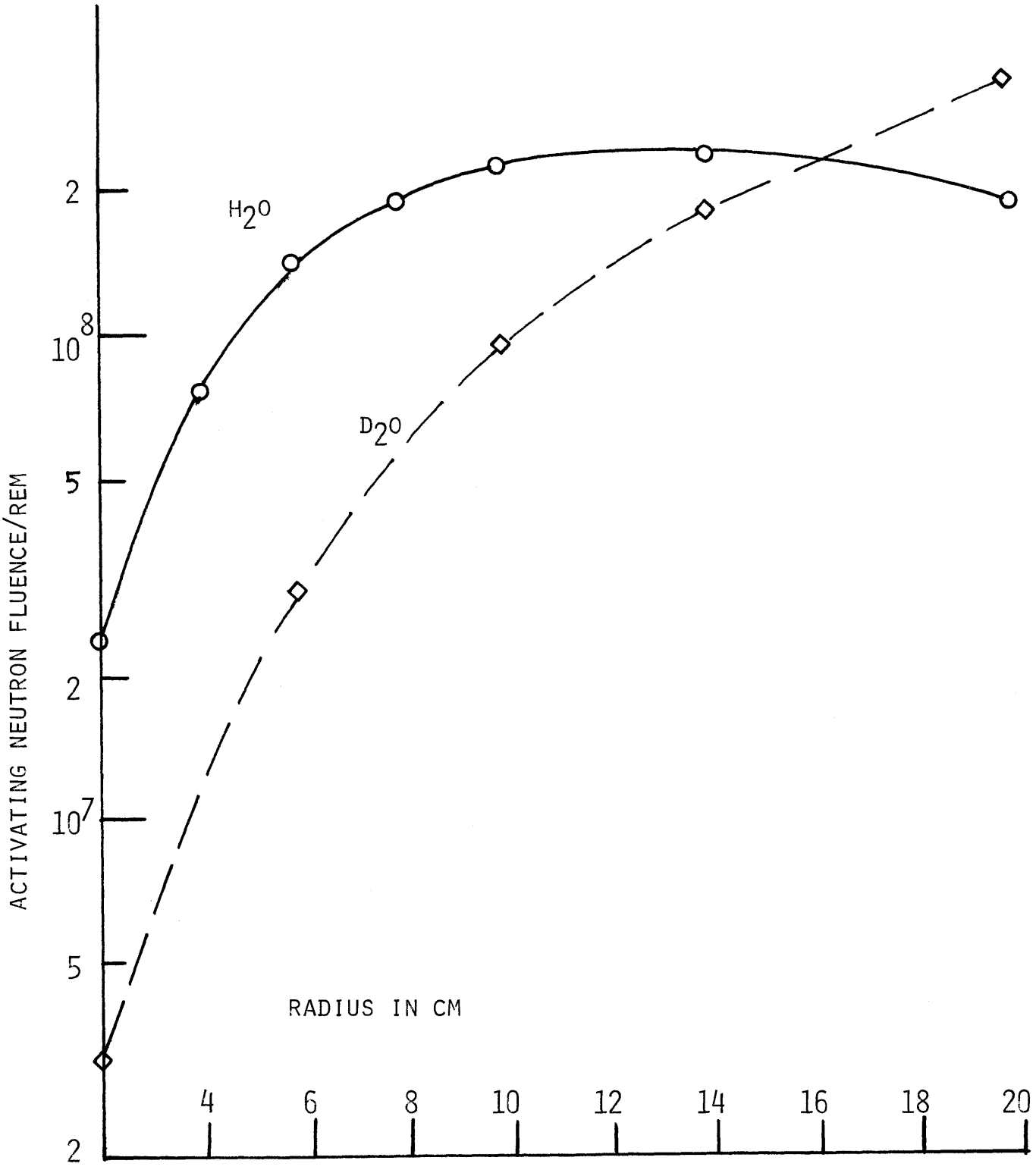

FIGURE 3.1 -- ACTIVATING NEUTRON FLUENCE PER REM AS A FUNCTION OF RADIAL DISTANCE FROM A 800 μG ^{252}Cf SOURCE IN A 30 CM SPHERE.

have to be ~120 cm. Similarly if a source to hand distance of 6cm is used, the diameter of this facility would be ~100cm If we assume a square cylindrical geometry, the first facilty has a volume ~1.7 times the volume of the second, and would therefore cost (shielding) and weigh ~1.7 times as much also. Hence, from a practical cost-effectiveness approach, a small hand to source distance seems desirable. Since the signal to dose ratio is higher in H_2O (compared to D_2O) for source to hand distances that are practical (< 15cm), H_2O is the obvious moderator of choice. Note also, that the optimal source to hand distance in H_2O is ~6cm.

3.2.3 Multisource Bilateral Irradiation for Achieving Thermal Flux Uniformity

In order to optimize the thermal flux uniformity within a volume in which the hand might be placed for irradiation, a multiple source planar configuration is considered. The idea here is to first generate a uniform thermal flux distribution in a plane by arranging a set of four sources on the same plane. Then by superimposing the distributions from two planar sets of sources placed some appropriate distance apart, a uniform thermal flux region between the two source planes can be achieved.

Figure 3.2 shows a single set of four equal sources in a plane where the sources are symmetrically positioned on a circle of radius 8cm. The graph in Figure 3.2 labeled

FIG. 3.2 -- VARIATION OF THE ACTIVATING NEUTRON FLUX WITHIN A PLANE OF 4 ^{252}Cf SOURCES AND IN CORRESPONDING PARALLEL PLANES. NORMALIZATION = 4×10^{10} N-SEC^{-1}

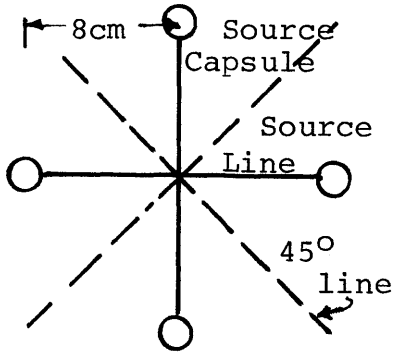

CROSS SECTION OF ^{252}Cf SOURCE PLANE

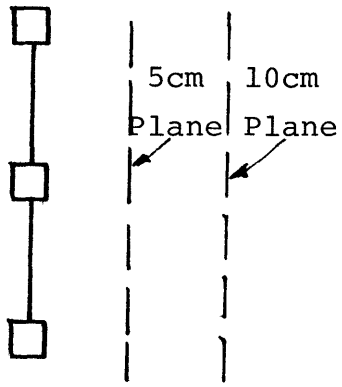

SIDE VIEW OF SOURCE PLANE

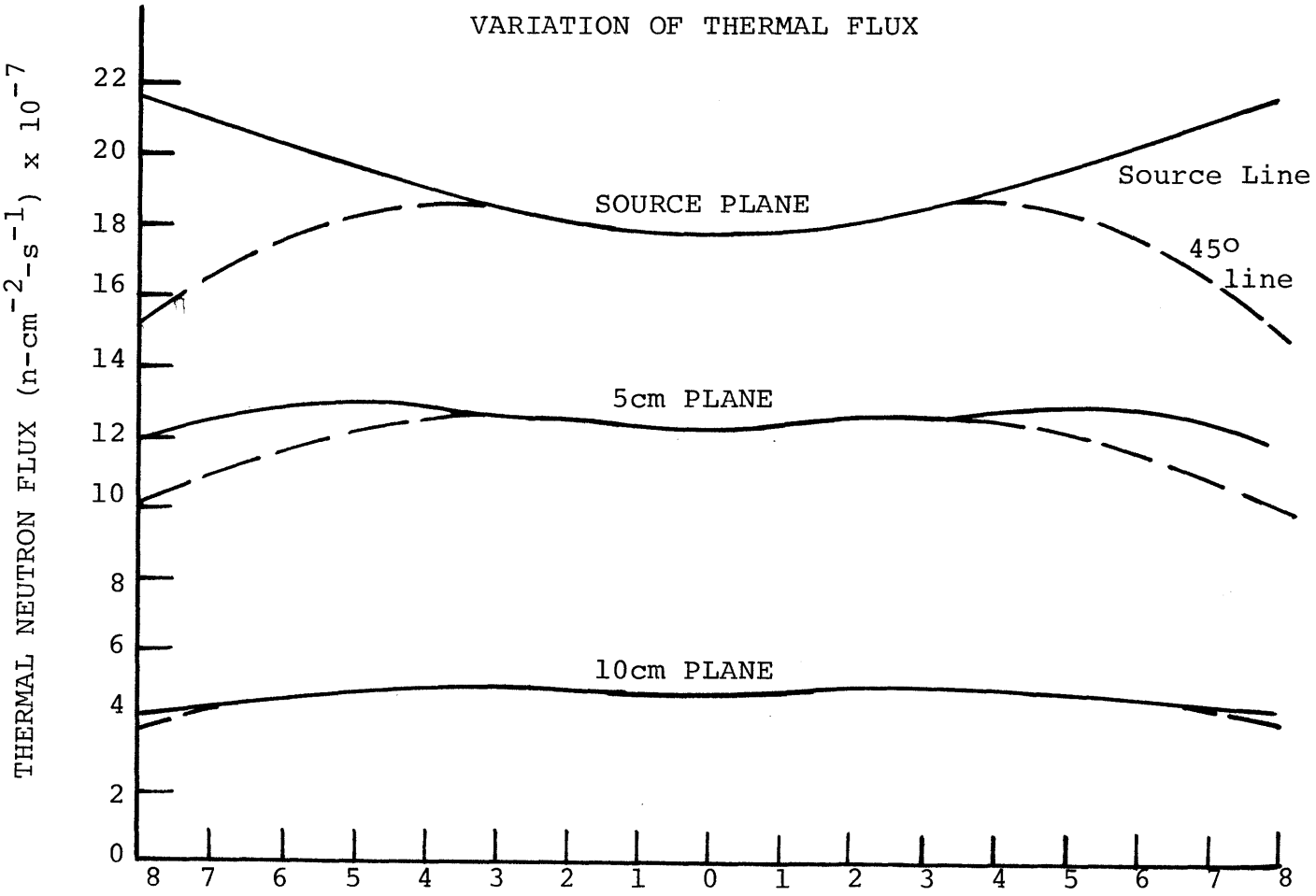

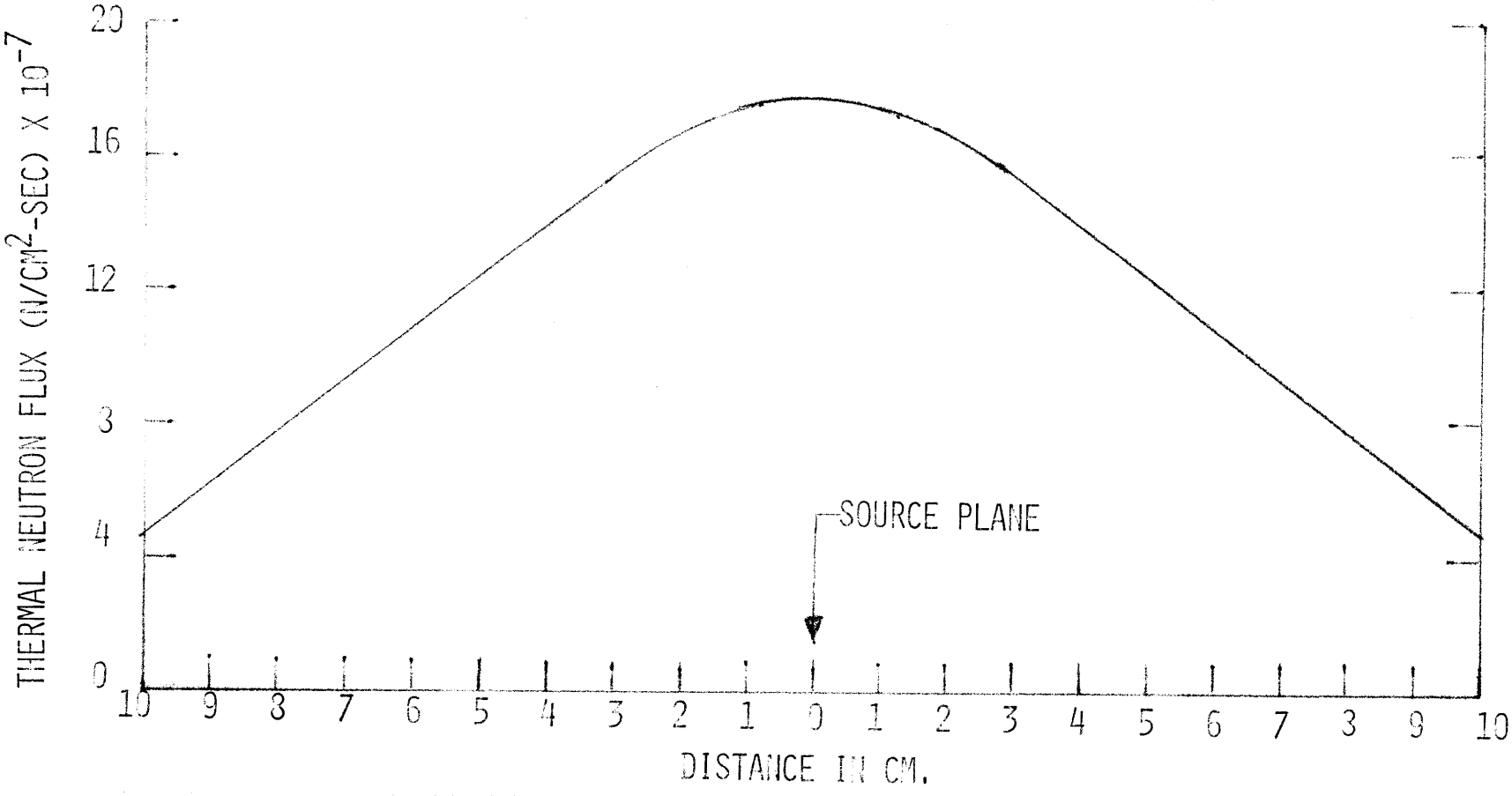

FIG. 3.3 -- THERMAL NEUTRON FLUX VARIATION ALONG CENTRAL AXIS NORMAL TO A PLANE OF 4 ^{252}CF SOURCES. NORMALIZATION = 4 X 10^{10} N-SEC^{-1}

FIG. 3.4 -- VARIATION OF THERMAL NEUTRON FLUX IN PLANES PARALLEL TO TWO SOURCE PLANES IN 8 SOURCE CONFIGURATION. NORMALIZATION = 4×10^{10} N-SEC^{-1}

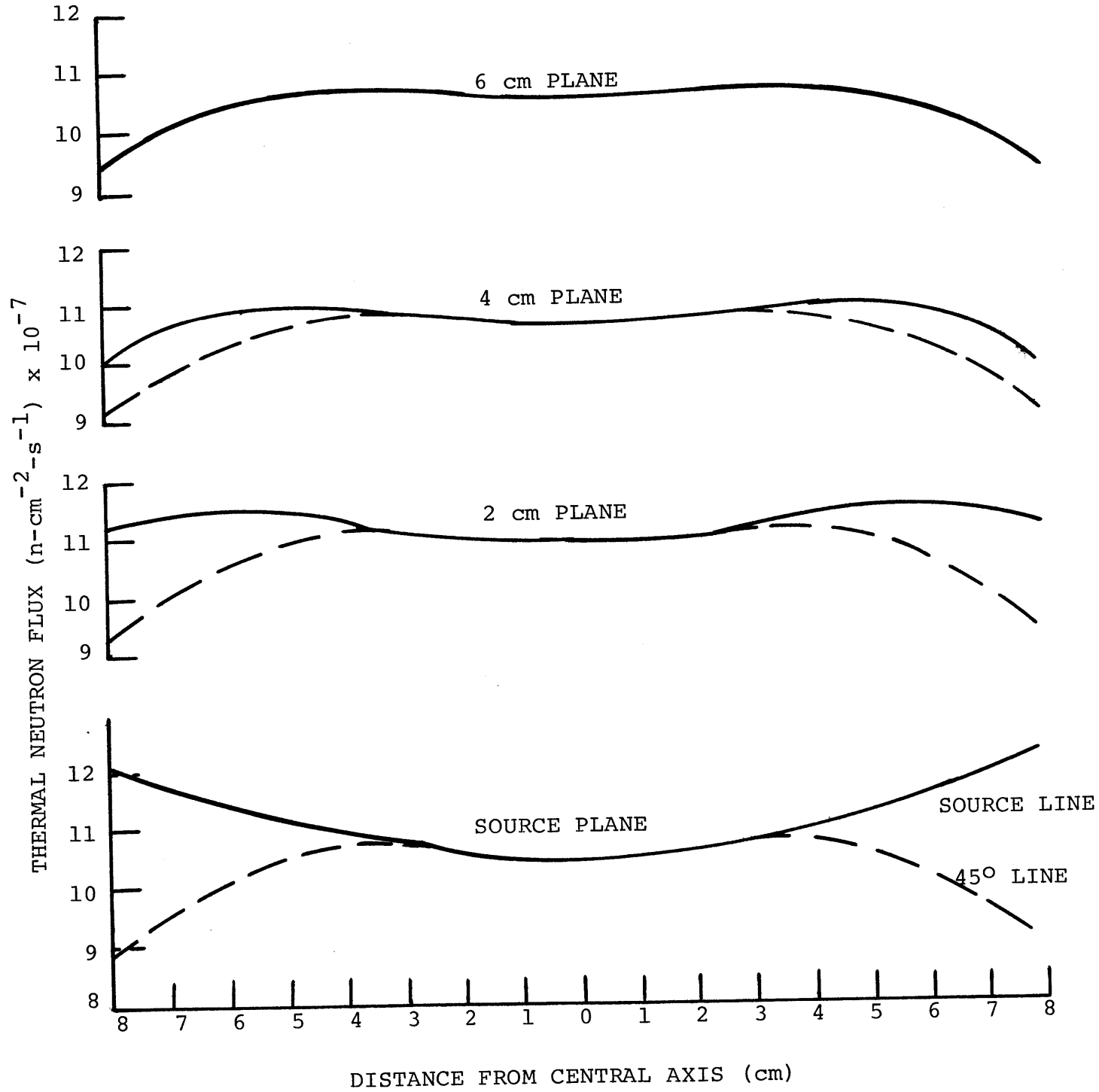

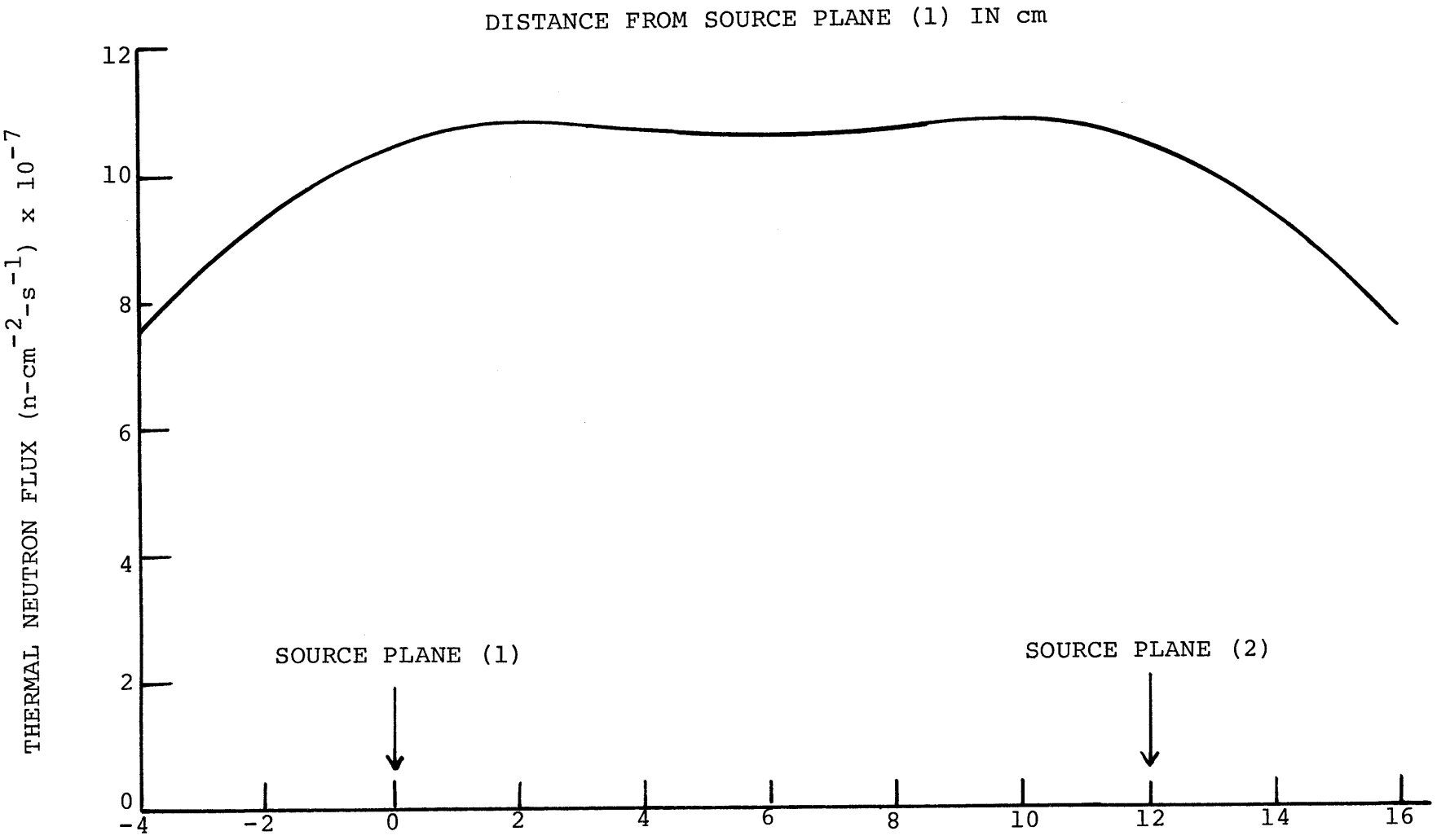

FIG. 3.5 -- VARIATION OF THERMAL NEUTRON FLUX ALONG CENTRAL AXIS OF 8 SOURCE CONFIGURATION. NORMALIZATION = 4 x 10^{10} N-SEC^{-1}

"source plane" shows the maximum variations in the thermal flux distributions in the source plane calculated along the two lines of symmetry. The two lines of symmetry are named (1) the "source line", which is the diagonal line that passes through the center of the plane and connects two sources, and (2) the "45° line" which is the line rotated 45° in the plane from the "source line". Similar plots of thermal flux in planes parallel to the source plane are also shown. Note that as the distance from the source plane increases, a greater degree of thermal neutron flux uniformity is realized. However, the decrease in the absolute thermal flux as a function of distance from the source plane is substantial as shown in Figure 3.3 .

Thermal flux uniformity along this direction, however, can be achieved by superimposing the thermal flux distributions from two planes of four sources each. The thermal flux uniformity along the centerline connecting two planes is shown in Figure 3.5, and appears to be excellent. These planes are separated by 12cm since it appears that this separation is optimal as indicated in Sections 3.2.1 and 3.2.2 . Figure 3.4 gives the thermal flux distributions within several planes normal to this centerline. From these figures, it appears that a fairly uniform thermal neutron flux can be obtained for a volume larger than the average human hand (~500 cm^3) by using eight ^{252}Cf sources moderated with H_2O.

3.3 Three Dimensional Monte Carlo Design Calculations

As a result of the ANISN studies, the optimal moderator (H_2O), source to hand distance (6 cm), and separation of the bilateral sources (12 cm) were determined. In addition, the ANISN calculations indicated that a multi-source bilateral configuration (previous section) is suitable for this application. Consequently a preliminary design of the ^{252}Cf hand irradiator facility was based on both the results of the ANISN calculations and upon the results of and experience gained in the design of the boron assay facility. This design was incorporated into an ANDY code three-dimensional calculational model in order to investigate the utility of the design in terms of (1) the Ca activation rate in the hand, (2) dose to the hand, (3) dose to the whole body, and (4) the Ca activations in the forearm as a source of noise. This Monte Carlo model os the hand irradiation facility is shown in Figure 3.8. The rationale for employing an ANDY calculation at this point, follows that given in Section 2.5. A description and explanation of the model follows.

3.3.1 Modeling Of The Hand and Arm

The hand was modeled as three elliptical disks comprising a "sandwich" of tissue, bone, and tissue regions (Figure 3.8). To estimate the average volume of the human hand and wrist, the volume of three adult hands were measured by placing them in a beaker filled with water and

measuring the displaced volume of water. The average thus obtained was 475 cm^3. The volume of the bone region was determined from the weight of bone in the hand and wrist (152 g in Reference Man, ICRP #23) and the density of bone (1.5 g/cm^3), to be ~100 cm^3. Consequently, the hand and wrist were modeled as a 475 cm^3 elliptical disc with a 100 cm^3 central region as bone.

Similarly, the arm was modeled as a 50 cm long, 6 cm diameter cylinder concentric with a 3.2 cm diameter region of bone with a total bone volume of 400 cm^3 [=600 g/1.5 $g\text{-}cm^{-3}$; Spiers (1957)]. Although the human arm bones comprise the humerus, and the radius and ulna (in the forearm), this simple model should be adequate for estimating the Ca activation in the bones of the forearm. A 5 cm thick natural Li-loaded polyethylene bracelet is placed at the end of the forearm. The bracelet and arm models are separated by .1 cm from the hand model to facilitate the ANDY code calculations.

3.3.2 Modeling of the Facility

The proposed ^{252}Cf neutron activation facility for the hand has eight 100 microgram ^{252}Cf sources moderated by H_2O. Four sources are positioned symmetrically in each of two parallel annular rings of bismuth separated by 12 cm in a tank of H_2O with the dimensions of 50 cm diameter by 55 cm high. The tank is shielded by 20 cm of natural lithium loaded polyethylene on all sides. The more detailed version of this model, which was employed for computational purposes,

is shown in Figures 3.9, 3.10. and 3.11. In these calculations, as in the boron assay calculations, bismuth was simulated by using the Pb cross sections with the thermal group (group 30) absorption cross section adjusted by a factor of 1/5 (i.e. $\sigma_a^{Bi}/\sigma_a^{Pb} = 1/5$).

3.3.3 Investigation of the Utility of the Design

As stated in Section 3.3, the objective of the Monte Carlo calculation was to investigate the design of the hand irradiation facility in terms of (1) the Ca activation in the hand, (2) dose to the hand, (3) dose to the whole body and (4) the Ca activations in the forearm as a source of interference. The results of this investigation are given below.

The Monte Carlo calculated dose rates are:

	Neutron (Rad/Hr.)	Induced Gamma (Rad/Hr.)
Hand	8.0 $\pm$<1%	5.5 $\pm$<1%
Top of Facility	$1.7\times10^{-3}\pm$ 1%	$2.8\times10^{-3}\pm$ 1%
Side of Facility	$6.0\times10^{-3}\pm$ 1%	$0.8\times10^{-3}\pm$ 1%
Bottom of Facility	$3.8\times10^{-3}\pm$ 1%	$3.3\times10^{-3}\pm$ 1%

Since ^{252}Cf source gamma rays were not included in this calculation, only the neutron and induced gamma ray doses are shown. The primary (source) gamma ray does can, however, be estimated from the depth dose curves for a ^{252}Cf point source in H_2O which are given in Stoddard (1971). Since the ratio of the source gamma ray dose (in rem) to the neutron dose (in rem) is 0.10 at ~6cm [Stoddard (1971)], the source

gamma ray dose to the hand in this facility is estimated to be ~8 rad/hr using quality factors of 10 for neutrons and 1 for gamma rays.

The dose at the surface of the facility represents the upper limit dose to the whole body. Again, the unshielded source gamma dose is estimated from Stoddard (1971) to be ~140 mrad/hr. The bismuth annuli should, however, reduce this dose by a factor of ~.01, so that the approximate source gamma ray is ~ 1.4×10^{-3} rad/hr.

In the hand and wrist, and in the forearm, the calculated Ca activation rates are:

Hand & Wrist = 1,460 ± 7% Ca Activations/sec.
Forearm = 107 ± 30% Ca Activation/sec.

Thus a two minute irradiation will net (allowing for the decay of $^{49}Ca^*$ as it is produced) approximately 163,000 $^{49}Ca^*$ atoms in the hand.

To monitor the $^{49}Ca^*$ activity in the hand and wrist, it is proposed that the hand be placed flat in a reproducible position between two large NaI detectors. If the detectors are each 5" diameter by 5" thick, the full energy peak efficiency is estimated to be approximately 16% [Lazar (1956)] for a 3.1 MeV gamma ray entering normally to the face of the detector. Since the dimensions of the hand may be greater than 5 inches, and since some clearance between the detectors and the hand is necessary, a conservative estimate

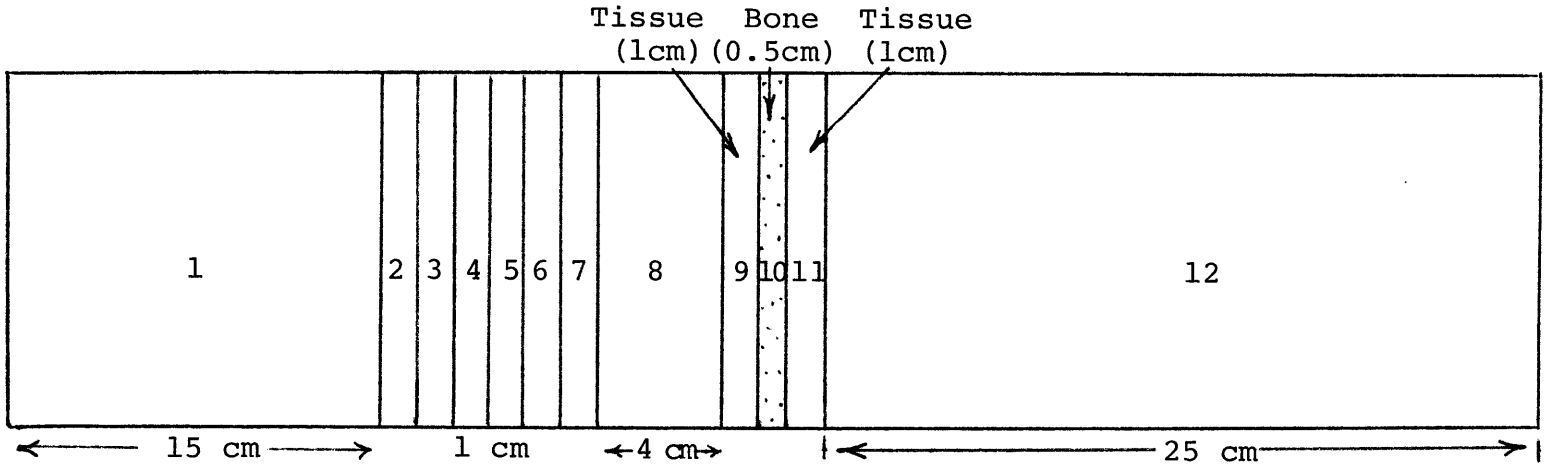

FIG. 3.6 -- MODEL USED FOR CALCULATION OF HAND REPOSITIONING UNCERTAINTY

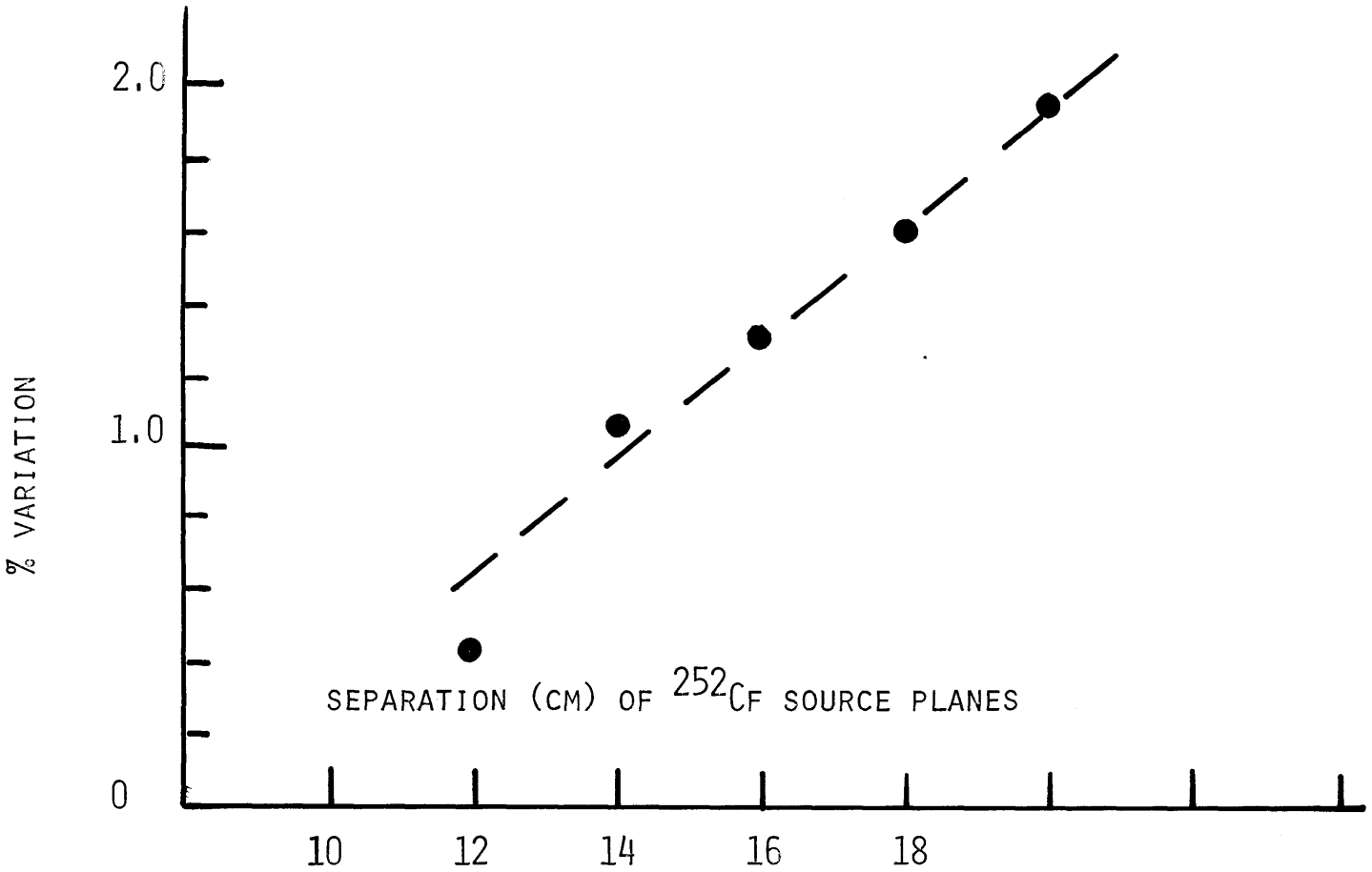

FIGURE 3.7 -- % VARIATION IN CA ACTIVATIONS IN HAND PHANTOM FOR A 1 CM DISPLACEMENT

RT. BDY. SOURCE-HAND DIST. CM	BILATERAL SOURCE SPACING CM	HAND CENTER $\sum_g \Phi_g^+ \chi_g {}^{252}Cf$ $^{49}Ca^*$/SOURCE NEUTRON	HAND→1CM DISPLACEMENT $^{49}Ca^*$/SC.NT.	%DIFF.
10	22.5	8.32(-7)		
9	20.5	1.03(-6)	1.05(-6)	+1.94
8	18.5	1.27(-6)	1.29(-6)	+1.57
7	16.5	1.55(-6)	1.57(-6)	+1.29
6	14.5	1.87(-6)	1.89(-6)	+1.07
5	12.5	2.23(-6)	2.24(-6)	+ .45
4	10.5	2.61(-6)		

Abbrev.: RT. BDY. = Right Boundary; χ_g = Fraction of a Source Neutron in Energy Group g; SC.NT. = Source Neutron

TABLE 3.2 -- RESULTS OF THE ANISN ADJOINT MODE CALCULATION OF THE HAND REPOSITIONING UNCERTAINTY

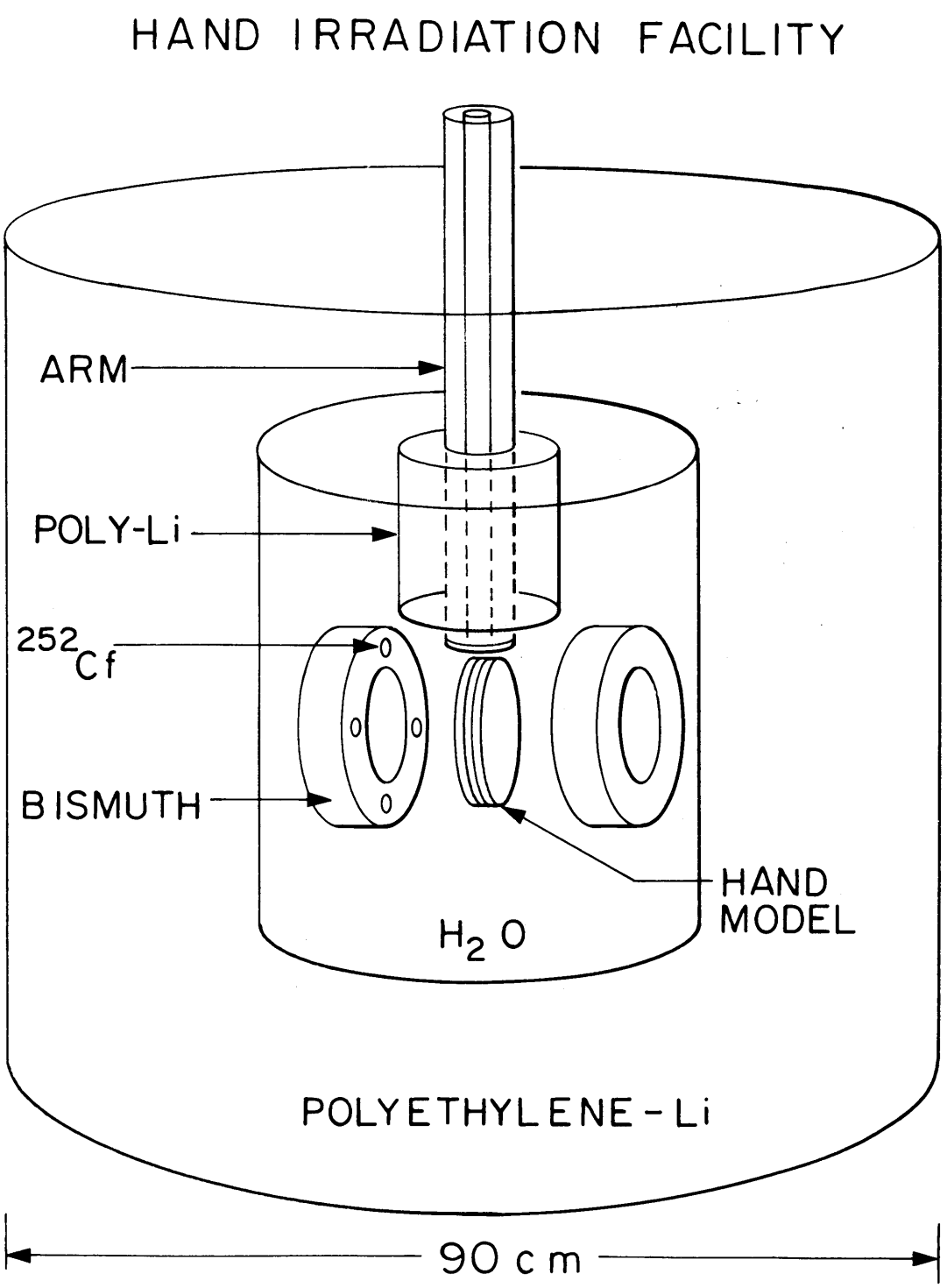
HAND IRRADIATION FACILITY
ARM
POLY-Li
252Cf
BISMUTH
HAND MODEL
H2 O
POLYETHYLENE - Li
90 cm

FIGURE 3.8

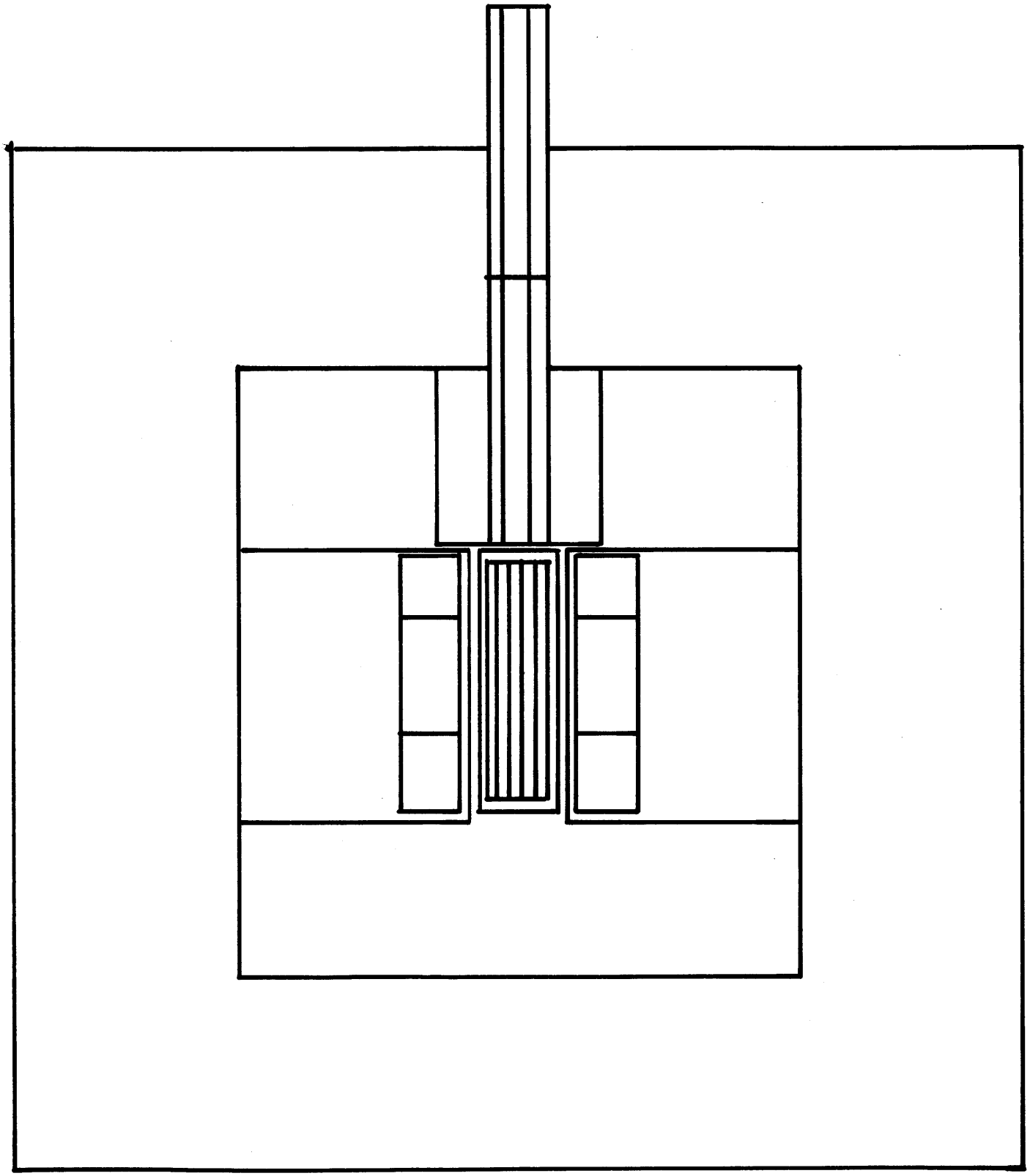

FIGURE 3.9 -- MONTE CARLO MODEL IV OF THE BORON ASSAY FACILITY. FRONT VIEW.

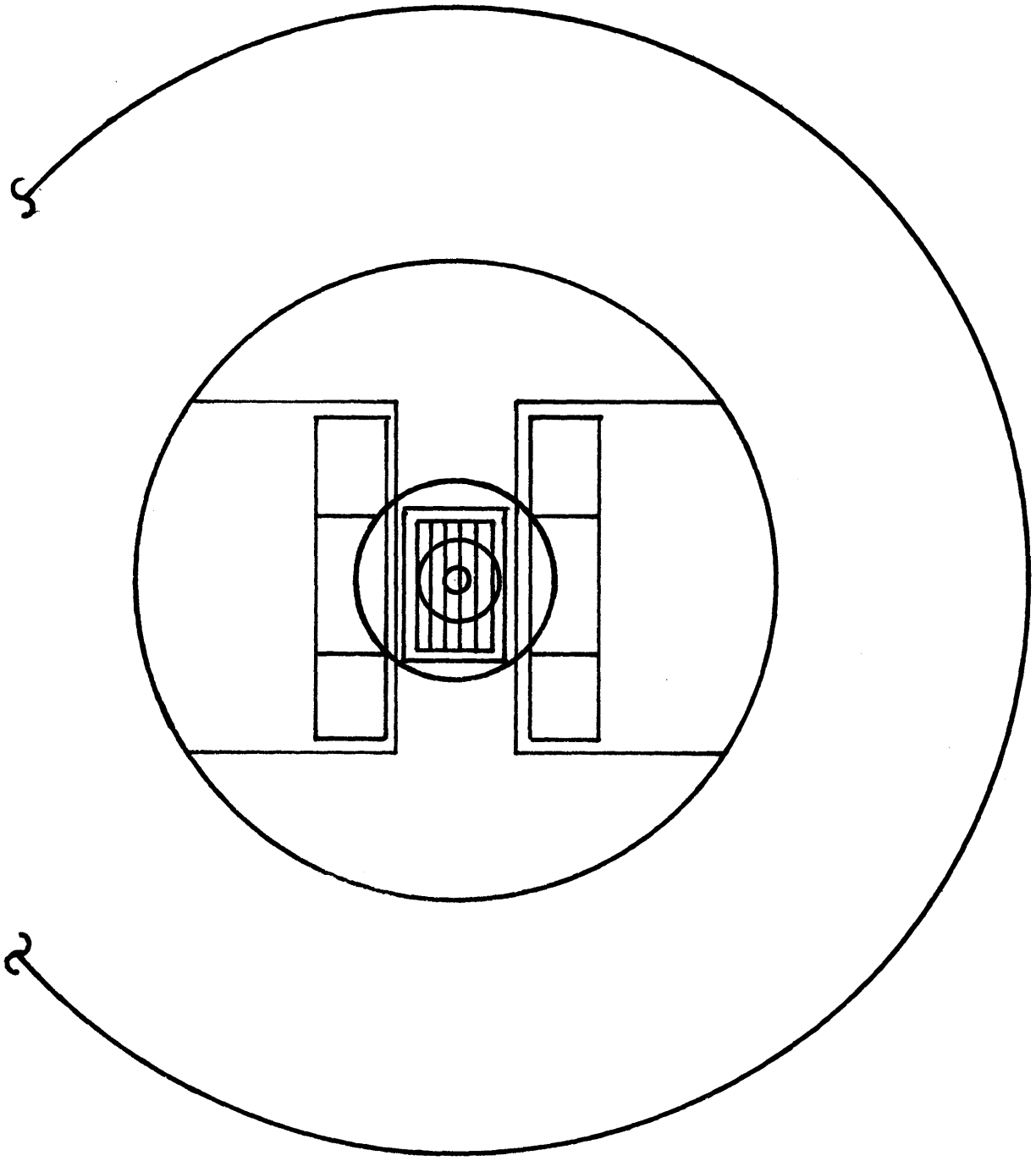

FIGURE 3.10 — MONTE CARLO MODEL OF THE HAND IRRADIATION FACILITY. TOP VIEW.

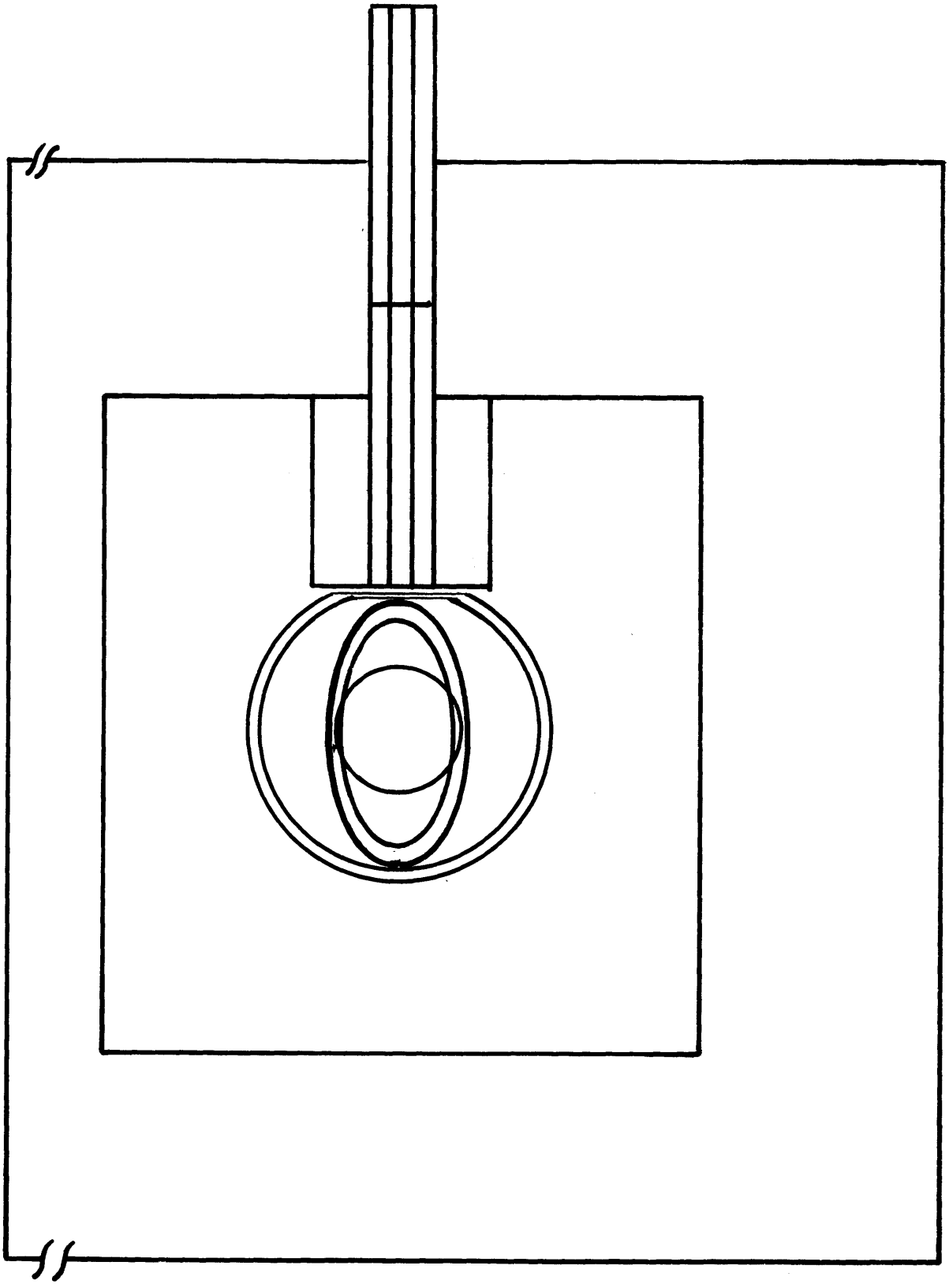

FIGURE 3.11 -- MONTE CARLO MODEL OF THE HAND IRRADIATION FACILITY. SIDE VIEW.

for the total solid angle subtended by the detector is ~2π steradians. This means that if the counting time were 2000 seconds following a cooling time of 60 seconds, about 86% of the estimated 163,000 $^{49}Ca^*$ decays would be detectable with an efficiency of .16 x .86 x .5. Thus the 3.1 MeV full energy peak area would contain about 11.000 counts. The $^{49}Ca^*$ activity in the arm (about 7% of the $^{49}Ca^*$ produced in the hand) may be effectively shielded from the NaI detectors by Pb shielding placed around the forearm before the counting begins. A conservative estimate for the 3.1 MeV photon leakage through a 3" Pb shield is ~5%. Therefore, at the very worst, the $^{49}Ca^*$ activity in the arm would represent about .35% of the total ^{49}Ca activity monitored.

3.4 Calculation of Repositioning Uncertainty With ANISN In the Adjoint Mode

The model shown in Figure 3.6 was used for this calculation of the repositioning uncertainty with ANISN used in the adjoint mode. In this mode (Section 2.2) ANISN solves the adjoint equation to the Boltzman transport equation. Recall from Section 2.2 that in this calculation, when the Ca absorption cross sections are given as the source for a region, the adjoint function for which we solve describes the fractional increase in the Ca absorptions due to a single neutron of some energy group introduced in the region where the adjoint solution is obtained. To obtain the activations due to a ^{252}Cf source at this location, we need only to multiply this solution by a normal-

ized ^{252}Cf neutron spectrum [see Bell (1970)]. In this manner an estimate of the Ca activations in the bone (region 10) due to a ^{252}Cf source in any of the regions 2-7 of the model may be obtained. Assuming the principle of superposition, the bone Ca activations for the hand equally spaced between two sources is obtained by simply doubling the response from one source. To obtain the activations for a 1cm displacement of the hand, again we apply the principle of superposition in the following manner. If the hand is positioned equally between two sources then it is x cm away from both. After a 1cm displacement (lateral) occurs, the hand will be x+1 cm away from one source and x- 1 cm away from the other. Thus for two sources separated by 2x cm, the activations in the hand displaced 1cm is obtained simply by adding the response from a source x+1 cm away from the hand to the response from a source x-1 cm away from the hand. Table 3.2 and Figure 3.7 present the results of this adjoint calculation. For a 12 cm bilateral source spacing, these results indicate that a 1 cm lateral displacement of the hand from the central plane between the sources, would result in a 0.5% change in Ca activations.

Note that the transverse dimensions of this model (30 cm by 38 cm) were taken as the average of the transverse dimensions of the hand and H_2O tank in the Monte Carlo model. A buckling correction (code option, see Section 2.2) was used

to stimulate the effects that would be produced by these dimensions. The accuracy of the buckling correction employed by ANISN has been experimentally shown, at least in one instance, to be excellent [Zamenhof (1975)].

3.5 Predicted Total Uncertainty Of A Ca Measurement

The principal components of the total error for N counts of the $^{49}Ca^{*}$ decay gamma ray are (1) Poisson statistics, (2) repositional error and (3) analysis (systematic) errors. For a measurement of Ca which produces N counts (of the 3.1 MeV photon), the total statistical and analysis error is approximated by

$$\sigma_n = [\sigma_p^2 + (\sigma_a x n)^2]^{1/2} \quad \text{where}$$

σ_p^2 = variance of the mean due to Poisson statistical fluctuation = N

σ_a = fractional analysis or systematic error $\equiv$ .005 (assumed)

Thus for a two minute irradiation and approximately half hour counting period netting ~11,000 photon counts, the error (one standard deviation) due to Poisson statistics and analysis is ~1.1% (of N). Assuming that the total uncertainty of a Ca measurement is a linear sum of the total statistical and analysis error, and the error due to hand displacement, the total measurement error is estimated to be ~1.6% (one standard deviation). The assumed systematic error is an estimate of the error due to interference from Ca activations

in the forearm and to some extent from contributions of the Na 2.75 MeV peak to the background under the 3.1 MeV peak.

3.6 Comparison With Other Existing Facilities

The designed ^{252}Cf hand irradiation facility as is shown in Table 3.1 can be very favorably compared to other facilities presently in use. The facility in Orsay (France) uses both ^{238}Pu-Be, and ^{252}Cf neutrons since it was designed to measure both Ca and P. The higher energy ^{238}Pu-Be neutrons are needed to excite the $^{31}P(n,\alpha)^{28}Al$ reaction which has a threshold of a 3.5 MeV: The Hammersmith Hospital facility (London) uses cyclotron produced neutrons produced from 16 MeV deuterons on Be for the same type of study. This facility uses 4-6 cm of paraffin wax to moderate the fast neutrons as well as the H_2O in the hand. For both irradiation facilities, the hand is in air rather than H_2O. Catto's facility does have the hand surrounded by H_2O, but it employs one ^{241}Am-Be source and is designed so that the hand is closely centered around the source.

The lower dose per Ca count delivered by the hand irradiator presented in this thesis is attributable to (1) the H_2O moderator between the sources and the hand and (2) the location of the hand at a distance where the signal to dose ratio is near optimal. The superior precision is no doubt due to the engineered thermal flux uniformity.

It should be noted, however, that a true comparison

FACILITY	HAND DOSE (RADS)		C_A COUNTS	PRECISION (1 S.D.)	C_A COUNTS FOR 1 RAD NEUTRON DOSE
	NEUTRON	GAMMA			
MAZIERE (ORSAY)	1.4	1.0	5,000	± 3%	3,570
CATTO (SCOTLAND)	0.5	0.5	2,000	± 5%	4,000
SPINKS (HAMMERSMITH)	1.5	-	5,500	~ ± 2%	3,670
M.I.T. (DESIGNED)	0.3	0.3	10,500	± 2%	35,000

TABLE 3.1--INTERCOMPARISON OF THE M.I.T. DESIGNED HAND IRRADIATION FACILITY WITH SIMILAR FACILITIES AROUND THE WORLD

between this facility, and the Orsay and Hammersmith facilities cannot be made since the latter facilities are designed to measure both Ca and P. Consequently these facilities must employ fast neutrons (En>3.5MeV) which deliver a larger dose than would be required if only Ca were to be measured.

III. EXPERIMENTAL STUDIES

4. CHARACTERIZATION OF ^{10}B ASSAY FACILITY

Several experiments were carried out to experimentally meaure the important performance parameters of the boron assay facility (Section 2) and to determine the accuracy of the design calculations. The specific goals were:

(1) Measurement of the thermal flux distributions along sample tubes #1, #2, and #3 (Figures 4.1 and 4.2), using Mn and Cd covered Mn foils.

(2) Measurement of the Mn-Cd ratios along sample tubes #1, #2, and #3.

(3) Measurement of the fast neutron flux in the detector portal using threshold foils.

(4) Measurement of the surface dose rates using standard survey meters.

(5) Measurement of the background photon spectrum at the detector portal using a Ge(Li) detector.

4.1 Foil Measurements

4.1.1 Thermal Neutron Flux Distributions and Mn-Cd Ratios

The thermal neutron flux distributions within the boron assay facility were measured along the tubes labeled #1, #2, and #3 in Figures 4.1 and 4.2. The measurements were carried out using bare and Cd covered

Mn (81.3 wt. %) in Cu foils placed in a slotted stainless steel tube (diameter = 1.2 cm and wall thickness = .08 cm) to maintain precise foil positioning. Six foils, positioned at 5 cm intervals, were used so that the thermal flux distribution along approximately one-half the length of each sample tube was measured for each irradiation. The dimensions of the Mn in Cu foils were .05 mm thick and 0.95 mm in diameter. The self shielding of these foils was estimated to be negligible (Beckurts (1964)). The cadmium covers were slightly thicker than 1.0 mm (.040"). A cutoff energy of .678 eV has been calculated for this thickness of Cd when 1/v absorbers are used (Stanford (1964), Westcott (1958)).

The Thermal Flux is determined from the basic relation:

$$\text{Reaction rate} = R = N \int_0^\infty n(E) v \, \sigma_a(E) \, dE \text{ reactions per second} \qquad (4.1)$$

where

N = total number of target atoms

$\sigma_a(E)$ = absorption cross section at energy E

$n(E)$ = number of neutrons per unit volume per unit energy interval

v = neutron velocity

For a foil which has a 1/v absorption cross section below the Cd cutoff energy the following relation holds

$$R_{E_{Cd}} = N\ \sigma_{TH}\ v_{TH} \int_0^{E_{Cd}} n(E)\ dE \tag{4.2}$$

$$= N\ \sigma_{TH}\ (n\ v_{TH}) \tag{4.3}$$

where

$R_{E_{Cd}}$ = reaction rate due to neutrons below the cutoff energy

E_{Cd} = Cd cutoff energy

σ_{TH} = absorption cross section at 2200 m/sec

v_{TH} = 2200 m/sec

Thus the thermal flux stated at the neutron velocity of 2200 m/sec is

$$\phi_{2200} = \frac{R_{E_{Cd}}}{N\ \sigma_{TH}} \tag{4.4}$$

If bare and Cd covered foils are used to determine $R_{E_{Cd}}$, then

$$\phi_{2200} = \frac{(R_{bare}/N_{bare}) - R_{covered}/N_{covered})}{\sigma_T} \tag{4.5}$$

The reaction rates of the bare foil (R_{bare}) and the Cd covered foil ($R_{covered}$) are determined from the measured activity, A, of each foil by:

$$A = R\ (1 - e^{-\lambda t_i})\ (e^{-\lambda t_w} - e^{-\lambda t_c})\ x\ \varepsilon \qquad (4.6)$$

where:

λ = decay constant of the activated nuclide

t_i = time of irradiation

t_w = time from end of irradiation to beginning of count

t_c = time from end of irradiation to end of count

ε = fraction of the emitted photons which is detected (total detection efficiency for the counting geometry and the energy Cd of the monitored photon).

The cadmium ratio, CdR is given by

$$CdR = \frac{(R_{bare}/N_{bare})}{(R_{covered}/N_{covered})} \qquad (4.7)$$

Equations 4.5 and 4.6 were used to determine the thermal flux and equation 4.7 was used to determine the cadmium ratios. The measurements of the Mn-Cd ratios and of the thermal flux distributions were carried out in the following manner. First, each set of six bare foils was irradiated for approximately 12 or more hours, so that the saturation activity was obtained. These foils were then counted with a Ge(Li) detector, and 1024 channel multichannel analyzer, and

associated electronics. The total counts under the Gaussian shaped ^{56}Mn peak (E_γ = .847 MeV) were recorded and the background counts were subsequently subtracted. The background was determined by averaging over the counts in 3 channels on both sides of the peak and multiplying by the number of channels in which the ^{56}Mn peak was recorded (6 channels). The absolute detection efficiency (i.e. fraction of emitted photons that are detected) for the foil counting geometry employed, was determined as a function of energy using calibrated disc shaped standards. These were ^{54}Mn, ^{60}Co, ^{137}Cs, and ^{22}Na standards with ±3% precise activity calibrations. A straight line on a full logarithmic plot of the detection efficiency as a function of energy was obtained so that accurate interpolating of the absolute detection efficiency at the energy of the ^{56}Mn decay gamma ray (.847 MeV) was possible. Moreover, the ^{54}Mn standard E_γ = .835 MeV) provided a measurement of the absolute efficiency at an energy only .012 MeV from the energy of the ^{56}Mn decay gamma ray emitted from the activated foil. Thus the error in the measured absolute detection efficiency for the .847 MeV photon is estimated to be, at worst, ~±3%.

After the bare Mn foils were irradiated and removed from the facility, they were replaced by Cd covered foils at identical locations. Thereafter these Cd

covered foils were treated in the same manner as were the bare foils, and the resulting measured activities were used in equation 4.5 to determine the absolute thermal flux.

The thermal neutron flux distributions determined in this manner are plotted in Figures 2.13, 2.14, and 2.15. These are the thermal flux distributions measured along tubes #1, #2, and #3 of the boron assay facility and are compared to the corresponding Monte Carlo calculations of these distributions. In view of the geometrical complexity of the assay facility (four different materials and four separated sources), the small size (30 cm of D_2O is $\sim$ 1/4 diffusion length), and a large variation in thermal flux values (factor of 30 difference between the minimum and maximum values), the overall agreement between the experimental and calculated distributions is remarkable.

The experimental and calculational agreement along tube #1 is most outstanding. These two sets of thermal flux values agree to well within 1 standard deviation of each value over the entire length of the tube. The same results agree equally as well in tube #2 along parts of the tube which are not in the region of the cluster of bismuth cylinders, (i.e. the outermost 8 cm on both ends of tube #2). The agreement within the region of the cluster of four bismuth cylinders is the poorest in the

facility - the calculated values are approximately 30% higher than the experimental ones. The results for tube #3 also show two levels of agreement. Along the positive half of the tube (in the direction below the fourth source), the agreement again is within the error limit of one standard deviation. Along the negative half of the tube, the calculated thermal flux values are approximately 25% lower than the experimentally measured values.

There are several factors and effects which may produce the differences that are observed in figures 2.14 and 2.15. One possible explanation might be shifts in the thermal spectrum due to leakage and absorption which cannot be accounted for in the calculations because of the broad thermal group structure (E_T = $\sim$ 0 - .152 eV) and corresponding group averaged cross sections. Following this reasoning, the decrease in the thermal flux (in comparison to the calculated flux) in the region of the B_i cluster along tube #2 might be due to the removal of low energy neutrons by the Bi which has a macroscopic absorption cross section $\sim$ 30 times larger than D_2O and a σ_a/σ_s ratio $\sim$ 50 times larger than D_2O. Consequently, the average energy of the thermal neutrons increases. Since the Mn foils are 1/v absorbers, this absorption hardened neutron distribution activates these foils at a lower rate (than would a Maxwellian

distribution). The result is a measured thermal flux which is lower than calculated. The difference observed along the negative half of tube #3 (moving away from the detector portal) might be explained in terms of the phenomenon known as diffusion cooling. In this case there is a preferential leakage of neutrons from the high energy end of the thermal spectrum at locations far away from the source and near boundaries. The result is a neutron distribution which is somewhat depleted in the faster neutrons. This "softer" spectrum, therefore, activates the 1/v Mn detectors at a higher rate and results in a higher measured flux than was calculated since such shifts in the thermal neutron spectrum are not calculated by the present code.

Another possible source of these differences could be errors in the elemental cross sections, which could lead to inaccurately calculated fluxes in the vicinity of the Bi or along the floor of the tank near the Li - polyethylene. These reasons are offered as possible explanations and not definitive ones. Additional calculations with codes which compute thermal flux distributions should be carried out to further investigate this difference.

Finally, the Mn-Cd ratios at several points in the three tubes are presented in table 4.3. These range from about 7 inches the middle of tube #2 (between the

cluster of Bi cylinders) to approximately 25 near the middle and negative end of tube #3. At the face of the detector portal, the Mn-Cd ratio is $\sim$ 7. It is of interest to note that for a pure 1/v detector (foil), which measures neutron density, the following relations hold:

CdR = 2	50% of the neutron density is below the Cd cutoff energy
CdR = 7	86% of the neutron density is below the Cd cutoff energy
CdR = 25	96% of the neutron density is below the Cd cutoff energy

These relations are obtained from the definition of the Cd ratio, used in computing the fraction of the total measured neutron density below the Cd cutoff energy. This fraction is given by:

$$\frac{\text{Bare Activity - Cd Covered Activity}}{\text{Bare Activity}} = \frac{\text{CdR-1}}{\text{CdR}}$$

4.1.2 Neutron Spectrum in the Detector Portal

The differential and integral neutron spectra in the detector portal were measured using the

spectrum measurement service of EG & G*. These spectra were computationally (computer code) determined with activation data from gold, cadmium covered gold, arsenic and sulfur foils. These foils wer irradiated for $\sim$ 72 hours within the detector portal, approximately 2.5 cm from the face of the D_2O "cup", so that the integral fast neutron spectrum was determined precisely at the center of the Ge crystal location (within the GeLi detector crystal. The spectrum determination procedure involves iteratively fitting an initially assumed moderated fission spectrum to the foil activation data. Figures 4.4 and 4.5 give the differential and integral neutron spectra as determined by EG & G. Estimated errors here range from 5%-18%. A comparison of the measured and calculated thermal and fast flux values is given below. Note however, that the calculated values are averaged over the volume in region 41 of the Monte Carlo model (IV).

	Calculated ($n\text{-}cm^{-2}s^{-1}$)	Measured ($n\text{-}cm^{-2}s^{-1}$)
Thermal flux	$1.4 \times 10^3 \pm 43\%$	$4.6 \times 10^3 \pm 18\%$
Fast flux (E>500eV)	$2 \times 10^3 \pm 30\%$	$1.4 \times 10^3 \pm 18\%$

*EG & G Nuclear Science and Instumentation Laboratory, 130 Robin Hill Road, Goleta, California 93017.

^{252}CF NEUTRON IRRADIATION FACILITY
FOR BORON ASSAY

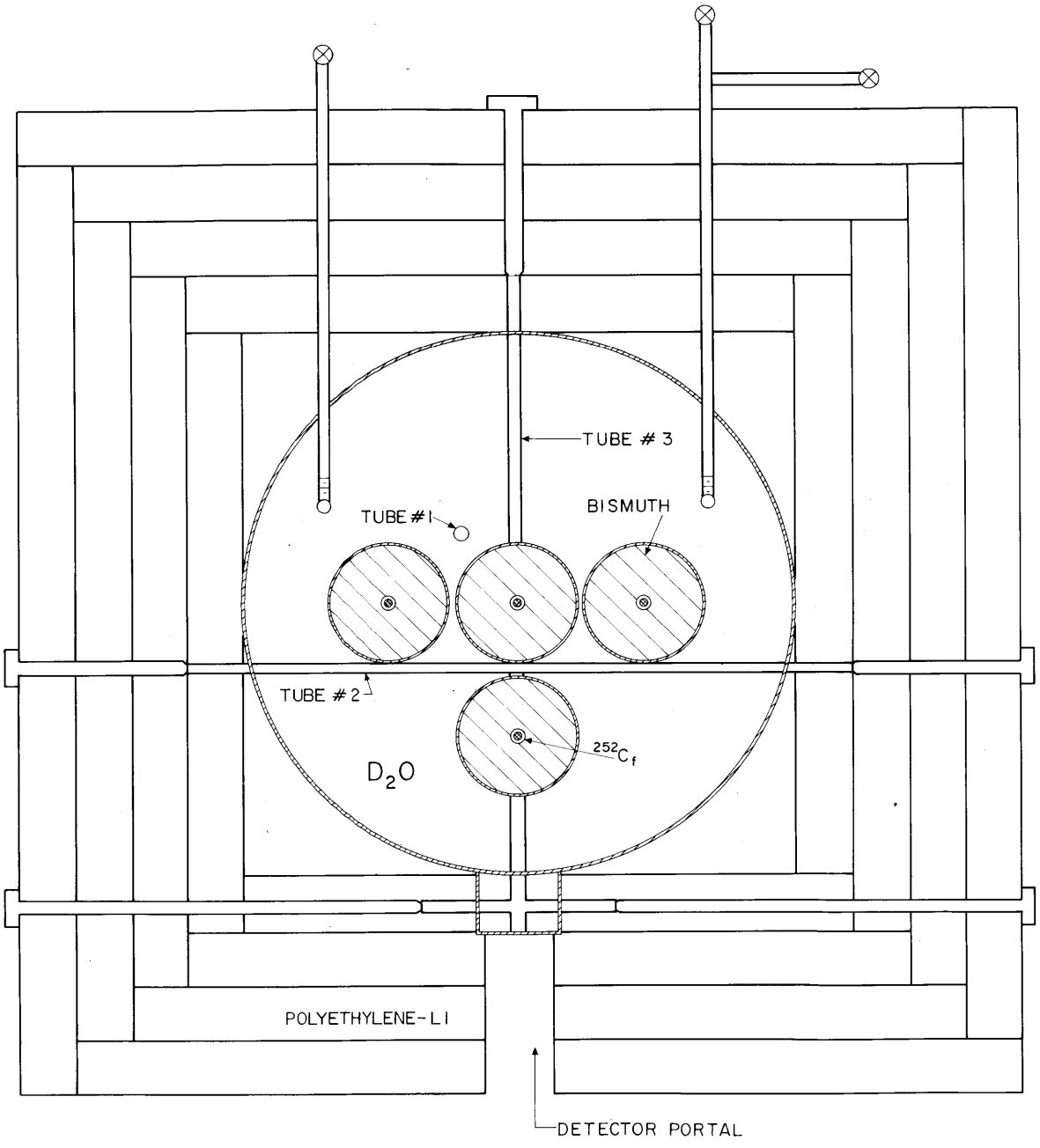

FIGURE 4.1--TOP VIEW

^{252}CF NEUTRON IRRADIATION FACILITY
FOR BORON ASSAY

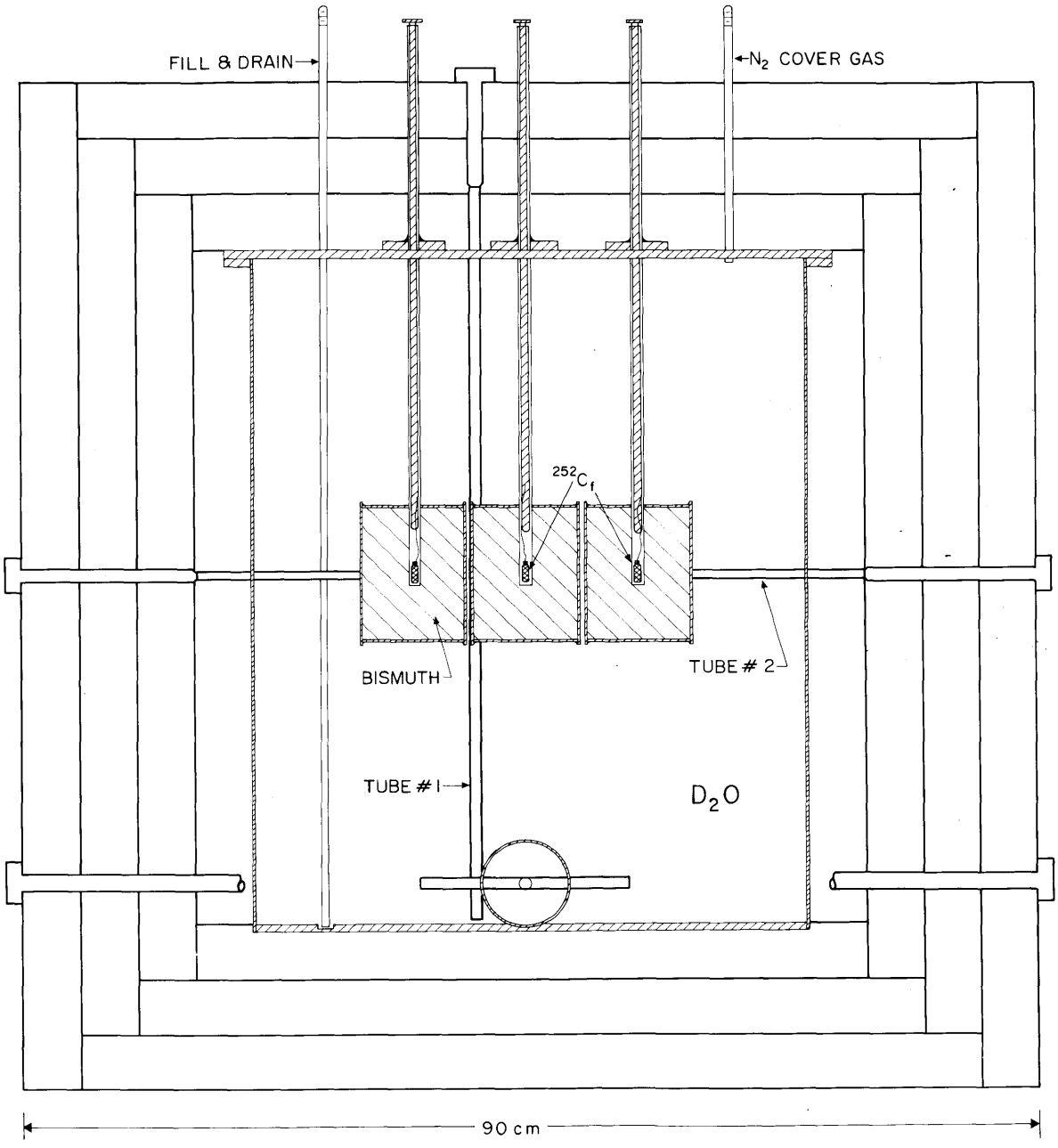

FIGURE 4.2--VIEW FROM THE DETECTOR PORTAL SIDE

FIG. 4.3 -- BORON ASSAY FACILITY SHOWING EXPERIMENTAL ARRANGEMENT USED FOR TEST MEASUREMENTS

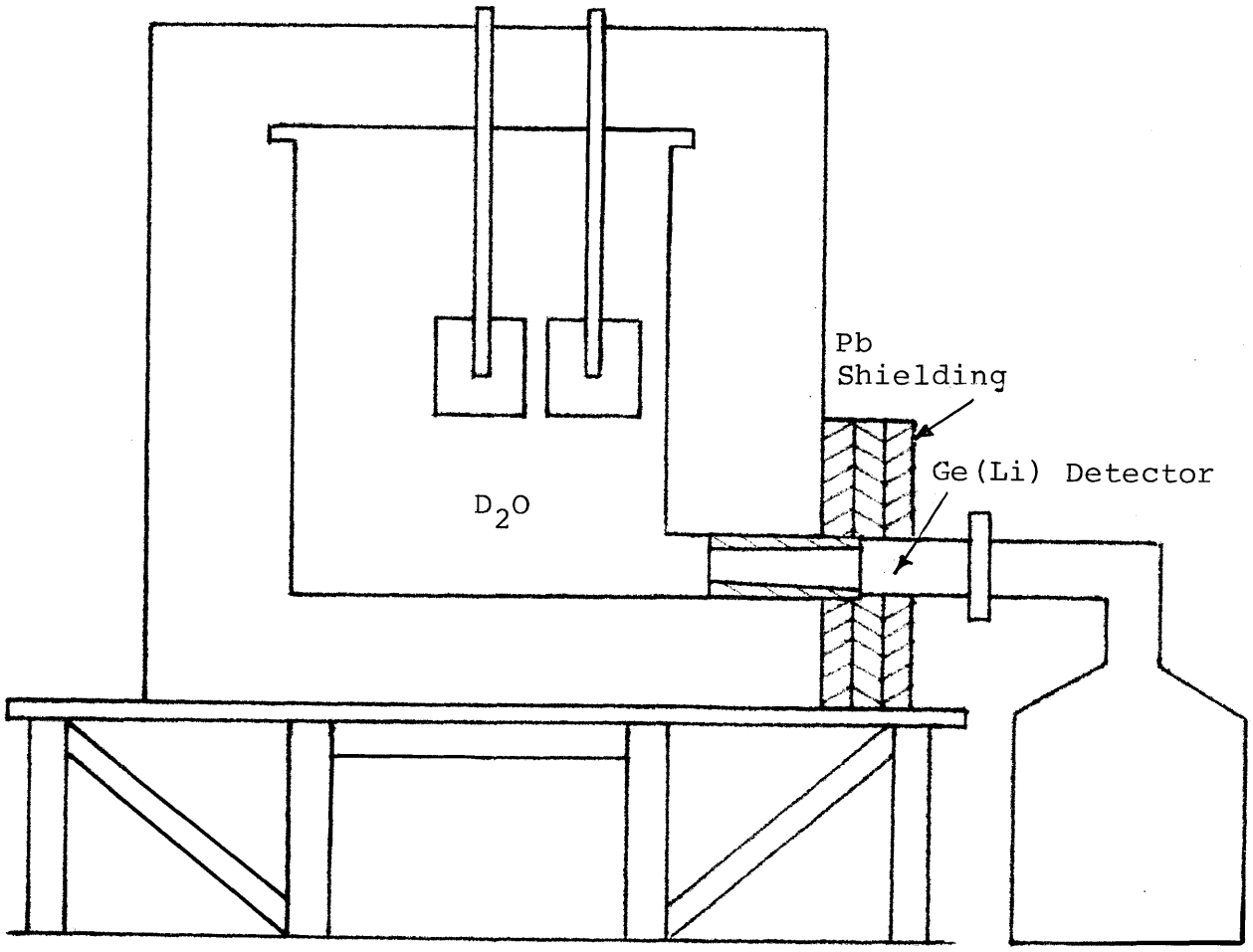

FIGURE 4.4--MEASURED INTEGRAL NEUTRON SPECTRUM IN THE DETECTOR PORTAL OF THE BORON ASSAY FACILITY

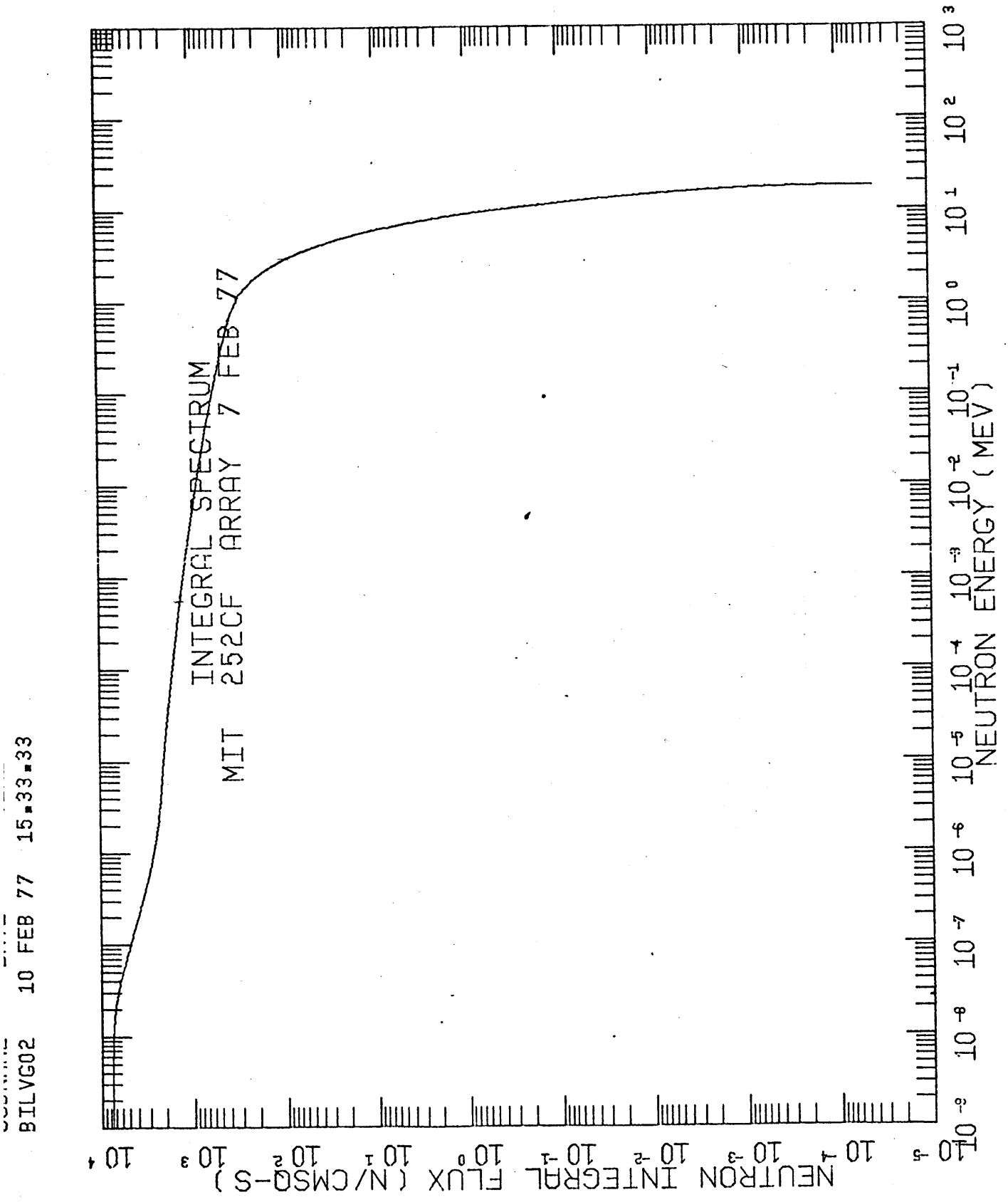

FIGURE 4.5--MEASURED DIFFERENTIAL NEUTRON SPECTRUM IN THE DETECTOR PORTAL OF THE BORON ASSAY FACILITY

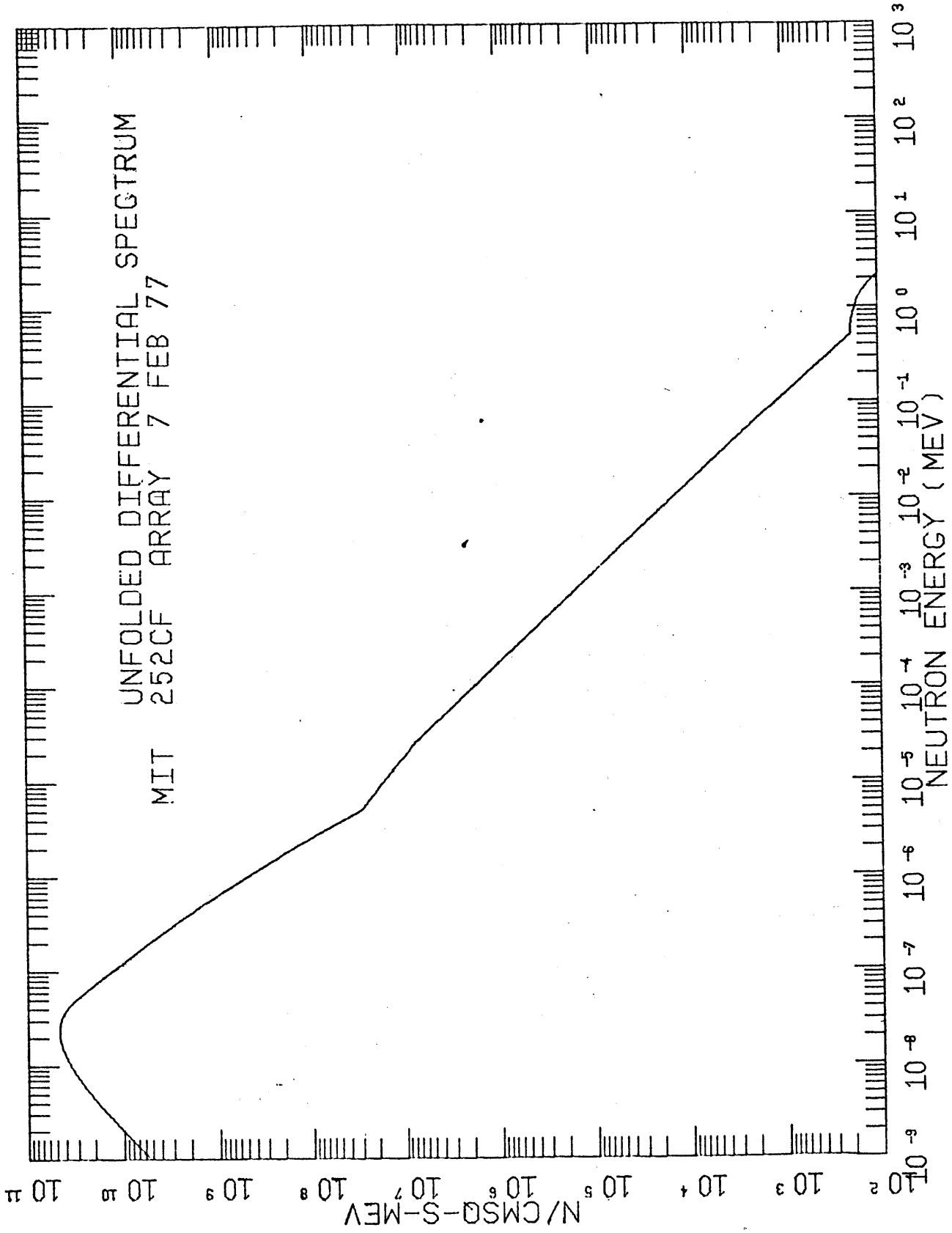

BILVG02 10 FEB 77 15.33.33

SURFACE	DOSE IN MREM/HR.					
	Thm n	Fast n	Total n	Ind γ	Pri γ	Total γ
FRONT: Y Plane						
Calculated	<.01	51 $\pm$ 5	51 $\pm$ 5	12.3 $\pm$ .5	4.3 $\pm$ .04	16.6 $\pm$ .7
Measured			50 $\pm$ 5			15 $\pm$ 1.5
BACK: $-$Y Plane						
Calculated	<.01	21 $\pm$ 4	21 $\pm$ 4	8.4 $\pm$ .3	2.7 $\pm$ .03	11.1 $\pm$ .5
Measured			20 $\pm$ 2			13 $\pm$ 1.3
LEFT: $-$X Plane						
Calculated	<.01	47 $\pm$ 8	47 $\pm$ 8	11.8 $\pm$ .7	3.7 $\pm$ .04	15.5 $\pm$ 1
Measured			35 $\pm$ 3.5			13 $\pm$ 1.3
RIGHT: X Plane						
Calculated	<.01	38 $\pm$ 6	38 $\pm$ 6	9.3 $\pm$ .4	3.7 $\pm$ .04	13.0 $\pm$ .5
Measured			35 $\pm$ 3.5			13 $\pm$ 1.3
TOP: Z Plane						
Calculated	<.01	17 $\pm$ 4	17 $\pm$ 4	11.2 $\pm$ 3.4	3.1 $\pm$ .03	14.3 $\pm$ 4.3
Measured			20 $\pm$ 2			50 $\pm$ 5

TABLE 4.1 -- CALCULATED AND MEASURED DOSE RATES AT VARIOUS SURFACES OF THE BORON ASSAY FACILITY CONTAINING 320 μG OF ^{252}Cf.

ENERGY GROUP	ENERGY MeV	INDUCED ϕ_{γ_1} (γ-cm^{-2}-s^{-1})	% OF TOTAL IND γ DOSE
31	9 - 10	1.7×10^{1}	<1
32	8 - 9	1.5×10^{1}	<1
33	7 - 8	1.5×10^{2}	10
34	6 - 7	1.1×10^{2}	7
35	5 - 6	1.1×10^{2}	6
36	4 - 5	3.1×10^{2}	15
37	3 - 4	2.5×10^{2}	10
38	2 - 3	7.0×10^{2}	23
39	1 - 2	2.3×10^{2}	5
40	.5 - 1	7.1×10^{2}	9
41	.1 - .5	2.5×10^{3}	13
42	.01 - .1	1.3×10^{2}	<1

TABLE 4.2 --CONTRIBUTION TO THE TOTAL INDUCED GAMMA RAY DOSE BY THE INDUCED GAMMAS IN EACH ENERGY GROUP AT THE SURFACE OF THE BORON ASSAY FACILITY

DISTANCE FROM CENTER OF TUBE (cm)	Mn-Cd RATIOS TUBE #1	TUBE #2	TUBE #3
30			7.5 ± 20%
28	16.6 ± 5%		
25		16.5 ± 4%	15.6 ± 17%
23	18.7 ± 5%		
20		6.4 ± 3%	16.8 ± 13%
18	13.1 ± 5%		
15		6.7 ± 3%	23.3 ± 9%
13	11.2 ± 4%		
10		6.0 ± 3%	22.0 ± 7%
8	10.2 ± 4%		
5		5.4 ± 3%	19.7 ± 6%
3	8.4 ± 3%		
0		5.3 ± 3%	19.2 ± 6%
-3	10.3 ± 3%		
-5		5.8 ± 3%	20.8 ± 6%
-8	7.5 ± 4%		
-10		5.8 ± 3%	20.2 ± 8%
-13	10.7 ± 5%		
-15		7.2 ± 3%	24.7 ± 10%
-18	10.3 ± 5%		
-20		7.2 ± 4%	24.0 ± 13%
-23	20.4 ± 5%		
-25		7.4 ± 4%	
-28	17.3 ± 5%		

TABLE 4.3 -- MN-CD RATIOS WITHIN TUBES #1, #2, AND #3 OF THE BORON ASSAY FACILITY

MATERIALS USED IN THE CONSTRUCTION OF THE BORON ASSAY FACILITY

Tank:

Stainless Steel, Types 304 and 316

Fe ~ 70%
Ni ~ 18%
Cr ~ 8%
Mn ~ 2%

Source Photon Shielding:

Bismuth

Moderator:

Reactor Grade D_2O

Biological Shielding:

10% by Weight Natural Lithium Loaded Polyethylene

Lithium Carbonate

CH_2
$N_H = 5.5 \times 10^{22}$ Hydrogen atoms/cc
$N_{Li} = 1.07 \times 10^{22}$ Lithium atoms/cc
$\rho = 1.25$ gm/cc

TABLE 4.4

4.2 EXTERNAL DOSE MEASUREMENTS

4.2.1 Experimental Measurements and Calculated Values

Both the neutron and total gamma ray doses were measured at the four side surfaces and at the top surface of the constructed boron assay facility. Because of a lack of access to the bottom surface, no dose measurements were made there. The following survey meters were used to measure neutron and gamma ray doses:

(1) Neutron Dose Rate Meter

Type: ^{6}LiI(Eu) scintillation detector with 10" high density polyethylene spherical moderator

Make: Ludluar Measurements Inc., model 42-4

Accuracy: $\pm$ 10%

(2) Gamma Ray Dose Rate Meter

Type: Geiger counter

Make: Precision Radiation Inst. Inc., Model 121

Accuracy: $\pm$ 10%

Table 4.1 presents the Monte Carlo calculations of the thermal neutron dose, fast neutron dose, induced

gamma ray dose, and the dose delivered by primary or source gamma rays at the various facility surfaces. The measured neutron dose is compared to the calculated total neutron dose, and the measured gamma ray dose is compared to the calculated total gamma ray dose. As shown, most of the calculated doses and corresponding experimental measurements of the doses agree to within one standard deviation, and all except one, agree to well within two standard deviations. The one exception is the measured gamma ray dose at the top surface. This measurement is approximately 3 times the calculated value, and this difference is attributed to an increased gamma ray flux which results from the absence of Bismuth (just above the sources) within the source tubes. Neither of these tubes nor the openings around them were included in the calculational model.

Note that one correction factor was employed in calculating the induced gamma ray doses. This correction factor, which results from the use of Pb cross sections to simulate Bi, is explained in the next section.

4.2.2 Analysis of Dose Components

A complete knowledge of the total dose components and their origins is necessary if design improvements, to effectively reduce

dose rates, are to be realized. In table 4.1, the thermal neutron, fast neutron, primary gamma ray and induced gamma ray doses at the surface of the facility are itemized. The first three doses are due to direct radiations from the source and hence can be attenuated further by simply adding appropriate shielding. The latter dose, on the other hand, is due to gamma rays induced by neutrons so that an addition of shielding or other materials could increase this component of the total dose. Since this total dose component arises from a number of nuclear reactions in several materials in a small complex geometry, it is not an easy task to precisely identify and determine the relative contribution of the radiations from the various possible reactions to the dose. Nonetheless, a general analysis of the induced gamma ray dose can be made.

We begin by examining the induced gamma ray dose at the surface. An analysis of the induced gamma ray dose components can be made by examining the induced gamma ray dose as a function of energy at the surface of the facility. The multigroup induced gamma ray spectrum and the fractional contribution of each energy group flux to the dose (induced gamma) is given in table 4.2. In this calculation, the group 33 (E = 7-8 Mev) fluxes were adjusted by a factor of 1/5

to account for the factor of 5 larger photon production cross sections of Pb (E_γ = 7.38 MeV) which were used in the simulation of Bi. This correction, of course, assumes that all of the gamma rays in group 33 (7-8 MeV) are the 7.3 MeV radiative capture gamma rays from Pb. This is a reasonable assumption since the value of the group 33 flux at the surface of Monte Carlo model II of the boron assay facility (which contained no Pb) is < 2% of the same flux in model IV. Recall, however, that the correct thermal neutron absorption cross section of Bi was employed in the Monte Carlo calculations. This cross section is separate and distinct from the photon production cross section.

Several conclusions are apparent when the induced gamma ray spectrum at the surface of Model IV of the facility is compared to the spectra at the surface of Model II. Recall that Model II differs from IV primarily in that it has an AL D_2O tank, no Pb or "Bi", and 15 cm of Polyethylene-Li shielding on the sides.

Since apparently most ($\sim$ 98%) of the group 33 flux is due to the Pb 7.3 MeV radiative capture gamma, then we conclude from table 4.2 that 10% of the total dose is contributed by Pb capture gamma rays. If the correct Bi gamma production cross sections had been used, however, the gamma flux which now appears in group 33 would appear instead in group 36 (4-5 MeV).

Since the dose factor for group 36 is ∿0.7 the dose factor for group 33, the total dose from these Bi capture gammas would decrease by this factor. It is difficult, however, to conjecture on the basis of these calculations what per cent of the total dose group 36 would then contribute since the source of the present group 36 gamma ray is not known for certain. However, a simple calculation of the iron radiative capture reaction rate in the 0.16 cm thick stainless steel (~75% Fe) wall of the D_2O tank, and a comparison of group 37-34 flux is at the surfaces of the various calculational models, indicates that Fe (n,γ) radiation comprise as much as 90% of the included gamma rays in these groups. [Rasmussen (1969)]. Therefore, it appears that capture gammas from the steel tank may contribute as much as ∿30% of the induced gamma dose. The exact percentage cannot be determined since some of the gamma rays in group 24-27 are due to downscattered Pb gamma rays. In the context of the total dose at the surface of the facility, this component is not very significant, however, a better understanding of its present contribution and potential contributions in other systems requires further investigation.

In addition to these large components of the induced gamma dose, it appears that (1) the 2.22 MeV

radiative captive gamma rays from hydrogen in the polyethylene may produce as much as $\sim$ 20%, (2) the .511 MeV annihilation gamma rays induced primarily in the Bi by pair production reactions of Bi prompt x-rays may produce as much as $\sim$ 9%, and (3) the .477 MeV x-rays from the inelastic scattering reaction ^{7}Li (n,n') may contribute as much as $\sim$ 13% of the induced gamma dose. These percentages are upper limit values as it is impossible to determine them precisely for the reasons previously explained. The presence in the actual facility of the principle reactions cited, has been demonstrated experimentally and is discussed in the next section.

4.3 Photon Spectroscopy - Measurement and Analysis of Background Spectrum

A number of background spectra were taken at various positions around the boron assay facility. In the absence of a Ge(Li) detector, the background spectrum was first measured with a 2" x 2" NaI(Tl) detector. A typical NaI(Tl) spectrum at the detector portal is shown in figure 4.5. The most outstanding feature of this spectrum is the .511 MeV annihilation gamma ray peak. The count rate associated with this peak was observed to be correlated to the source to

detector distance. The maximum .511 MeV count rate was observed with the detector at the center of the front side (+ x plane in Monte Carlo model) of the shielding, the external position closest to the effective center of the four source configuration. Generally, this concurs with the Monte Carlo calculations which indicate that the .511 MeV annihilation gamma rays predominately originate in the Bi around the sources. Two channels of .511 MeV gamma ray production in the Bi are likely. First, as discussed in section 4.2.2, the 4.17 MeV radiative capture gamma rays produced within the Bi cylinders (which are in a high thermal neutron flux region), have a pair production coefficient to total attenuation coefficient ratio of $\sim$ 0.5. Thus approximately 50% of these radiative capture gammas which interact within the Bi cylinders do so by pair production. Secondly, the source gammas which have a spectrum of energies from 0-10 MeV also have an appreciable probability of interacting within the Bi by pair production. If one assumes that all the .511 MeV annihilation gamma rays which are generated within their last mean free path of Bi ($\sim$ 2 cm) escape, and computes the flux of these gamma rays at the surface of the facility, a rough accounting of the group 40 (.5-1 MeV) flux computed by ANDY can be made.

A final possible major source of measured 0.511 MeV annihilation radiation is the large ammount of Pb detector shielding which gives rise to annihilation gammas after high energy gamma rays emerging from the assay facility interact by pair production in the Pb.

Unfortunately, the resolution of the NaI(Tl) crystal ($\sim$ 9% FWHM at .511 MeV) precludes use of this detector for measuring small amounts of ^{10}B. The futility of using NaI(Tl) as a detector for this application was realized after repeated attempts with various shielding configurations failed to produce a resolvable ^{10}B signal. Further, the intensity of the background and the high NaI(Tl) efficiency combine to yield high counting dead times of 20-25% even with 2.5 cm of Pb in front of the detector.

The first Ge(Li) background spectrum was taken at approximately 170 cm from the front side surface of the assay facility. This spectrum revealed an additional prominent and important peak which was not observed before. Unfortunately, this peak was due to the $^{7}Li(n,n')$ reaction which gives rise to a .477 MeV from the first excited state of the recoiling ^{7}Li nucleus. Recall that this gamma ray is identical to the .477 MeV gamma ray emitted from the recoiling excited ^{7}Li nucleaus produced in the ^{10}B (n,α) ^{7}Li reaction. Consequently,

this inelastic scattering reaction which has a threshold at approximately .5 MeV produces a .477 MeV peak with the same doppler broaden shape which is characteristic of the .477 MeV from the $^{10}B\ (n,\alpha)^{7}Li$ reaction. Because this $^{7}Li\ (n,n')$ reaction has a threshold at approximately .5 MeV with a cross section at 1 MeV of $\sim$ .175 barns, it was not at the time the facility was constructed expected to significantly contribute to the background spectrum. In retrospect, however, its presence and intensity can be fully accounted for.

In accounting for this peak, it is convenient to relate it to a peak with which we are familiar such as the H capture gamma peak. Estimations of the macroscopic cross section of the polyethylene-Li are:

$$\Sigma_{is}^{^{7}Li}\ (1MeV) = .00198\ cm^{-1}$$

$$\Sigma_{a}^{H}\ (TH) = .0167\ cm^{-1}$$

From the ANDY calculations it was found that within the polyethylene shielding the thermal neutron flux is approximately equal to the integral neutron flux above 1 MeV (i.e. $\phi(TH) \sim \int_{1\ Mev}^{\infty} \phi\ (E)$). Hence, the ratio of the .477 MeV gammas to the 2.22 MeV H capture

gammas produce in the polyethylene-Li shielding can be approximated by:

$$\sim \frac{\sum_{is}^{^7Li}(1\ MeV)}{\sum_{a}^{H}(TH)} = .12$$

Thus the expected ratio of the .477 MeV count rate to the 2.22 MeV count rate is approximately:

$$\frac{\text{detected .477 MeV } \gamma/\text{sec}}{\text{detected 2.22 MeV } \gamma/\text{sec}} \sim \frac{.12 \times \text{detector } \varepsilon \text{ at .477 MeV}}{\text{detector } \varepsilon \text{ at 2.22 MeV}}$$

$$\sim .12 \times \frac{.15}{.01} = 1.8$$

This ratio was observed in the background spectrum (measured at 170 cm) to be $\sim$ 1.4, where the detected .477 MeV background activity at this distance was $\sim$14 counts per second.

In addition to this verification of the intensity of the ^{7}Li inelastic gamma ray, the absolute count rate at 170 cm can be roughly calculated by assuming that all of the .477 gamma rays produced in their last mean free path of polyethylene-Li ($\sim$ 12 cm) escape and constitute an isotropic plane source (Lamarsh (1975)). When the fraction of these gamma rays which would be counted by the detector is computed, the approximate measured value of $\sim$ 10 cps is obtained. An integrated

threshold neutron flux of 10^4n $cm^{-2}S^{-1}$ was assumed in the polyethylene in this calculation.

At 4 cm from the detector portal (figure 4.3) the Ge(Li) background spectrum contained more features than were observed at 170 cm. A background spectrum was recorded with a Pb shielded detector in the geometry shown in figure 4.3, and with a waterfilled standard 7 ml vial positioned 40 cm from the detector in tube #3. This spectrum was identical to the spectrum (Figure 5.1) without the doppler broaden .477 MeV background peak from the ^{7}Li (n,n') reaction. This result is of course attributed to the Pb detector shield and collimator assembly, and demonstrates its effectiveness.

The other identifiable background peaks are shown in this spectrum (Figure 5.1). These include several Ge radiative capture peaks, some decay gamma ray peaks from neutron activated nuclei, and one electron conversion peak from the ^{72}Ge (n,n') reaction. As expected from the analysis of the calculated outer surface spectrum discussed in section 4.2.2, the principal radiative capture lines of Fe (from the stainless steel tank) and of Ge (in the detector) are evident. The energies and relative intensities of these peaks are in agreement with those given in MITNE 85 [Rasmussen (1969)].

Decay gamma ray peaks at .835 MeV, and .847 MeV are identified from the radioisotopes ^{54}Mn and ^{56}Mn. The ^{54}Mn and ^{56}Mn are produced by $^{54}Fe(n,p)\ ^{54}Mn$ and $^{56}Fe(n,p)^{56}Mn$ reactions in the stainless steel tank. The reactions have thresholds at 0.2 MeV and 0.5 MeV respectively, and their cross sections at 1 MeV are 5.5 barns and 0.75 barns. [Nucl. Data Tables, 11, 8-9 (1973)]

One peak of particular interest is the one at .693 MeV which is produced by the $^{72}Ge(n,n')$ reaction within the detector (Stelson(1971)). This reaction provides an on line monitor of the integral fast neutron flux. Stelson experimentally detemined that for ^{252}Cf neutrons, the approximate fast fluence in the detector can be obtained by multiplying 18 times the area under this peak. The shape of this peak is due to the imperfect conversion of the electrons emitted from the first excited level of the recoiling ^{72}Ge atom.

5. PERFORMANCE OF BORON ASSAY FACILITY

A number of measurements of quantities of ^{10}B were made to evaluate the boron assay facility. Because of two conditions, however, this evaluation of the facility as constructed had to be made with the detector external to the detector portal. Therefore, the quantities of ^{10}B which can be measured using this facility with the detector in its intended location (the detector portal) is extrapolated from the results obtained with the detector outside of the detector portal. The reasons for this test geometry are explained in the next sections.

5.1 Experimental Restrictions

5.1.1 Susceptibility of Detector to Fast Neutron Damage

A severe limitation on the use of the detector is imposed by its susceptibility to fast neutron damage. Although both the foil measurements and the ANDY calculations indicated that the detector could reside within the detector portal for $\sim$ 80 hours (receiving a fast fluence of 6×10^{8} n-cm^{-2}) before suffering a 50% degradation in the energy resolution, fear of irreparable damage of this particular detector prevented its insertion into the detector portal (recall from section 4.3 that this detector had already been redrifted several times).

We therefore chose to perform the various measurements with the detector position external to the detector portal, in a region where the fast neutron flux is a factor of 10 lower(than in the detector portal). Obviously with the detector positioned in this fashion, the solid angle it subtends at the sample (located in the moderator) is diminished. This factor is experimentally taken into account as described in section 5.2.1.

5.1.2 Interfering Photons in the Background From ^{7}Li (n,n') Reactions

In section 4.3.2, the presence of a .477 MeV peak, identical to the .477 MeV peak from the ^{10}B (n,α) ^{7}Li reaction, was noted in the background spectrum and accounted for as originating from the ^{7}Li (n,n') reaction in the Li loaded polyethylene shielding. Recall that this peak (identical to the ^{10}B peak width to within the detector resolution) was relatively intense with 14 cps at 170 cm from the facility. Since the expected count rate for probable amounts of ^{10}B is of the order of 1-10 counts per seconds, this background peak presents a very serious interference problem. Abatement of this problem, without changing the shielding material, requires a moderate amount of detector shielding and collimation. Since the detector portal, as constructed, is too small to accomodate any effective amount of detector shielding,

a second reason for positioning the detector outside of its intended portal, was to locate it so that adequate shielding would be possible. Obviously if this facility is to be used with the present materials which comprise it, the detector portal must be enlarged so that it can accomodate the necessary shielding. This is certainly feasible and should present little or no problem.

5.2 ^{10}B Measurements in Test Geometry

5.2.1 Experimental Setup: Test Geometry vs. Design Geometry

For the reasons explained in the previous section the detector was set up in a test assay geometry shown in Figure 4.3. Recall that in this geometry the detector is positioned so that it is directly in front of the detector portal and 5 cm from the biological shielding. The Pb annulus fits over both the detector and the 5 cm extension of the Pb collimator. At the outermost end of the collimator, the internal opening is sufficiently large to expose the entire active area of the face of the Ge(Li) detector (~13.85 cm^2).

As will be shown, this test assay geometry differs significantly from the design assay geometry where the detector is fully inserted into the detector portal.

With the detector at ~5 cm from the detector portal, the optimal sample location in tube #3 was calculated and experimentally determined. The calculation predicted that with the detector at this position, the product of the thermal neutron flux to which the sample is exposed and the solid angle subtended by the detector at the sample (Δ), would be a maximum with the sample 40 cm from the detector. This point is 10 cm from the center of tube #3, and is the point of maximum thermal neutron flux which is closest to the detector. This calculated optimal sample location was corroborated experimentally.

Because of the smaller solid angle subtended by the detector in this test geometry, the detected count rate per unit sample will be lower than with the detector fully inserted into the portal (design geometry). The detection sensitivity (i.e., count rate per unit sample) for these two different irradiation-detection geometries are related by the following:

$$\frac{\text{TEST geometry sensitivity}}{\text{DESIGN geometry sensitivity}} = \frac{\phi_T(10\text{cm}) \times \Delta(40\text{cm})}{\phi_T(28\text{cm}) \times \Delta(2\text{cm})} \approx \frac{1}{30}$$

where for TEST assay geometry:

sample-detector distance = 40 cm

Δ = .0007

sample distance from tube center = 10 cm

$\phi_T = 1.6 \times 10^5$ n-cm^{-2}-s^{-1}

and for DESIGN assay geometry:

sample-detector distance = 2 cm

Δ = .28

sample distance from tube center = 28 cm

$\phi_T = 1.2 \times 10^4$ n-cm^{-2}-s^{-1}

This solid angle (Δ) for the sample in the design geometry was calculated [Etherington (1958)] assuming that the 7 ml cylindrical sample vial (~5 cm length by 1.6 cm diameter) was positioned parallel to the plane of the detector face.

5.2.2 Results for a ^{10}B Test Sample, Performance Projections, And Comparison With Calculations

Since the maximum count rate per unit sample obtainable with the detector in the design position is thirty times that obtainable with the detector in the est position, the ^{10}B test sample was loaded with thirty times the design basis amount of ^{10}B, i.e. 30x0.1mg=3mg of ^{10}B. Therefore, it was reasoned that the results obtained with this 3mg ^{10}B sample in the test geometry would approximate the results obtainable with a 0.1mg ^{10}B sample in the design geometry. Implicit in this reasoning is the assumption that the photon background can be reduced in the detector portal to the approximate background level that was recorded with the detector in the test

DISTANCE FROM CENTER OF TUBE (cm)	^{10}B SIGNAL + BACKGROUND (sec^{-1})	^{10}B SIGNAL (sec^{-1})	STATISTICAL PRECISION FOR 500 sec COUNT
10 cm	87.89	12.46	± ~5%
	88.19	12.64	
	88.00	12.45	
16 cm	82.20	11.79	± ~5%
	81.73	11.32	
	81.56	11.15	
21 cm	81.10	11.07	± ~5%
	81.37	11.34	
	80.65	10.61	
26 cm	77.41	8.23	± ~7%
	77.56	8.38	
	76.94	7.76	
28 cm	72.79	3.27	± ~16%
	72.66	3.14	
	73.14	3.54	

TABLE 5.1 -- MEASUREMENT DATA FOR A 3 MG ^{10}B TEST SAMPLE AS A FUNCTION OF DISTANCE WITHIN TUBE #3 OF THE BORON ASSAY FACILITY

position. This is not a poor assumption since ANDY calculates that the background in the detector portal will increase by a factor of ~2.3. This increase can be compensated for by adding approximately one-half thickness of Pb or Bi for ~1 MeV gammas (~1 cm) to the minimum thickness of shielding required externally. Table 5.1 presents the measurement results for a 3 mg ^{10}B test sample at various positions within tube #3. (The detector is in the test position.) The net ^{10}B count rates with the sample at 10 cm from the center is of particular interest since it approximates the expected count rate for a .1 mg sample located 28 cm from the tube center with the detector in the portal.

Note that with the test sample at the 10 cm position the average ^{10}B count rate is 12.5 ± .6 counts per second with an average background count rate of 75.5 ± .01 counts per second. If we require that the ^{10}B signal have a statistical standard deviation of 5% then we compute a required counting time of less than 450 seconds. Therefore, if the detector is inserted into the portal and a 0.1 mg ^{10}B sample is positioned 28 cm from the tube center, the ^{10}B count rate should be approximately twelve counts per second. The background counts under the ^{10}B peak from the Compton edge of the ^{1}H 2.22 MeV peak will increase roughly by a factor of 30 since the quantity of H_2O in this sample (~.1 mg ^{10}B/7ml H_2O) will

be the same as was in the test sample (3mg ^{10}B/7 ml H_2O). The count rate under the ^{10}B peak due to the hydrogen Compton tail in the test geometry was experimentally determined to be ~1.5 cps by making measurements with and without 7 ml H_2O samples. Thus an estimate of the total background count rate under the ^{10}B peak in the design geometry is ~120 [= 75 + 30(1.5)] counts per second for 7 ml of H_2O. With this background count rate, a 5% statistically precise measurement of .1 mg ^{19}B in 7 ml H_2O should require ~1000 seconds if the same is 28 cm from the tube (#3) center and the shielded detector is in the portal.

Another important conclusion from the results in the test geometry involves extrapolating a lower detection limit for the design assay geometry. In this case, the goal is to determine the smallest quantity of ^{10}B which can be measured with 5% precision within one hour with the detector in its portal. Assuming again that the background can be shielded to its approximate level as recorded in the test geometry, a lower practical ^{10}B detection limit can be estimated. Note from Table 5.1 that the 3 mg test sample can be measured with ~16% precision in 500 seconds with the sample 28 cm from the tube's center. If the detector were moved from the external test position into its portal, 2cm away from the sample, the count rate would increase by the ratio of the solid angles (a factor of ~120). Thus if the amount of this test sample

	CALCULATED* (ANDY)	MEASURED
^{10}B Signal counts/sec 3mg Sample - Test Geometry	9.5 ± 1	12.4 ± .6
Background Under ^{10}B Peak (counts/sec) - Test Geometry	~90	~75
ϕ_F in Detector Portal ($n\text{-}cm^{-2}\text{-}sec^{-1}$)	$2 \pm .6 \times 10^3$	$1.4 \pm .3 \times 10^3$
ϕ_F at Detector in Test Position ($n\text{-}cm^{-2}\text{-}sec^{-1}$)	$\sim 4.2 \times 10^2$	$\sim 3.2 \times 10^2$

TABLE 5.2 -- CALCULATED AND MEASURED PERFORMANCE PARAMETERS OF THE BORON ASSAY FACILITY

*See Section 5.2.2

were decreased by exactly that factor, the count rate would remain unchanged. We, therefore, conclude that with the detector in its portal, and with adequate shielding 3.0 mg ^{10}B x $\frac{1}{120}$ = .025 mg ^{10}B can be measured with a statistical standard deviation of ~16% in ~1000 seconds when the increase in the H Compton edge is accounted for. Accordingly, if we count for 3600 seconds, a statistical precision of 8.5% can be achieved when measuring .025 mg of ^{10}B in 7 g of H_2O. This, then, is approximately the smallest practical quantity of ^{10}B which is assayable with the desired precision within one hour if the present facility, is used with the addition of shielding around the detector portal.

A general comparison between some of these measured parameters and their calculated values can be made with some qualifications. Table 5.2 gives the measured values of three important parameters. A measured value for one parameter ϕ_F at two locations is given. All of these parameters do not have corresponding calculated values for the identical locations at which they were measured. Thus calculated values for locations which approximate those at which the measurements were made are tabulated. This table is intended only to show a basic agreement between the Monte Carlo calculations and experimental data. In two instances, this is not a true comparison since the calculated values of the background in the 16Kev window

GAMMA RAY SPECTRUM PRODUCED FROM 3 mg ^{10}B IN 7g H_2O IRRADIATED IN THE ^{252}Cf NEUTRON IRRADIATION FACILITY

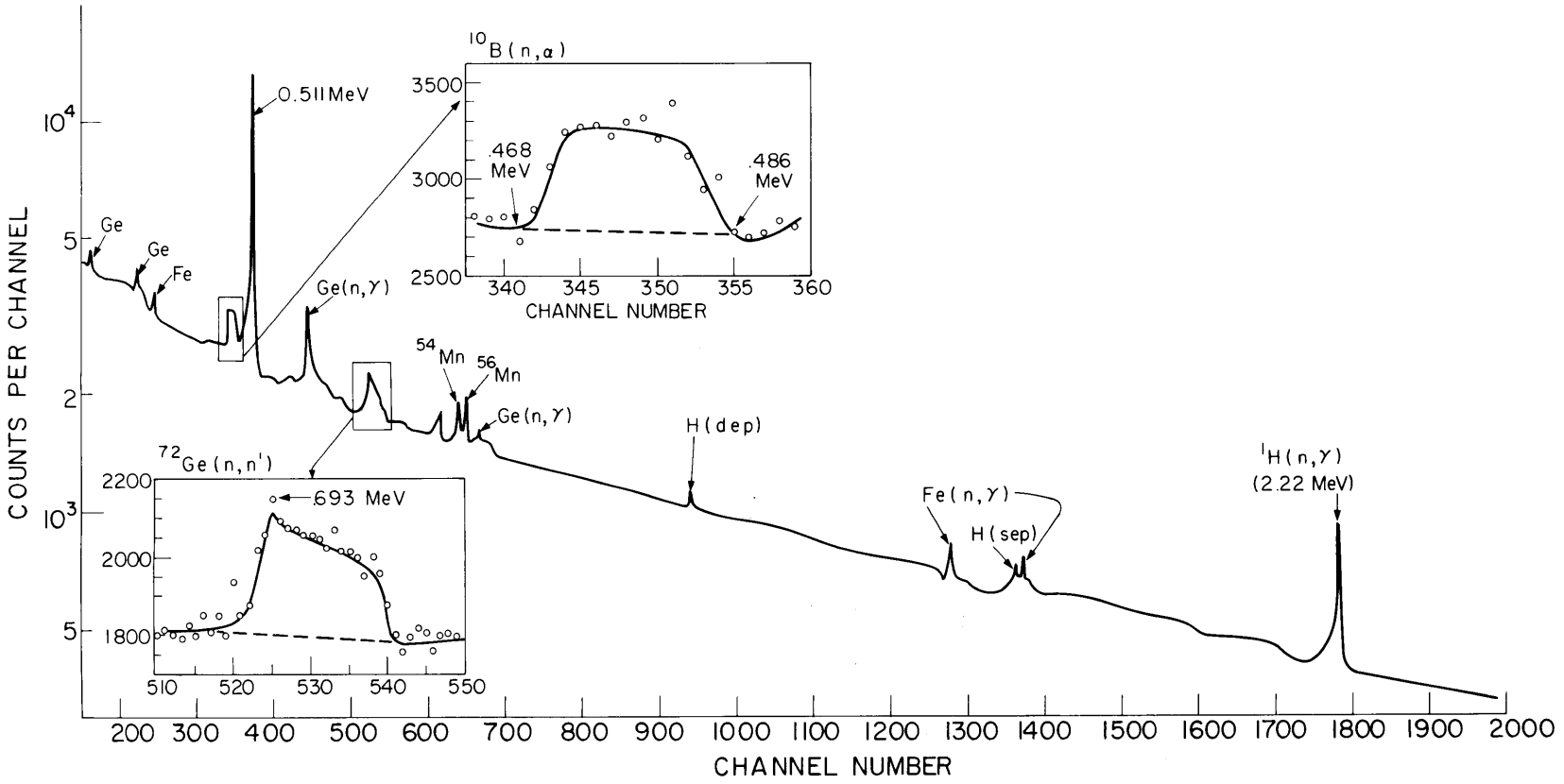

FIGURE 5.1

about .477 MeV and (2) ϕ_F in the detector, need to be multiplied by small correction factors (detector in test position). Unfortunately, calculations of these correction factors require more information than is available. In both cases, however, these correction factors will be <1. and probably between .5 and 1. Thus a general comparison of these ANDY derived results and experimental ones can be made with the above qualifications in mind.

Finally, Figure 5.1 is a photon spectrum recorded with the 3 mg ^{10}B Test sample located 10 cm from the tube center and the detector in the Test position, i.e., external to the detector portal. The features of this spectrum with the exception of the ^{10}B peak, were explained in Section 4.3. The width of the ^{10}B peak is due to and can be accounted for by a first order ($\pm$ v/c) doppler broadening of the .477 MeV gamma ray emitted from the recoiling ^{7}Li nucleus.

5.3 Conclusions

Although a number of conclusions have already been stated within the previous few sections, there are several which should be clearly reiterated.

(1) The fast neutron flux in the lithium loaded polyethylene shielding is sufficiently high to produced a significant background of .477 MeV photons from the $^{7}Li(n, n')$ reaction. These

.477 MeV photons can be eliminated from the background spectrum with a moderate amount (~10 cm) of Bi or Pb.

(2) If one modification of the boron assay facility, as it is now constructed, is made, it will more than meet all design criteria. This modification is the inclusion adequate of a Pb or Bi annulor detector shield around the detector portal. The approximate annular thickness required can be determined semi-empirically.

(3) With the above modification, .1 mg of ^{10}B can be measured with a statistical precision of 5% in less than 1000 seconds. The fast neutron flux of $\phi_F \sim 2 \times 10^3 n/cm^2$-sec would thus allow 300 of these measurements before a fast fluence of $6 \times 10^8 n/cm^2$ is incurred by the detector. Assuming that it may cost $1,600 to redrift a Ge(Li) detector (Canberra industries), the effective cost per measurement is ~$5.00. Note that Stelson (1975) has reported that once a Ge(Li) detector is redrifted after fast neutron damage there is no apparant "memory" of the damage.

(4) The apparent practical lower detection limit of ^{10}B is .025 mg with a ±8.5% precision.

6. ^{10}B ASSAY STUDIES USING MITRII NEUTRON BEAM

An experimental study of the feasibility of using a neutron beam for the assay of boron was conducted. The experimental arrangement employed, the principal results, and a comparison of this system with the ^{252}Cf facility are given in this section.

6.1 Experimental Setup

The irradiation-detection geometry used (in this study) is illustrated in Figure 6.3. The sample is positioned in the neutron beam by means of a small neutron detector to determine the point of maximum flux. As shown, the Ge(Li) detector is aligned at a right angle to the neutron beam and views the sample from a distance of 56 cm. The detector is recessed in a 44 cm long 15 cm thick annular Pb shield. In front of the Pb shield is placed a 2.5 cm thick slab of Li-polyethylene, with an 8 cm diameter central hole, to minimize thermal neutron activations in and immediately around the detector. The data is collected and the energy spectrum recorded by a 2048 multi-channel analyzer (and associated electronics). ^{60}Co, ^{137}Co, ^{54}Mn and ^{22}Na standards were used to calibrated the spectrometer so that one channel $\simeq$1.22 KeV.

6.2 System Calibration and Measurement of ^{10}B Samples

The objectives here are to (1) quantitatively correlate the detected ^{10}B signal to the quantity of ^{10}B present and

RADIATIVE CAPTURE GAMMA RAY SPECTRUM PRODUCED FROM 70 μg ^{10}B IN 7g H_2O IRRADIATED WITH A REACTOR NEUTRON BEAM

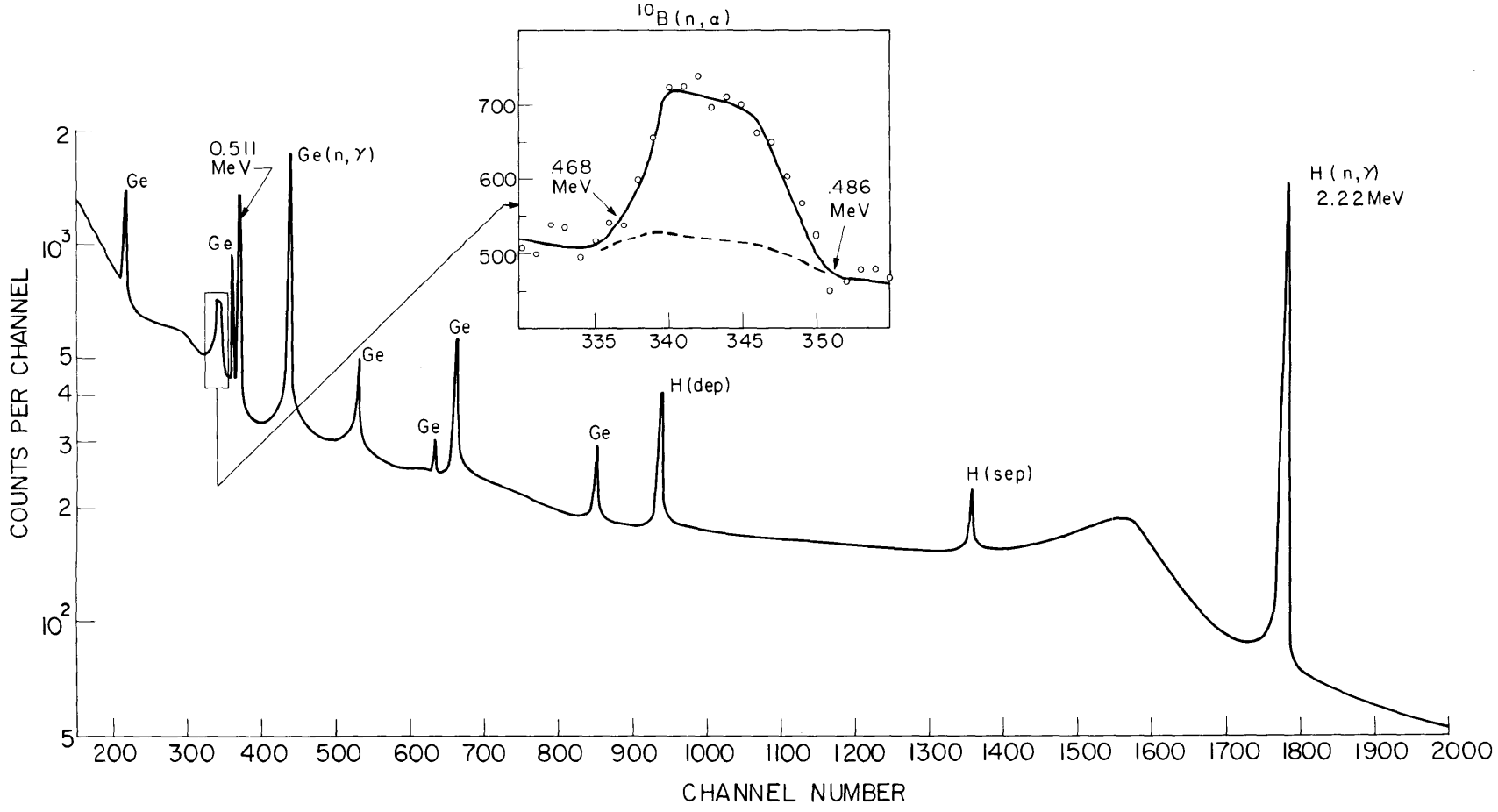

FIGURE 6.1

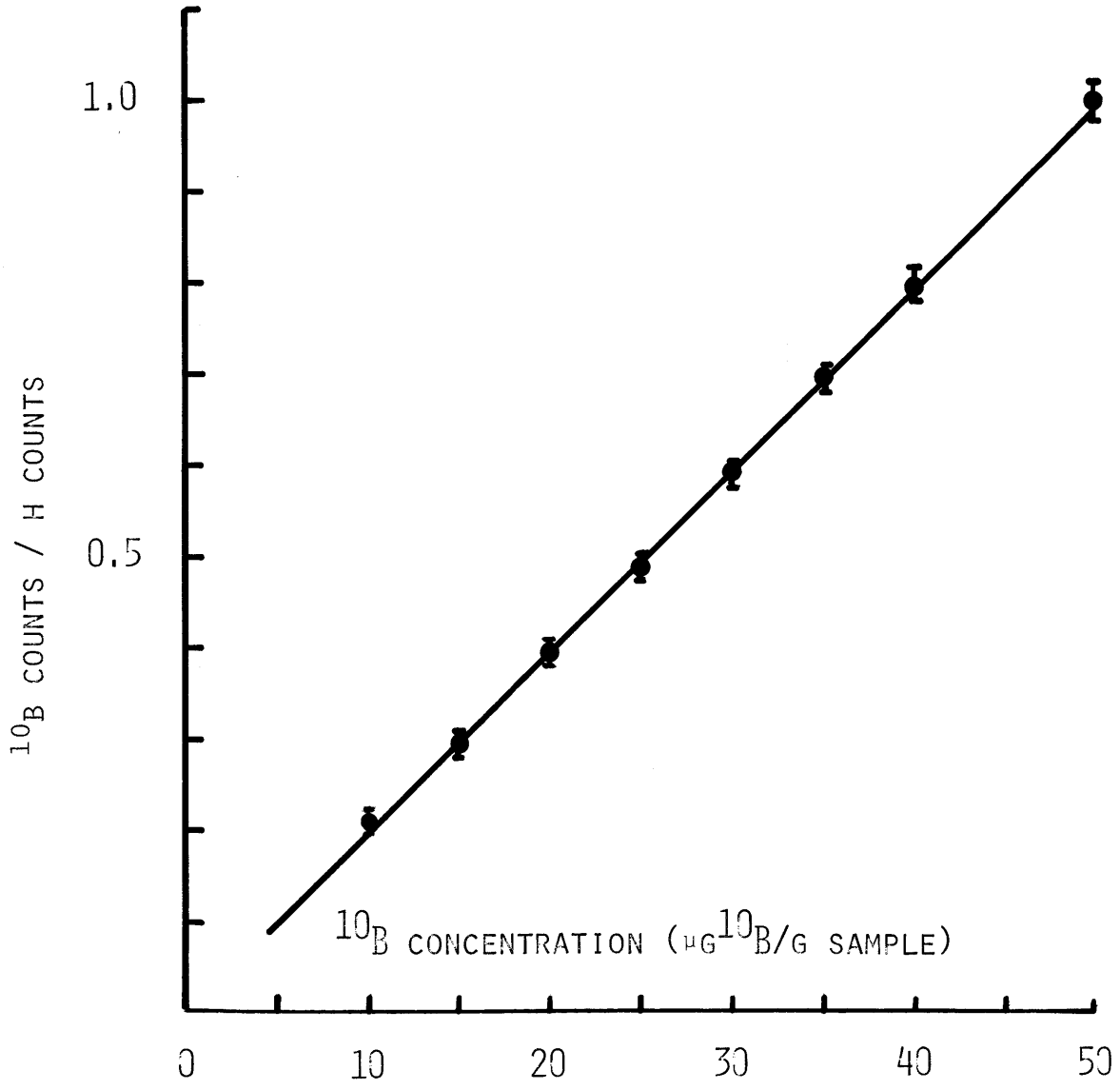

FIGURE 6.2 -- MEASURED ^{10}B PEAK AREA TO H PEAK AREA AS A FUNCTION OF ^{10}B CONCENTRATION IN 7G H_2O SAMPLES

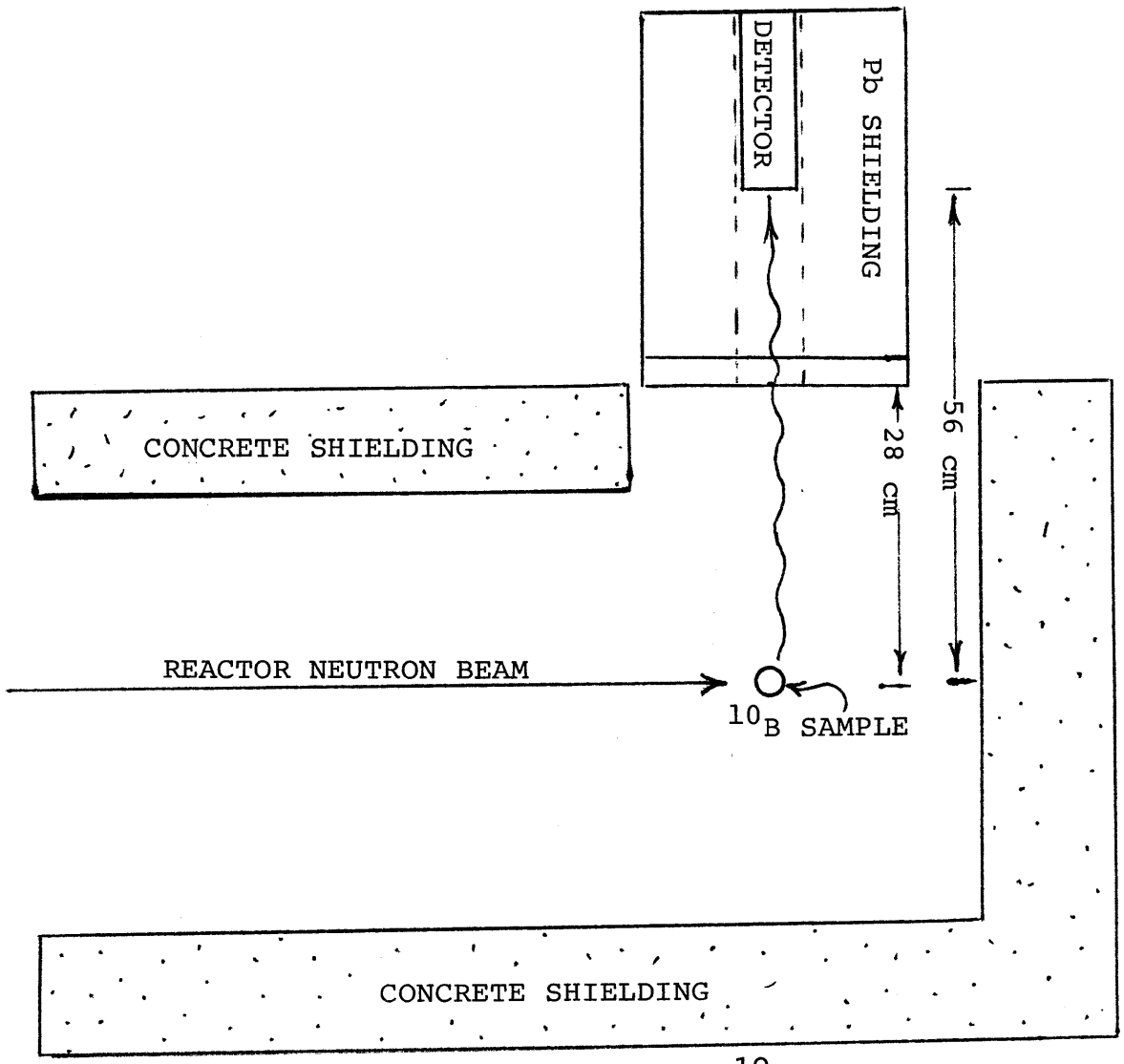

FIG. 6.3 -- REACTOR FACILITY USED FOR ^{10}B MEASUREMENTS

SAMPLE	$\mu g\ ^{10}B/g$ SAMPLE	TIME OF IRRADIATION	TOTAL COUNTS IN ^{10}B "WINDOW"	NET COUNTS FROM ^{10}B	COUNTS FROM HYDROGEN	$\frac{^{10}B\ COUNTS}{H\ COUNTS} = F$	$\frac{F}{^{10}B$ CONCENTRATION IN SAMPLE	σ_F
BLOOD	0.0	32,000 sec	208,268	-	198,178	-	-	-
	10.0	3,000	25,181	4,357	19,815	.2199	.02199	5.25%
	20.0	2,500	23,066	6,401	15,858	.4036	.02018	3.35%
	30.0	2,000	20,703	7,452	12,609	.5910	.01970	2.71%
	40.0	1,800	20,394	8,844	10,991	.8046	.02012	2.29%
H_2O	0.0	20,500 sec	130,726	-	130,749	-	-	-
	10.0	2,500	19,241	3,321	15,921	.2086	.02086	6.0 %
	15.0	2,550	20,325	4,606	15,721	.2930	.01953	4.41%
	20.0	3,000	26,740	7,575	19,168	.3952	.01976	3.08%
	25.0	1,600	14,838	4,804	10,035	.4788	.01915	3.53%
	30.0	1,660	16,341	6,076	10,266	.5919	.01973	2.94%
	35.0	1,660	17,366	7,147	10,221	.6853	.01959	2.58%
	40.0	1,400	15,654	6,953	8,702	.7990	.01998	2.54%
	50.0	1,250	15,437	7,753	7,685	1.0088	.02018	2.3%

TABLE 6.1 -- ^{10}B ASSAY CALIBRATION DATA USING REACTOR NEUTRON BEAM

(2) determine the lower limits of ^{10}B quantities that can be assayed. To calibrate the detected ^{10}B signal, a set of independently prepared ^{10}B standards were used. These standard samples consisted of 7 ml vials of H_2O and 7 of blood which were injected with concentrations of ^{10}B ranging from 0-50 μg ^{10}B/g sample. Using these standards a plot of the detected ^{10}B signal as a function of ^{10}B concentration was obtained.

A calibration plot obtained with the H_2O standards is shown in Figure 6.2. A similar graph was obtained with the blood standards. The data for both graphs is given in Table 6.1. Two features of these graphs are important. First note that along the ordinate of the graph is plotted the ratio of the ^{10}B .477 Mev γ peak area to the hydrogen 2.22 Mev γ peak area. Because of the frequent fluctuations in reactor power (~5%), and therefore in flux levels, the 2.22 MeV prompt gamma ray peak is used as a relative thermal flux monitor. Since both of these materials are always exposed to the same thermal flux levels the ratio of interest (i.e., ^{10}B counts/H counts) is invariant with changes in reactor power. Hence the ratio ^{10}B counts per sec/H counts per sec is used as the calibration parameter because it is insensitive to fluctuations in thermal flux levels. It should be pointed out that this ratio is actually a measure of the ^{10}B concentration in the sample, i.e. a measure of the ratio of the ^{10}B atoms to the H atoms. Consequently this

ratio is also insensitive to sample volume fluctuations. It should be noted that measurement of this ratio requires two types of background counts. One with a sample containing no ^{10}B to determine the background within the energy "window" about the ^{10}B peak. A second count should be taken without any sample to determine the H photon background from various materials in the experimental vicinity.

A complete table of data obtained in generating the two calibration curves is given in Table 6.2. Note that in both instances the $^{10}B/H$ ratio was measurable to within a statistical standard deviation of 6% in 3,000 seconds or less. Thus the lower practical detection limit of ^{10}B concentration is roughly 10 μg/gm sample for the sample detector distance used. Since this distance can be decreased by approximately one half, the level of sensitivity can be increased roughly by a factor of 4. This would lower the minimum ^{10}B concentration detection limit by approximately the same factor.

To test the effectiveness of this ^{10}B assay procedure, a "blind" study was conducted in which two samples prepared independently of the author were assayed. The ^{10}B concentrations of both samples, one H_2O and one blood, were know only to the chemist† who prepared them. The results of the assay agreed with the values recorded by the chemist, to within 1-2 standard deviations of the experimental values. Thus the efficacy of this approach is thereby demonstrated. This

†Dr. Glyn R. Wellum, Massachusetts General Hospital.

level of agreement greatly exceeds that obtainable by the wet chemistry techniques (~15%) referenced in the introduction. The results of these two measurements are given below:

(1) Blood Sample:

Actual concentration = 7.5 μg ^{10}B/g sample

Measured = 6.2 ± .8 μg ^{10}B/g sample

(2) H_2O Sample:

Actual concentration = 15 μg ^{10}B/g sample

Measured = 16.2 ± 1.4 μg ^{10}B/g sample

Figure 6.1 is a radiative capture gamma ray spectrum produced by irradiating 70 μg ^{10}B in 7 g of H_2O. See Table 6.1 for all the corresponding data. This boron assay system is compared to the ^{252}Cf assay system in Section 7.2.

7. SUMMARY, CONCLUSIONS AND RECOMMENDATIONS

7.1 Summary of Calculational and Experimental Studies

7.1.1 Rapid Boron Assay Facility

The first objective of this thesis was to design, construct, and evaluate a facility that would measure ^{10}B in human blood and tissue samples *in vitro* while meeting the following criteria:

a. Sensitivity: Detection of ^{10}B at levels of concentration of the order of 10 μg $^{10}B/g$ sample in 10g samples (i.e., ~.1mg^{10}B).

b. Precision: Statistical standard deviation of $\pm 5\%$ or less.

c. Time required to complete a measurement: less than one hour.

d. Portable: The completed facility should have sufficient compactness and pose a sufficiently low radiation hazard to allow an in-hospital siting.

This objective was achieved with certain qualifications, which will be explained later. The constructed facility, shown in Figure 4.1, employs a Ge(Li) detector to monitor the 0.447 MeV prompt gamma ray from the ^{10}B (n, α)^{7}Li reaction. This facility was designed in several steps employing both one-dimensional discrete ordinates and three-dimensional Monte Carlo radiation transport computer codes.

The one-dimensional discrete ordinate code, ANISN, was used to (1) design a suitable moderator configuration, (2) optimize the relative source-sample-detector distances, and (3) investigate biological shielding materials, so that an initial basic design could be made.

Moderating materials, H_2O, D_2O and Be, were evaluated in terms of three important parameters. These were the thermal neutron flux (ϕ_T), the fast neutron flux (ϕ_F), and the background photon flux (ϕ_γ). These parameters are related to the ^{10}B activation rate, the fast neutron detector [Ge(Li)] damage, and background count rate respectively. Accordingly, the moderators were compared in terms of both the ϕ_T/ϕ_F ratio (i.e., signal per unit detector damage), the ϕ_T/ϕ_γ ratio (i.e., signal to background), and the absolute ϕ_T levels (measurement time). These calculations were carried out with models of 30cm spheres of moderators.

The optimal location for the sample and detector within the moderator was determined by computing the number of required (by the design criteria) measurements that could be made before the detector suffers sufficient fast neutron damage to decrease the energy resolution by 50%, (after incurring a fast fluence of 6×10^8 n cm^{-2}).

Composite biological shielding materials were evaluated in terms of fast neutron removal, thermal neutron absorption and minimal radiative capture gamma ray production.

The principal findings were the following:

(1) A suitable moderator configuration for this application consist of the source shielded with 5 cm of Bi within a 30 cm radius sphere of D_2O. The Bi shielding reduces the source gamma ray flux at the external moderator surface to 0.04 of the gamma flux that would be present with no Bi around the sources. At radial distances greater than 15 cm, the ϕ_T is reduced by only 10%.

(2) Since the ratios, ϕ_T/ϕ_F, and ϕ_T/ϕ_γ, increase as the radial distance from the source increases, the best location for the detector is at the surface of the moderator and the best sample position is at the detector.

(3) A thickness of 20cm of either lithium loaded polyethylene or lithium loaded glycerin will reduce the surface dose rate to approximately 40 millirem/hr.

Several Monte Carlo three-dimensional calculations were carried out to effect a more realistic evaluation of the preliminary design and resulting modifications. The final Monte Carlo optimized version of the initial ANISN design corresponds to the constructed facilty shown in Figures 4.1 and 4.2. The Monte Carlo calculations indicated that this facility would meet all design criteria.

The constructed assay system was experimentally characterized and evaluated. First the thermal flux distributions in

the various sample tubes were measured using Mn and Cd covered Mn foils. The absolute agreement between these measured distributions and the corresponding calculated ones was excellent, as illustrated in Figures 2.13, 2.14, and 2.15. The agreement between the measured and calculated fast neutron flux in the detector portal, and dose rates at the surfaces of the facility were in similar agreement. Generally, the agreement between experimental data and calculated values was within 1-2 standard deviations.

Measurements of the background photon spectrum revealed a background of .477 MeV photons from the $^{7}Li(n, n')$ reaction. Those photons, however, were satisfactorily shielded against with a moderate amount of Pb. With this Pb shield, we were able to make a test measurement of ^{10}B (Figure 5.1). Since the Ge(Li) detector available for these studies had been redrifted several times, fear of irreparable fast neutron damage prevented its insertion into the detector portal. Thus a measurement of ^{10}B was made with the detector external to the portal where the fast flux was an order of magnitude lower ($\sim 3 \times 10^{2}$ n cm^{-2} S^{-1}). Since the sample detector geometry had a detection sensitivity 30 times less than it would be if the detector were in the portal, a test H_2O sample containing 30 times 0.1mg (see criterion a.) was used. The quantity was measurable with 5% statistics in ~500 seconds (Figure 5.1). Allowing for the increase in the background counts with a shielded detector in the portal, we extrapolate the following. With the detector in the portal, around which Pb shielding is

included, 0.1 mg of ^{10}B can be measured with 5% statistics in ~1000 seconds. This would meet all design criteria.

Finally a study was conducted to evaluate the feasibility of using a reactor neutron beam to assay ^{10}B. In this study we were able to measure ^{10}B levels as low as 10μg ^{10}B/g sample in 7g samples. Measuring this quantity, the time required to obtain 5% counting statistics (1 standard deviation) was ~1 hour (Figure 6.1). Since the sample-detector distance in this study can be reduced by 1/2, we should be able to reduce this counting time by ~1/4.

7.1.2 Partial Body In Vivo Neutron Activation Analysis Facility for the Measurement of Calcium

The second objective of this thesis, was to design a facility that would measure small changes in the calcium content of a human hand and wrist with a precision of ±2% or less and a fast neutron hand dose of less than 10 rem. In this system, ^{48}Ca in the hand and wrist is activated (^{48}Ca (n,γ) $^{49}Ca^*$) and the 3.1 MeV decay gamma ray is subsequently monitored with two large NaI(Tl) detectors.

This hand irradiation facility was designed in multiple steps employing both the discrete ordinates code ANISN and the general geometry Monte Carlo code, ANDY.

ANISN was used to evaluate two likely moderators, H_2O and D_2O, in terms of (1) the thermal flux to dose ratio (i.e. $^{49}Ca^*$ signal to dose), (2) thermal flux levels (irradiation

time) and (3) the spatial uniformity of the thermal flux (to determine the repositioning uncertainty). The calculated model consisted of a ^{252}Cf point source centered in a sphere of 30 cm radius. The results of these calculations indicated that for this application H_2O is the moderator of choice for the following reasons:

(1) The maximum thermal neutron flux level is 7 times higher in H_2O than in D_2O. Moreover the poor uniformity of the thermal flux distribution in H_2O from one point source can be made adequately uniform by superimposing the distributions from two sources separated by two times the distance over which the peak thermal flux falls by a factor of 1/2 (i.e., 2 x 6cm = 12 cm source sepearation).

(2) For practical source to hand distances of 15 cm or less, the thermal flux to dose ratio is higher in H_2O.

By applying the principle of superposition, we similarly determined that a set of four equal sources symmetrically positioned on a circle with an 8cm radius would produce, in H_2O, a uniform thermal flux distribution in the plane of the sources and in planes parallel to this plane. Furthermore, by using two sets of sources separated by 12cm, the thermal flux is uniform (few % variation) both laterally (between source planes) and within the planes parallel to the source plane

such that:

(1) ϕ_T varies by ~1% over 10 cm (approximate handwidth) in the plane parallel to, and equidistance from the two source planes.

(2) ϕ_T varies by <1% over $\pm$2cm laterally (approximate hand thickness) from the centerpoint between the two sources.

These findings lead to the design shown in Figure 3.8, which is the Monte Carlo model of the facility. This model was used to determine (1) the Ca activations in the hand and the wrist, (2) the dose to the hand and the body and, (3) the Ca activation in the forearm as a source of background activations. The results indicated that a two-minute irradiation will prodice (a) ~ 163,000 $^{49}Ca^*$ atoms in the hand (b) a fast neutron hand dose of ~.3 rad (c) an induced gamma ray hand dose of ~.2 rad, (d) <.06 mrad fast neutron whole body dose, (e) <.1 mrad induced gamma ray whole body dose, and (f) 11,000 $^{49}Ca^*$ nuclei in the forearm. Assuming a total photo peak efficiency of 8% for the 3.1 MeV gamma ray, ~11,000 counts under the Ca peak should be realized with 1% counting statistics.

Since an <u>in vivo</u> neutron activation analysis facilty would be used clinically to serially monitor the Ca content in the hand and wrist of each paient, allowance for repositioning errors during each irradiation has been made. To test the sensitivity of the hand irradiator to lateral changes

in the hand position, an ANISN calculation(adjoint solution) was carried out. This calculation estimated that the change in Ca activations in the hand for a 1cm hand displacement from the center position is in the range of ~0.5%. Calculations to estimate the effects of vertical changes in the hand position have not been made.

We conclude that with a two minute irradiation of the hand followed by a thirty minute counting period, a measurement of the Ca in the hand and wrist can be made with <2% precision. Table 3.1 compares this facility with other similar facilities presently in use.

7.2 Conclusions

A number of detailed conclusions have already been drawn throughout the thesis. The following is a summary of the major conclusions:

(1) The constructed rapid boron assay facility should perform as required if the detector portal is modified to accommodate a Ge detector shielded with a Pb annulus. The thickness of the annulus should be determined empirically. A rough calculation indicates that about 8 cm would be adequate.

(2) If the above modification is made, both calculations and experiments predict that about 300 5% precise (statistical standard deviation) measurements of 0.1 mg ^{10}B can be made per detector life (time for fast fluence of 6×10^{8} n-cm^{-2}). Assuming a detector

repair cost of approximately $1600, the effective cost per measurement is about $5.00. Surprisingly enough, this compares quite well with the reactor facility, where a similar measurement requiring 1000 seconds, would cost about $6.00 per measurement.

(3) The existing reactor facility in the assay of boron meets all required measurement criteria. This facility, however, could be improved. The present detector shield, which allows a minimum sample-detector distance of approximately 28 cm, should be optimized with respect to sample detector distance and background levels.

(4) The designed hand irradiation facility, when compared with similar facilities presently in use around the world, has the highest figure of merit for the measurement of Ca (i.e., measured $^{49}Ca^{*}$ activity per dose).

7.3 Recommendations For Future Investigation

7.3.1 Boron Assay Facility

Since the possibility of fast neutron damage to the Ge(Li) detector is a major concern, some of the calculations in Section 2.3 have been reviewed to determine if the present facility can be significantly improved in terms of the exposure of the detector to fast neutrons. Since the figure of merit, as defined in Section 2.2.3, is about a factor

of 40 greater at the surface of a 50 cm sphere of D_2O than at the surface of a 30 cm sphere of D_2O, it appears that such an improvement can be realized if some of the compactness of the facility (an original concern) is sacrificed. An investigation of the utility of a reflector which could be added to the present system, is therefore recommended for future work.

From the presently available information (Section 2.3.4) it appears (following the procedure in Section 2.3.4) that if 20 cm of D_2O reflector is added to the existing facilty, the optimal sample and detector locations would be at $r \approx 45$ cm for both. Positioning the sample here would expose it to approximately the same thermal flux level present at $r \approx 28$ cm (the optimal sample position) in the existing facility. This should ensure at least no longer measurement times than are presently required. The large increase in the figure of merit would be due to approximately a factor of 20 decrease in the fast neutron flux, and a factor of 2 decrease in the background gamma ray flux. Since graphite has a larger albedo than D_2O for equal slab thicknesses of less than 20 cm, it should also be investigated as a reflector.

Note, however, that the macroscopic fast neutron removal cross section for polyethyline is about 35% higher than for graphite, and about 25% higher than for D_2O. Consequently, if existing polyethylene-Li biological shielding is replaced

with an equal thickness of either graphite or D_2O the surface fast neutron dose rates will increase by roughly the above percentages respectively. Therefore some biological shielding (~10 cm of polyethylene) will be necessary.

7.3.2 Hand Irradiation Facility

The need for reproducible Ca activation within the hand and wrist can be met by imaginative engineering design. Although the present facility has been engineered to allow for a small displacement of the hand, the problems of how to reposition the hand, restrain the hand from large displacements, and repeatedly affix the lithium bracelet to the forearm within the moderator need to be seriously considered if the full potential of the design is to be realized with the constructed facility . Replacing the H_2O with polyethylene for example, may have certain practical advantages. If this were done, a cylindrical hand portal could be a part of the constructed facility. Each patient's hand could be fitted with a polyethylene cylinder that could in turn be inserted into the hand portal. This cylinder might also include the polyethylene-Li bracelet. The feasibility of such an arrangement, which might include air ducts or voids, should be investigated in terms of thermal flux uniformity and other important parameters.

BIBLIOGRAPHY

N.N. Ajitanand, "Prompt Gamma-Ray Emission in the Spontaneous Ternary Fission of Californium-252," Nucl. Phys. A133, 625 (1969).

R.L. Bach and R.S. Caswell, "Energy Transfer to Matter by Neutrons," Rad. Res., 35, 1 (1968).

K.H. Beckhurts and K. Wirtz, Neutron Physics, New York: Springer-Verlag (1964).

G.I. Bell and S. Glasstone, Nuclear Reactor Theory, New York: Van Nostrand Reinhold Co. (1970).

K. Boddy, S. Hashimi and J. Boyle, "An Assessment of the Probable Errors in Determining Calcium in Sections of Bone by In Vivo Activation Analysis," S.R.R.C. Report #SRRC 30/69, East Kilbride, Scotland (1969).

K. Boddy, I. Holloway, A. Elliot, D. Glaros, I. Robertson and B. East, "Low Cost Facilities for Partial-Body and Total Body Activation Analysis in the Clinical Environment," Nuclear Activation Techniques in the Life Sciences, IAEA-SM-157/20, 589, I.A.E.A., Vienna (1972).

K. Boddy, I. Robertson and D. Glaros, "The Development of a Facility for Partial-Body In Vivo Activation Analysis Using ^{252}Cf Neutron Sources," Phys. Med. Biol., 19, 853 (1974).

K. Boddy, D. Glaros and I. Robertson, "Measurement of Calcium in Sections of a Human Skeleton using a Reactor Spectrum-In Vivo Activation Analysis Technique," Phys. Med. Biol., 20, 80 (1975).

J.W. Boldeman, "Prompt-Neutron Yield from the Spontaneous Fission of Californium-252," Nucl. Sci. Eng., 55, 2 (1974), 188-220.

A.R. Boulogne and A.G. Evans, "Californium-252 Neutron Sources for Medical Applications," Int. J. Appl. Radiation Isotopes, 20, 453 (1969).

J.C. Browne and F.S. Dietrich, "Hauser-Feshbach Calculation of the Californium-252 Spontaneous-Fission Neutron Spectrum," Phys. Rev., C10(6), 2545 (1974).

G.L. Brownell, A.H. Soloway and W.H. Sweet, "Boron Capture Therapy," in Modern Trends in Radiotherapy, Vol. I, p. 132, T. Deeley and C. Wood, Eds., London: Butterworth, Inc. (1967).

G.L. Brownell, B.W. Murray, W.H. Sweet, G.R. Wellum and A.H. Soloway, "A Reassessment of Neutron Capture Therapy in the Treatment of Cerebral Gliomas," Proc. Seventh Natl. Cancer Conf., 827 (1973).

Californium-252, Its Use and Market Potential, USAEC, Savannah River Operations Office, Aiken, South Carolina (1970).

Californium-252 Progress, Number 7, p. 42, USAEC, Savannah River Operations Office, Aiken, South Carolina (1971).

J.R. Cameron and J. Sorensen, "Measurement of Bone Mineral In Vivo; An Improved Method," Science, 142, 230 (1963).

L.L. Carter and E.D. Cashwell, Particle-Transport Simulation with the Monte Carlo Method, Oak Ridge: USERDA Technical Information Center (1975).

G.R. Catto, J.H. McIntosh and M. Macleod, "Partial Body Neutron Activation Analysis In Vivo: A New Approach to the Investigation of Metabolic Bone Disease," Phys. Med. Biol., 18, 508 (1973).

R.L. Chase, Nuclear Pulse Spectrometry, New York: McGraw Hill, Inc. (1961).

S.H. Cohn, C.S. Dombrowski and R.G. Fairchild, "In Vivo Neutron Activation Analysis of Calcium in Man," Int. J. App. Rad. Iso., 21, 127 (1970).

S.H. Cohn and C.S. Dombrowski, "Measurement of Total Body Calcium, Sodium, Chlorine, Nitrogen, and Phosphorus in Man by In Vivo Neutron Activation Analysis," J. Nucl. Med., 12, 499 (1971).

S.H. Cohn, R.G. Fairchild and K.K. Shukla, "Theoretical Considerations in the Selection of Neutron Sources for Total Body Neutron Activation Analysis," Phys. Med. Biol., 18, 648 (1973).

C. Colbert, "Precision of Measuring Bone Mineral from Radiographs." Submitted for publication to Science.

J.L. Crandall, "Survey of Applications for ^{252}Cf, Iso. and Rad. Tech., 7, No. 3, 306 (1970).

R.L. Currie, F.J. McCrosson and P.B. Parks, "Flux Enhancement with ^{252}Cf Source in a Subcritical Assembly," Neutron Sources and Applications: Proceedings of the American Nuclear Society National Topical Meeting, April 19-21, 1971, Augusta, Ga.

O.L. Deutsch, Unpublished MIT Nuclear Engineering Department Report: Users Guide to ANDY, M.I.T., Cambridge, Ma. (1974).

O.L. Deutsch and B.W. Murray, "Monte Carlo Dosimetry Calculation for Boron Neutron Capture Therapy in the Treatment of Brain Tumors," Nucl. Tech., 26, 320 (1975).

D. Duffey, A. El-Kady and F. Senftle, "Analytical Sensitivities and Energies of Thermal-Neutron-Capture Gamma Rays," Nucl. Instr. Methods, 80, 149 (1970).

D. Duffey, J.P. Balogna and P.F. Wiggins, "Techniques with ^{252}Cf for Neutron Capture Gamma Ray Spectroscopy," Bull. Amer. Phys. Soc., Series II, 19, 530 (1974).

D. Duffey, J.P. Balogna and P.F. Wiggins, "Analysis of Geothermal Power Plant Water Using Gamma Rays from Capture of Californium-252 Neutrons," Nucl. Tech., 27, 488 (1975).

F.C. Engesser and W.E. Thompson, "Gamma Rays Resulting from the Interaction of 14.7 MeV Neutrons with Various Elements," J. Nucl. Energy, 21, 487 (1967).

W.W. Engle, A User's Manual for ANISN, a One-Dimensional Discrete Ordinates Transport Code with Anisotropic Scattering, Report #K-1693, Union Carbide Corporation (1967).

R.D. Evans, The Atomic Nucleus, New York: McGraw-Hill Co. (1968).

R.A. Forster and H.O. Menlove, "Moderator Investigations of ^{252}Cf for Non-Destructive Assay of Fissionable Materials," Neutron Sources and Applications: Proceedings of the American Nuclear Society National Topical Meeting, April 19-21, 1971, Augusta, Ga., USAEC Report CONF-710402, Vol. III (1971).

D.C. Glaros, "Partial Body In Vivo Neutron Activation Analysis - A Technique for Measuring Minerals in Bone," Ph.D. thesis, University of Strathclyde, U.K.

L. Green, "^{252}Cf Fission Neutron Spectrum," Trans. Am. Nucl. Soc., 14, 119 (1971).

L. Green, J. Mitchell and N. Steen, "Californium-252 Fission Neutron Spectrum from 0.5 to 13 MeV," Nucl. Sci. Eng., 50, 257 (1973).

Guide for Fabricating and Handling ^{252}Cf Sources, USAEC Report, National Technical Information Service, Aiken, South Carolina, SRO-153 (1971).

D.R. Harris, "ANDY MG3, The Basic Program of a Series of Monte Carlo Programs for Time Dependent Transport of Particles and Photons," LA-4539, Los Alamos Scientific Laboratory (1970).

W.H. Harris and R.P. Heaney, Skeletal Renewal and Metabolic Bone Disease, Boston: Little, Brown and Company (1970).

J.E. Harrison, W.C. Williams, J. Watts and K.G. McNeill, "A Bone Calcium Index Based on Partial Body Calcium Measurements by In Vivo Activation Analysis," J. Nucl. Med., 16, 116 (1974).

H. Hatanka and K. Sano, "A Revised Boron-Neutron-Capture Therapy for Malignant Brain Tumors," Z. Neurol., 204, 309 (1973).

D.M. Hegsted, "Balance Studies," J. Nutrition, 106, 307 (1976).

E.K. Hyde, The Nuclear Properties of the Heavy Elements. Part III Fission Phenomena, Englewood Cliffs, N.J.: Prentice-Hall (1964).

I.C.R.P., Recommendations of the International Commission on Radiological Protection, Brit. J. Radiol., Supplement 6 (1955).

I.C.R.P., Report of the Task Group on Reference Man, ICRP Report #23, Pergamon Press (1975).

H. Ing and W. Cross, "Spectra and Dosimetry Related to Neutron Irradiations of the Human Body," Phys. Med. Biol., 20, 906 (1975).

T.D. Jones, "Particle Current to Fluence Conversion for Instruments of Detection and for Monte Carlo Simulated Radiation Transport," Health Phys., 28, 451 (1975).

A. Kaczmarczyk, "Rapid Method for Determination of Boron in Biological Material," Anal. Chem., 43, 271 (1971).

D. Kedem and M. Lemanska, "Computational Experiments with a Californium-252 Source for Possible Use in Neutron Radiography," Nucl. Tech., 28, 152 (1976).

H. Kramer, C. Chasman and K. Jones, "Effects Produced by Fast Neutron Bombardment of Ge(Li) Gamma Ray Detectors," Nucl. Instr. Methods, 62, 173 (1968).

J.R. Lamarsh, Introduction to Nuclear Reactor Theory, Reading, Mass.: Addison Wesley (1966).

K.D. Lanthrop, "Discrete-Ordinates Methods for the Numerical Solution of the Transport Equation," Reactor Tech., 15, No. 2, 107 (1972).

LASL, Report in Californium-252 Progress, Number 7, p. 42. USAEC Savannah River Operations Office, Aiken, South Carolina (1971).

E.A. Lorch, "Neutron Spectra of ^{241}Am/B, ^{241}Am/Be, ^{241}Am/F, ^{242}Cm/Be, ^{238}Pu/^{13}C and ^{252}Cf Isotopic Neutron Sources," Int. J. Appl. Rad. and Iso., 24, 585 (1973).

B. Maziere, D. Comar and D. Kuntz, "In Vivo Measurement of the Ca/P ratio by Local Activation with Isotopic Neutron Sources," in Proc. of 2nd East Kilbride Conf. on Progress and Problems of In Vivo Activation Analysis, S.U.R.R.C., East Kilbride, Scotland, April 1976.

K.G. McNeill, B.J. Thomas, W.C. Sturbridge and J.E. Harrison, "In Vivo Neutron Activation Analysis for Calcium in Man," J. Nucl. Med., 14, 502 (1973).

B.W. Murray, O.L. Deutsch, R.G. Zamenhof, R.I. Pettigrew, R.A. Rydin, G.L. Brownell, in Biomedical Dosimetry, 179, IAEA, Vienna (1975).

R.M. Neer, Massachusetts General Hospital (priv. comm., 1977).

J.P. Nichols, "Design Data for ^{252}Cf Neutron Source Experiments," Nucl. Appl., 4, 382 (1968).

L.C. Northcliffe and R.F. Schilling, "Range and Stopping Power Tables for Heavy Ions," Nucl. Data Tables, A7, 223 (1970).

N.R. Ortiz, I.C. Rickard, M.J. Driscoll and N.C. Rasmussen, "Instrumental Methods for Neutron Spectroscopy in the MIT Blanket Test Facility," M.I.T. Internal Report, Dept. of Nucl. Eng., MITNE-129, Cambridge, Ma. (1972).

R.I. Pettigrew, O.L. Deutsch and B.W. Murray, "^{252}Cf Partial Body In Vivo Neutron Activation Analysis Facility," Proc. of 2nd East Kilbride Conference on Progress and Problems of In Vivo Activation Analysis, S.U.R.R.C., East Kilbride, Scotland, April 1976.

R.I. Pettigrew, O.L. Deutsch and B.W. Murray, "Partial Body In Vivo Neutron Activation Analysis Using ^{252}Cf," Proc. of 4th Int. Conf. on Medical Physics, 32, 9.1, Ottawa, July 1976.

P.Q. Quitter, Gamma-Ray Spectroscopy, London: Adam Hilger Ltd. (1972).

D.E. Raeside, "Monte Carlo Principles and Applications," Phys. Med. Biol., 21, No. 2, 181 (1976).

N.C. Rasmussen, Y. Hukai, T. Inouye and V.J. Orphan, "Thermal Neutron Capture Gamma-Ray Spectra of the Elements," M.I.T. Internal Report MITNE-85, M.I.T., Cambridge, Ma. (1969).

W.C. Renig, "Advantages and Applications of ^{252}Cf as a Neutron Source," Nucl. Appl., 5, 24 (1968).

J.J. Ritts, M. Solomito and P.N. Stevens, "Calculation of Neutron Fluence-to-Kerma Factors for the Human Body," Nucl. Appl. Tech., 7, 89 (1969).

A. Roy and K.V. Iyengar, "Solid-Angle Correction Factors for Ge(Li) Detectors," Nucl. Instr. Methods, 114, 29 (1974).

R.A. Rydin, "Fast Neutron Spectroscopy and Dosimetry of the MIT Reactor Medical Therapy Facility Beam," Sc.D. thesis, M.I.T. Department of Nucl. Eng., Cambridge, Ma. (1964).

H.A. Sandmeir, G.E. Hansen, R.E. Seamon, T.J. Hirons and A.H. Marshall, "Coupled Neutron-Gamma Multigroup-Multitable Cross Sections for 29 Materials Pertinent to Nuclear Weapons Effect Calculations Generated by LASL/TD Division," LA-5137, Los Alamos Scientific Laboratory (1974).

F.E. Senftle, "Construction Materials for Neutron Capture-Gamma-Ray Measurement Assembly Using Californium-252," Nucl. Tech., 10, 204 (1971).

F.E. Senftle and P. Philbin, "Relative Shielding Properties of Ammonium Metatungstate for Neutrons and Gamma Rays from ^{252}Cf," Health Phys., 23, 529 (1972).

K. Siegbahn, Alpha, Beta and Gamma-Ray Spectroscopy, in K. Siegbahn (Ed.), North Holland Publishing Co., Amsterdam (1965).

W.S. Snyder, M.R. Ford, G.G. Warner and H.L. Fisher, Nucl. Med. Suppl. 3, Pamphlet 5.

A.H. Soloway and J.R. Messer, "Determination of Hydrolytically-Stable Boron Hydrides in Biological Materials," Analytical Chem., 36, 433 (1964).

T.J. Spinks, D.K. Bewley, G.F. Joplin and A.S.O. Ranicar, "Neutron Activation Measurement of Metabolic Activity of Sodium in the Human Hand," J. Nucl. Med., 17, 724 (1976).

P.H. Stelson, J.K. Dickens, S. Raman and R.C. Trammell, "Deterioration of Large Ge(Li) Diodes Caused by Fast Neutrons," Nucl. Instr. Meth., 98, 481 (1972).

D.H. Stoddard and H.E. Hootman, "^{252}Cf Shielding Guide," AEC Report #DP-1246, Savannah River Laboratory, Aiken, South Carolina (1971).

D.H. Stoddard and R.A. Moyer, "Calculated and Measured Effectiveness of Californium-252 Source Shielding," Proc. ANS Topical Meeting on Neutron Sources and Applications, Augusta, Ga., April 19, 1971.

G.S. Stanford, "Attenuation of Epicadmium Neutrons by Cadmium Foil Covers," in ANL-7010, Argonne National Laboratory, Argonne, Ill., 203 (July 1963).

D. Vartsky and B.J. Thomas, "In Vivo Neutron Activation Analysis; Preliminary Investigations of a Technique for Improving the Uniformity of Thermal Neutron Flux in the Body," Phys. Med. Biol., 21, 139 (1976).

J.P. Veerling, Jr., G. Oliver and E. Moore, "A Storage and Handling Facility for Californium-252 Medical Sources," Health Phys., 25, 163 (1973).

C.H. Wescott et al., "Effective Cross Sections and Cadmium Ratios for the Neutron Spectra of Thermal Reactors," AECL-612 (1958).

R.G. Zamenhof, B.W. Murray, G.L. Brownell, G.R. Wellum and E.T. Toplin, "Boron Neutron Capture Therapy for the Treatment of Cerebral Gliomas; I. An Evaluation of the Efficacy of Various Neutron Beams," Med. Phys., 2, 47 (1975).

R.G. Zamenhof, "The Measurement of Body Elemental Composition by Radiative Capture Gamma Ray In Vivo Neutron Activation Analysis," Ph.D. thesis, M.I.T. Interdepartmental Program in Biomedical Eng. and Dept. of Nucl. Eng., Cambridge, Ma. (1977).